Journal of Chemistry

Chemical Management and Treatment of Agriculture and Food Industries Wastes

Lead Guest Editor: Gassan Hodaifa
Guest Editors: Alberto J. López and Christakis Paraskeva

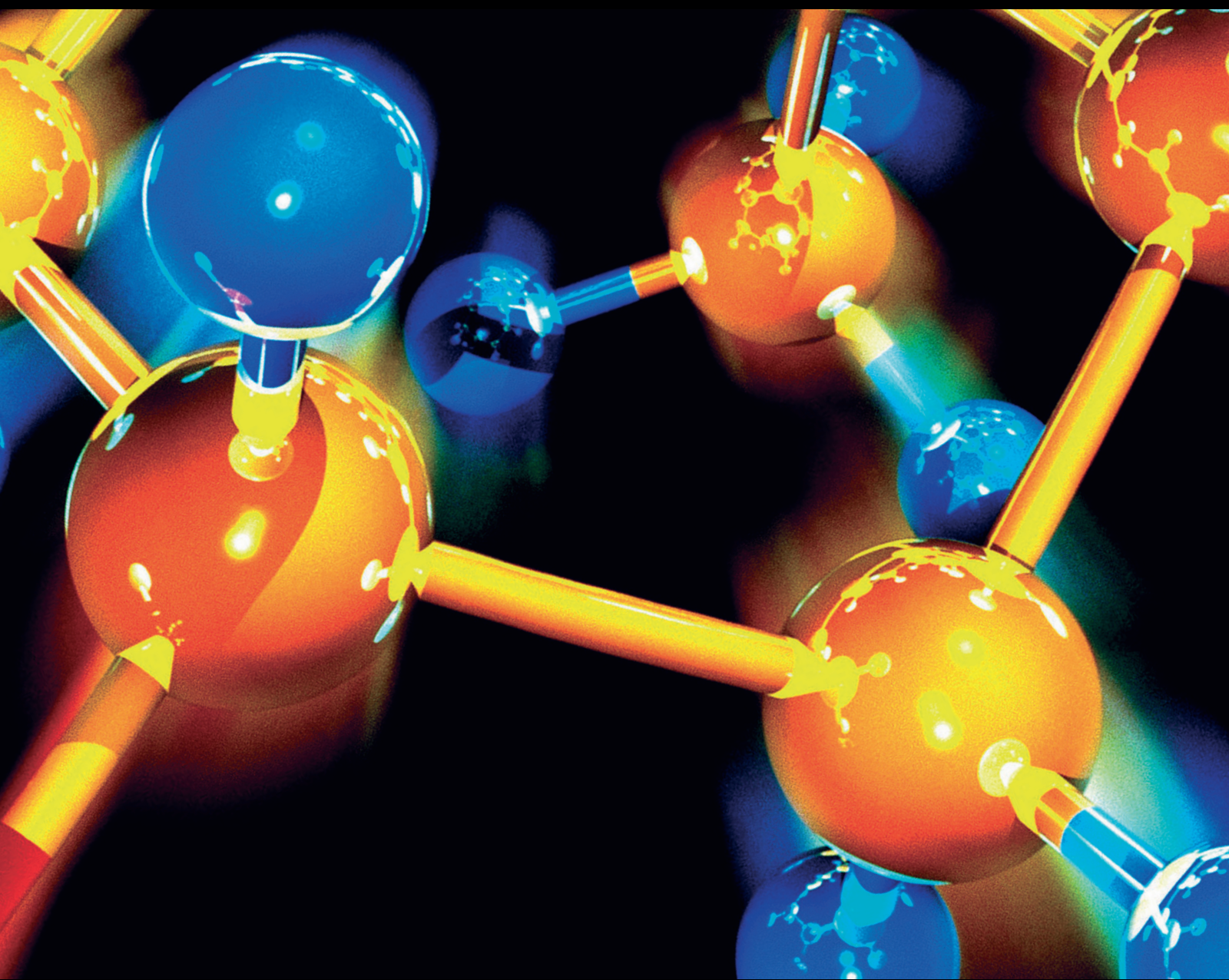

Chemical Management and Treatment of Agriculture and Food Industries Wastes

Journal of Chemistry

Chemical Management and Treatment of Agriculture and Food Industries Wastes

Lead Guest Editor: Gassan Hodaifa
Guest Editors: Alberto J. López and Christakis Paraskeva

Contents

Hindawi
Journal of Chemistry
Volume 2019, Article ID 4089175, 3 pages
https://doi.org/10.1155/2019/4089175

Editorial

Chemical Management and Treatment of Agriculture and Food Industries Wastes

Gassan Hodaifa,[1] **Alberto J. Moya López**,[2] **and Christakis Paraskeva**[3]

[1]*University of Pablo de Olavide, Seville, Spain*
[2]*University of Jaén, Jaén, Spain*
[3]*University of Patras, Patras, Greece*

Correspondence should be addressed to Gassan Hodaifa; ghodaifa@upo.es

Received 3 March 2019; Accepted 6 March 2019; Published 19 March 2019

Agriculture and related industries are one of the most strategic sectors for many countries. Agricultural residues are obtained from crops and livestock residues. Currently, the worldwide total harvest areas of cereals, primary oil crops, pulses, roots and tubers, and primary fiber crops are around 721.4×10^6, 301.9×10^6, 85.2×10^6, 61.9×10^6, and 37.7×10^6 ha, respectively. The worldwide industrial production of raw centrifugal sugar, molasses, oil palm, and oil soybean is around 176.9×10^6, 61.0×10^6, 57.3×10^6, and 45.7×10^6 tones, respectively. In general, the agrofood industry is increasingly modern and automated with a single objective that is to increase its production to meet the needs of the market and fulfil the economic objectives.

Parallel to these agricultural and industrial activities, large volumes of solid and liquid residues are generated that present a serious environmental problem in the case of not being well treated or managed. Considering the current social and scientific development, all these residues nowadays can be transformed to by-products with the aim to be reused as a new product useful to the society.

The special issue covers a very wide field as the agrofood industries generate various wastes, and there are an infinite number of applications and possible reuses of such wastes. In our initial proposal, we have tried to establish the state of the art for the agricultural and food industries residues, either in the solid or liquid state. The special issue has indicated that welcome manuscripts about the management and treatment methods of solid and liquid wastes and special attention will be given to works about the valorization of wastes as a source for sustainable bioenergy, water recirculation, and waste composting, where conventional and unconventional techniques are used. In addition, methods for the exploitation of forest and municipal wood wastes for energy generation will also be considered. In addition, potential topics to accept have been indicated. By way of example, it has been pointed the following:

(i) Agricultural crop residues for energy recovery and animal feed
(ii) Food industries residues for water and energy regeneration
(iii) Wastes management and composting
(iv) Residues from industrial oil crops: management and treatment
(v) Residues of olive industries: management and treatment
(vi) Lignocellulosic wastes as feedstocks for biofuels and biochar production
(vii) Conversion of waste to biogas, compost, and fertilizers
(viii) Wastewater treatment methods
(ix) Waste management and policies
(x) Advances in the liquid and solid state wastes treatment techniques and management
(xi) Separation of phenolic compounds with a high added value from agroindustrial wastes
(xii) Valorization of agriculture and industrial by-products to new useful products

From the first moment, we have been aware of the complexity that can reach the special issue. In fact, the seven accepted articles published in this special issue have dealt with different topics of high interest to the scientific community as well as to the industrial technology sector, as indicated below:

The article by E. Ramos-Zambrano et al. entitled "Cochineal Waxy Residues as Source of Policosanol: Chemical Hydrolysis and Enzymatic Transesterification" compares the chemical and enzymatic transesterification reactions for obtaining policosanol from waxy waste of cochineal insects generated in the carmine industry. First, in chemical reactions, different bases and solvents were evaluated; then, during transesterification, the use of molecular sieves, two lipases, and the effect on the reaction product yields of different alcohols as acyl receptors were analysed. The results obtained show an option to valorise the waste generated by the carmine industry. The policosanol obtained was composed mainly of triacontanol, an alcohol with a great commercial value due to its properties as the plant growth promoter. Triacontanol yields of up to 13% were attained through chemical hydrolysis and up to 19% by a novel method of enzymatic transesterification. Enzymatic transesterification was carried out with lipase *Candida antarctica* (CAL-Bn) in a reaction medium with toluene, molecular sieves, and different acyl receptors. This ecofriendly method can be applied to other wax sources to improve policosanol extraction.

The article by B. Bai et al. entitled "Lauric Acid-Modified Nitraria Seed Meal Composite as Green Carrier Material for Pesticide Controlled Release" presents a novel hydrophobic carrier LA-NSM, modified *Nitraria* seed meals with lauric acid, was fabricated through a facile chemical-surface modification route. The structure, surface wettability, and morphology of the obtained LA-NSM were characterized by Fourier-transform infrared spectroscopy (FT-IR), contact angle measurements (CAM), and scanning electron microscopy (SEM). Moreover, the degree of esterification and the influence of pH, temperature, and soil humidity on the release capacity of LA-NSM@DEL were also studied. Generally, the controlled DEL release of the LA-NSM platform not only enhanced the service efficiency of agrochemicals but also extended the utilization of waste *Nitraria* seeds. The results obtained show an environmentally friendly LA-NSM carrier was successfully prepared through modifying waste NSMs with lauric acid. FT-IR, SEM, and CAM analyses confirmed the reaction between hydroxyl groups of NSMs and carboxyl groups of lauric acid. The loading experimental results indicate that the equilibrium loading capacity of DEL into the LA-NSM carrier can reach about 1068 mg/g. The pH of soil, environmental temperature, and soil humidity have an obvious influence on the releasing property of LA-NSM@DEL. Moreover, the release process fitted well to the Higuchi model. Of particular interest regarding this technology that deserves to be mentioned is that the present route not only makes good use of natural waste resources but also can significantly address and reduce multiple issues created by pesticides, in view of their handy, convenient, and inexpensive fabrication method.

The article by K. Le Van and T. L. Thi Thu entitled "Preparation of Pore-Size Controllable Activated Carbon from Rice Husk Using Dual Activating Agent and Its Application in Supercapacitor" presents activated carbons prepared from rice husk by chemical activation with dual activation agents to obtain activated carbons with high porosity and large specific surface area. Additionally, the effect of the NaOH/KOH ratio on the specific surface area, pore structure, morphology, and thermal stability of the final activated carbons was studied. Moreover, the obtained materials were characterized and evaluated for potential application as supercapacitor electrode materials.

The article by M. K. Daud et al. entitled "Potential of Duckweed (*Lemna minor*) for the Phytoremediation of Landfill Leachate" presents a phytoextraction of zinc, copper, lead, iron, and nickel from landfill leachate by duckweed (*L. minor*). Bioconcentration factor and removal efficiency were also calculated. Results of this study proved that *L. minor* significantly reduced the concentration of heavy metals in landfill leachate. Removal efficiency of *L. minor*, for all the metals, from landfill leachate was more than 70% with the maximum value for copper (91%). Reduction in chemical oxygen demand (COD) and biological oxygen demand (BOD) was observed by 39% and 47%, respectively. The value of bioconcentration factor (BCF) was less than 1 with the maximum figure for copper (0.84) and lead (0.81), showing that the plant is a moderate accumulator for these heavy metals. Finally, the authors present *L. minor* as a sustainable alternative candidate.

The article by J. Liu et al. entitled "Three-Dimensional Excitation and Emission Fluorescence-Based Method for Evaluation of Maillard Reaction Products in Food Waste Treatment" presents a method to characterize and quantify Maillard reaction products (MRPs) created by hydrothermal treatment of food waste. Molecular weight fractionation, indirect spectrometric indicators, and three-dimensional excitation-emission fluorescence (3DEEM) analysis identified MRPs. The 3DEEM method combined with fluorescence regional integration (FRI) and parallel factor (PARAFAC) analyses was able to differentiate clearly between MRPs and other dissolved organic compounds compared to other approaches.

The article by T.-L. Pham and H. M. Bui entitled "Comparison of Diazinon Toxicity to Temperate and Tropical Freshwater *Daphnia* Species" presents an acute 48 h assay and a chronic 14-day assay performed to study the effects of diazinon on two cladoceran species. The toxicity of diazinon to early life stages of the temperate species *Daphnia magna* was tested, and the toxicity on *D. magna* was compared to that on the tropical species *Daphnia lumholtzi*. The results will provide baseline information to establish the benchmark for organophosphate insecticides in tropical waters. The results obtained confirmed that diazinon poses significant risk to aquatic organisms, namely, nontarget *Daphnia* species. The population growth of *D. magna* and *Daphnia lumholtzi* was adversely affected by diazinon after a chronic exposure period. Compared with *D. magna*, *D. lumholtzi* showed even higher sensitivity to diazinon in the acute test. The results of this study are important for

prediction of toxic effects and environmental risk associated with insecticides. Further studies using additional organophosphate insecticides, different tropical test species, and test conditions are needed to assess the possible environmental risk associated with pesticides in tropical aquatic ecosystems.

The article by Z. Majbar et al. entitled "Co-composting of Olive Mill Waste and Wine-Processing Waste: An Application of Compost as Soil Amendment" presents the valorization of the olive mill wastes and by-products wine industry by co-composting. In addition, the evolution of the parameters describing the co-composting of mixtures of olive mill wastes and green waste was studied and the effect of the different composts produced on the performance and yield of radish in the field was tested. The results showed that the co-composting of olive mill wastes and the wine by-products with green waste has proved to be an effective means of producing an organic amendment for agricultural soils. The monitoring of the physicochemical parameters during this process has revealed a good progress of the co-composting process, a biodegradation of organic matter, and a bioconversion of unstable matter into a stable product rich in humic substances. This biotransformation was also confirmed by the phytotoxicity test of the compost extracts produced, which showed that the various composts produced are mature and show no phytotoxic effect.

Conflicts of Interest

The Guest Editor and Guest Co-editors declare that there are no conflicts of interest or agreements with private companies, which will prevent us working impartially in the editorial process.

Acknowledgments

The editors thank all the authors for their contributions.

Gassan Hodaifa
Alberto J. Moya López
Christakis Paraskeva

Hindawi
Journal of Chemistry
Volume 2019, Article ID 4547378, 10 pages
https://doi.org/10.1155/2019/4547378

Research Article

Cochineal Waxy Residues as Source of Policosanol: Chemical Hydrolysis and Enzymatic Transesterification

Emilia Ramos-Zambrano,[1] **Pedro Herrera-Serrano**,[1] **Jorge García-Dávila**,[2] **Gabriel Ríos-Cortés**,[3] **Antonio Ruperto Jiménez-Aparicio**,[1] **and Alma Leticia Martínez-Ayala**[1]

[1]*Instituto Politécnico Nacional, Centro de Desarrollo de Productos Bióticos, Carretera Yautepec-Jojutla, Km. 6, Calle CEPROBI No. 8, Col. San Isidro, Yautepec, Morelos 62731, Mexico*
[2]*Universidad Politécnica de Tlaxcala, Av. Universidad Politécnica No. 1, Tepeyanco, Tlaxcala 90180, Mexico*
[3]*Instituto Tecnológico de Orizaba, Avenida Oriente 9 No. 852, Colonia Emiliano Zapata, Veracruz 94320, Mexico*

Correspondence should be addressed to Alma Leticia Martínez-Ayala; alayala@ipn.mx

Received 20 September 2018; Revised 4 January 2019; Accepted 14 January 2019; Published 10 February 2019

Guest Editor: Christakis Paraskeva

The aim of this study was to obtain and characterise the long-chain alcohols present in policosanol derived from waste from the production of carminic acid, a natural colouring agent widely used in the food industry. The effectiveness of different methods designed for extraction of policosanol from waxy waste was investigated and its content and composition was determined. Triacontanol was the main component in policosanol produced by chemical processes, and it yields up to 13% by alkaline hydrolysis in water and chloroform extraction. Regarding enzymatic transesterification, policosanol was obtained using lipase *Candida antarctica* recombinant in *Aspergillus niger* (CAL-B*n*) in a reaction medium with toluene. To improve the reaction, different acyl receptors, propanol, butanol, and isopropanol, were tested and molecular sieves were employed to maintain an anhydrous reaction medium. In this case, the policosanol was made up of other long-chain alcohols, but triacontanol was obtained in yields of up to 19% using isopropanol as an acyl receptor. Triacontanol has a great commercial value due to its effect as a promoter of plant growth, and these results contribute to the use and application of this agroindustrial waste in obtaining value-added products.

1. Introduction

The carmine industry, which produces natural red dye food additives, generates a great quantity of waste, which includes wax, cuticles, and cocoons derived from female cochineal insects that are cultivated and maintained on *Opuntia* plants throughout their life cycle (90 days). The insects produce a waxy layer, which is renewed twice (ecdysis) and constitutes around 3% of the weight of the cochineal insect. Cochineal wax is a mixture of esters of cocceric acid and cocceryl alcohol (triacontanol) [1, 2]; therefore, cochineal wax could be a good source of policosanol.

Policosanol is a mixture of long-chain alcohols with a length of 20–36 carbons. It consists mainly of tetracosanol (24C), hexacosanol (26C), octacosanol (28C) and triacontanol (30C). It is found naturally, free or esterified, in different vegetable and animal sources [3–8]. The mixture has been shown to have distinct beneficial effects, such as hypolipemiant, antiatherosclerotic, and cholesterol-lowering as well as antiaggregatory and ergogenic properties [9–12]. Also, triacontanol is a valuable compound because it helps to increase the yields of various agricultural crops [13].

The most widely used procedure for obtaining policosanol esterified in waxes is through the chemical hydrolysis under alkaline conditions, followed by solid-liquid extraction with organic solvents [5, 14–16]. Recently, Ma et al. [17] presented a method via solvent-free reduction from insect wax using $LiAlH_4$. These methods are characterised by the use of substances highly harmful to the environment, requiring high energy expenditure because of the special treatments necessary for the purification of the wastewater generated [18]. On the contrary, the use of immobilised

enzymes in transesterification is considered an ecofriendly process. The enzymatic reaction of transesterification is chemo-, regio-, and stereoselective, as a result of which the products are obtained in high yield and purity, in contrast to chemical hydrolysis, and the method allows the continuous use of the enzyme [19].

Immobilised lipase from the yeast *Candida antarctica*, CAL-B, as well as recombinant lipases expressed in *Aspergillus oryzae* or *Aspergillus niger*, have been reported as efficient catalysts to perform hydrolysis and esterification in organic solvents [20]. Enzyme activity depends on different factors, such as the support type or immobilisation system maintaining the active conformation of the enzyme; other factors include the interaction between the enzyme and substrate, water content, substrate molecular size, amount of organic solvent, and support pore diameter [21, 22].

The water content is essential for the enzymatic reaction to be carried out; an excess affects the conversion rate, so it must be determined specifically for each reaction system [23, 24]. Molecular sieves have been used to control the humidity in the reaction system; however, if the lipases are immobilised on a hydrophilic support, the molecular sieves do not have an impact on the performance of the products [25]. The disadvantage of removing water and using an organic solvent is that the activity of the enzyme is greatly reduced and the reaction time is increased [26].

In this work, chemical and enzymatic transesterification reactions for obtaining policosanol from waxy waste of cochineal insects generated in the carmine industry were compared. First, in chemical reactions, different bases and solvents were evaluated; then, during transesterification, the use of molecular sieves, two lipases, and the effect on the reaction product yields of different alcohols as acyl receptors were analysed.

2. Materials and Methods

2.1. Raw Materials and Conditioning. The materials were provided by Campo Carmín S.P.R. of R.L., located in Morelos, México. Samples of waxy residues corresponding to adult cochineals were collected according to the periods of infestation and crop harvest, which was approximately 90 days after infestation. Lumps, particles, remaining insects, and other impurities were manually removed from the samples. After that, the screening of samples was performed with an electric sieve (Rotate, model RX-2) with mesh sizes 40–100, for 20 min. The finest fraction corresponding to cochineal wax (particles < 0.149 mm) was collected to determine the effectiveness of different policosanol extraction methods. The clean waxy residues were stored at room temperature for further processing.

2.2. Chemical Hydrolysis. Three methods of alkaline hydrolysis were evaluated to investigate their effectiveness in extracting policosanol from waxy residues of cochineal, based on the work performed by Magraner et al. [14] and by Jia and Zhao [15]. Each extraction was run in triplicate.

Method A. Hydrolysis in water by extraction with chloroform. One gram of cochineal wax residue was hydrolysed in 100 ml of NaOH (20% w/v) by stirring for 4 h at 90°C. The mixture was cooled and filtered, and the mud cake separated was extracted with chloroform in a Soxhlet system for 6 h. Finally, the extract was cooled, evaporated at atmospheric pressure, and dried completely in a desiccator with anhydrous sodium sulphate.

Method B. Hydrolysis in alcohol by extraction with ethyl acetate. One gram of cochineal wax residue was hydrolysed in a 100 ml solution of 5 g of KOH diluted in ethanol (25%). The hydrolysis was carried out by stirring for 4 h at 90°C. The mixture was cooled and filtered, and the mud cake separated was extracted with ethyl acetate in a Soxhlet system for 6 h. Finally, the extract was cooled, evaporated at atmospheric pressure, and dried completely in a desiccator with anhydrous sodium sulphate.

Method C. Hydrolysis in water by extraction with hexane. One gram of cochineal wax residue was hydrolysed in 100 ml of NaOH (12% w/v) and the mixture vigorously stirred on a heating plate for 4 h at 90°C. The mixture was cooled and filtered, and the mud cake separated was extracted with hexane in a Soxhlet system for 6 h. Finally, the extract was cooled and evaporated at atmospheric pressure and dried completely in a desiccator with anhydrous sodium sulphate.

2.3. Enzymatic Transesterification Reaction

2.3.1. Wax Purification and Crystallisation. To carry out enzymatic transesterification reactions, the clean waxy residue was purified in a Soxhlet system with cyclohexane for 4 h, followed by extraction with methanol and acetone. The fraction soluble in cyclohexane, corresponding to the wax, was filtered and crystallised, and the fractions soluble in methanol and acetone dried at room temperature. Each resulting powder fraction and the purified wax were characterised by GC-MS.

2.3.2. Enzymatic Transesterification Conditions. Two lipases from *C. antarctica* were used for enzymatic transesterification: CAL-B*o* recombinant from *A. orizae* immobilised on Immobead 150 and CAL-B*n* recombinant expressed in *A. Niger* immobilised on acrylic resin, both from Sigma-Aldrich (México).

Solubility tests were carried out, and toluene was chosen as a good solvent for the wax; this is classified as a type yellow solvent, compared to chloroform, the most common solvent to dissolve policosanol, which is classified as red [27].

The transesterification reaction was carried out as follows: The reaction was performed at 60°C, and 100 mg of enzyme per gram of purified wax was added and dissolved in 5 ml of toluene as a reaction medium; to the mixture was added 250 μl of different alcohols as acyl receptors (propanol, butanol, isopropanol, and terbutanol). Molecular sieves of 3 Å and 4 Å were incorporated in the mix to decrease the negative effect of water on the reaction. This

experiment was realised with continuous orbital stirring or sonication for 2 h for comparison.

The transesterification reactions assisted by sonication were carried out in an ultrasonic bath (Branson, model 1–291) which had a 60 min mechanical timer, a 40 kHz transducer, and heating to 60°C.

2.4. Characterisation and Quantification

2.4.1. FTIR Analysis. The policosanol obtained by chemical hydrolysis and triacontanol standard alcohol was analysed using Fourier transform infrared (FTIR) spectroscopy. A Bruker Vertex 70 FTIR spectrometer with Opus Quant® software (version 6.5) was used to obtain characteristic spectra. The technique of attenuated total reflectance (ATR) was used, with 120 scans per sample and 60 scans for the baseline at 4 cm^{-1} resolution, in a wavenumber range of 400–4000 cm^{-1}.

2.4.2. GC-MS. The characterisation of fractions and the policosanol obtained was carried out with a gas chromatograph (Agilent Technologies Automatic Injector 7890a) coupled to a mass spectrometer (Agilent Technologies 5975C Inert MSD with Triple-Aixs detector). Samples and standards were prepared in chloroform (Cromasol V. Plus, 99.9%, HPLC grade), derivatised with 100 μL of a silanising agent (MSTFA) and heated to 60°C for 15 min [5]. The peaks obtained were characterized, and identification of the long-chain alcohols was carried out by comparison with the mass spectral library [28].

The yield of triacontanol obtained was determined from the mass spectra collected with GC-MS. A standard curve method was adopted to guarantee reliable results. The abundance of the fragment ions, m/z, was taken into account to identify and quantify the triacontanol; the resulting fragment ions were 495, 479, 125.103, 83, and 75.

2.4.3. HPTLC. The enzymatic transesterification reactions were monitored at different times by applying extracts diluted in chloroform in duplicate to chromatographic plates of silica 60 F254 on glass support, incorporating a developer for UV light (CAMAG). A CAMAG-brand HPTLC equipment model I15020060200-0001-2013 was used, integrated with LINOMAT5, ADC2, and VISUALIZER.

Different solvent systems were tested, and a hexane/diethyl ether/acetic acid 85 : 15 : 2 (v/v/v) system was chosen to achieve a optimum separation. Triacontanol standard (Sigma-Aldrich México) was applied for comparison of Rf.

3. Results and Discussion

3.1. Chemical Hydrolysis. FTIR signals allowed monitoring of the hydrolysis reaction, so that it was also possible to distinguish changes in band patterns between the raw material and the policosanol obtained. The most significant changes related to the disappearance of the 1731 cm^{-1} signal, which indicated the rupture of the ester groups (COO^-) and the increase in the 1704 cm^{-1} band, signifying the presence of acid group (–COOH) (Figure 1(a)). Acids and long-chain alcohols are products of the hydrolysis reaction, so changes in these signals indicate good hydrolysis efficiency.

The FTIR spectra of the policosanol extracts were compared with triacontanol standard (Figure 1(b)). The triacontanol standard showed characteristic bands at 3294 (OH bond), 2916 (–CH links), 1461 (C–OH primary alcohol bonds), 1062 (–CO), and 729 cm^{-1}, which is indicative of the presence of at least four methylene groups ($-CH_2-$). The signals found were similar in all extracts and are consistent with those found in the characterisation of the policosanol obtained from *Agave furcroydes* L. wax [3].

However, the FTIR analysis did not allow characterisation and quantification of the policosanol obtained, so we resorted to analysis by GC-MS. The results obtained showed that triacontanol was the major long-chain alcohol present in these extracts, and unquantifiable octacosanol and hexacosanol traces were detected. Hydrolysis by method A resulted in the highest yield of policosanol 134.00 ± 16.58 g/kg of cochineal wax, compared to methods B (49.95 ± 14.21 g/kg) and C (14.25 ± 4.31 g/kg), although method A had the lowest purity (29%) (Table 1). The chloroform used in method A is a solvent commonly used to dissolve policosanol in chromatographic analysis [5, 29], and it also improves extraction, but is not very selective. On the contrary, the hexane used in method C, with polarity index of 0.1 compared to chloroform (4.1) and ethyl acetate (4.4), could be more selective for policosanol. Triacontanol is a nonpolar alcohol due to its long-chain structure of 30 carbons, and so could be more related to hexane. Notwithstanding, hexane was not sufficiently selective, so policosanol of 65% purity was obtained (Table 1). To obtain a high yield of policosanol and higher purity, this method could be complemented with extractions by solvents of different polarities. In the following experiments, methanol and acetone were tested for wax purification and showed good selectivity for long-chain alcohols.

3.2. Enzymatic Transesterification

3.2.1. Chemical Purification. For the enzymatic reaction, the finest fraction (particles < 0.149 mm) of the total cochineal wax residue was subjected to chemical purification to obtain pure wax with a yield of 28%. During wax purification, it was observed that fractions soluble in methanol and acetone contained long-chain alcohols, in comparison to the purified wax, as can be seen in the HPTLC plate shown in Figure 2. This means that methanol and acetone extractions were effective in the separation or extraction of long-chain alcohols. By characterising these fractions by GC-MS, we can conclude that the methanolic fraction composition was as follows: octacosanol, triacontanol, untriacontanol, dotriacontanol, and tritriacontanol, and the fraction obtained from acetone was found to be composed only of triacontanol (Figure 2).

3.2.2. Enzymatic Transesterification Reaction under Sonication. Once the wax was purified, it was used for the

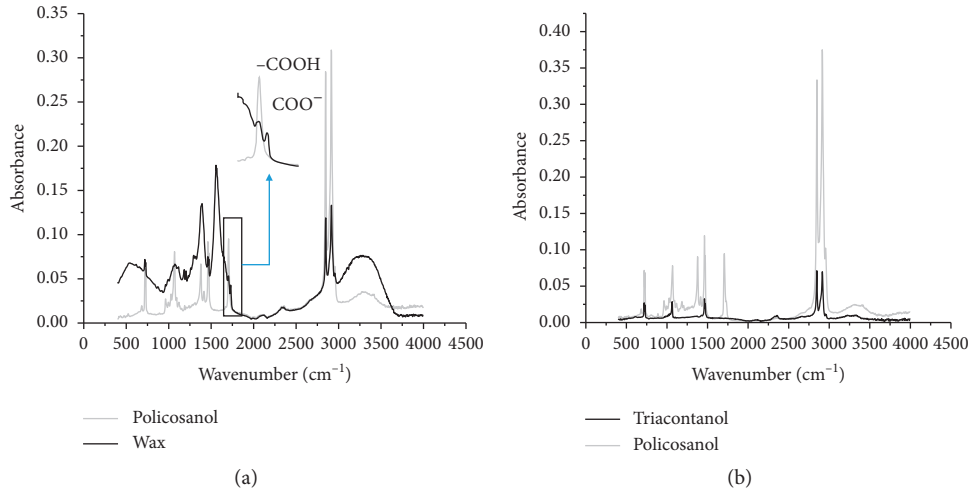

Figure 1: FTIR spectra of (a) policosanol and cochineal wax and (b) policosanol and triacontanol standard.

Table 1: Composition and quantification of policosanol in g/kg of cochineal wax obtained by chemical hydrolysis methods.

	Policosanol composition			Policosanol yield (%)	Policosanol purity (%)
	Triacontanol	Octacosanol	Hexacosanol		
Method A	134.00 ± 16.58^{a}	Traces	Traces	47	29.0
Method B	49.95 ± 14.21^{b}	Traces	Traces	10	51.0
Method C	14.25 ± 4.31^{c}	Traces	Traces	2	69.0

(Tukey $P < 0.05$).

evaluation of two enzymes in the transesterification reaction under sonication: lipase *C. antarctica* recombinant in *A. orizae* (CAL-B*o*) and lipase *C. antarctica* recombinant in *A. niger* (CAL-B*n*). The results obtained by HPTLC showed that CAL-B*o* showed no catalytic activity in any of the combinations of organic solvents, possibly due to the immobilisation support to which the enzyme was attached. Lipase *Candida* CAL-B*o* is immobilised in support Immobead 150, which is formed of methacrylate copolymers with epoxy functions, with an average particle size of 150–300 μm and presents a wide pore size range, with pores in the micropore and mesopore region [30]. In contrast, CAL-B*n* is immobilised on a macroporous acrylic poly resin (methyl methacrylate-*co*-divinylbenzene), having an average particle size of 315–1000 μm and a pore diameter of ~150 Å [31, 32]. Both supports show hydrophobic properties; however, the pore size of the enzyme CAL-B*o* (12–20 Å) is smaller than that of CAL-B*n* (~150 Å) and the pore size distribution is not homogeneous [30]. This characteristic is determinant for the enzyme-substrate coupling; a small pore size or inhomogeneous pore size allows only the smallest substrates to penetrate. The bigger substrates would clog the channels, resulting in a weaker affinity of the enzyme for the substrate by diffusion limitation in small pores [33, 34].

It has already been shown that the lipase enzyme of *C. antarctica* has good catalytic activity with toluene as a reaction medium at 60°C [32], and the use of alcohols as acyl receptors in the transesterification reaction has been proposed because they have a less negative effect on lipase stability [35]; nevertheless, more polar alcohols, such as methanol, change the polarity of the medium, decreasing the stability of the enzyme, while high concentration can lead to serious inactivation of the enzyme [35, 36].

It has been reported that the use of terbutanol as a cosolvent in enzymatic reactions helps to diminish the negative polar effect of methanol in transesterification reactions and therefore favours reuse of the enzyme [37]. In this case, the use of terbutanol as an acyl receptor did not allow obtaining policosanol, in contrast to butanol and isopropanol, which showed advantages in the enzymatic transesterification reaction and therefore obtaining of policosanol. It was found that lipases show different preferences for primary or secondary alcohols; Nelson et al. [38] found *C. antarctica* was suitable for secondary alcohols such as isopropanol or 2-butanol as acyl receptors, with 80% conversion. Alcohols could be modifying the organic system differently; it is well known that lipases show higher activity in hydrophobic than in hydrophilic solvents due to the three-dimensional structure of the enzyme being affected by the balance between hydrophobic interactions, electrostatic charge interactions, hydrogen bonding, disulphide linkages, and van der Waals forces with organic solvents. Solvents that can penetrate into the active sites of the enzyme can cause unfolding of proteins to occur due to disturbances in these forces [39]. As a result, transesterification reactions in organic solvents are strongly dependent on the polarity of the reaction medium [40]. Alcohol addition modifies the polarity of the organic system and affects solubility; maintaining solubility is essential for the transesterification

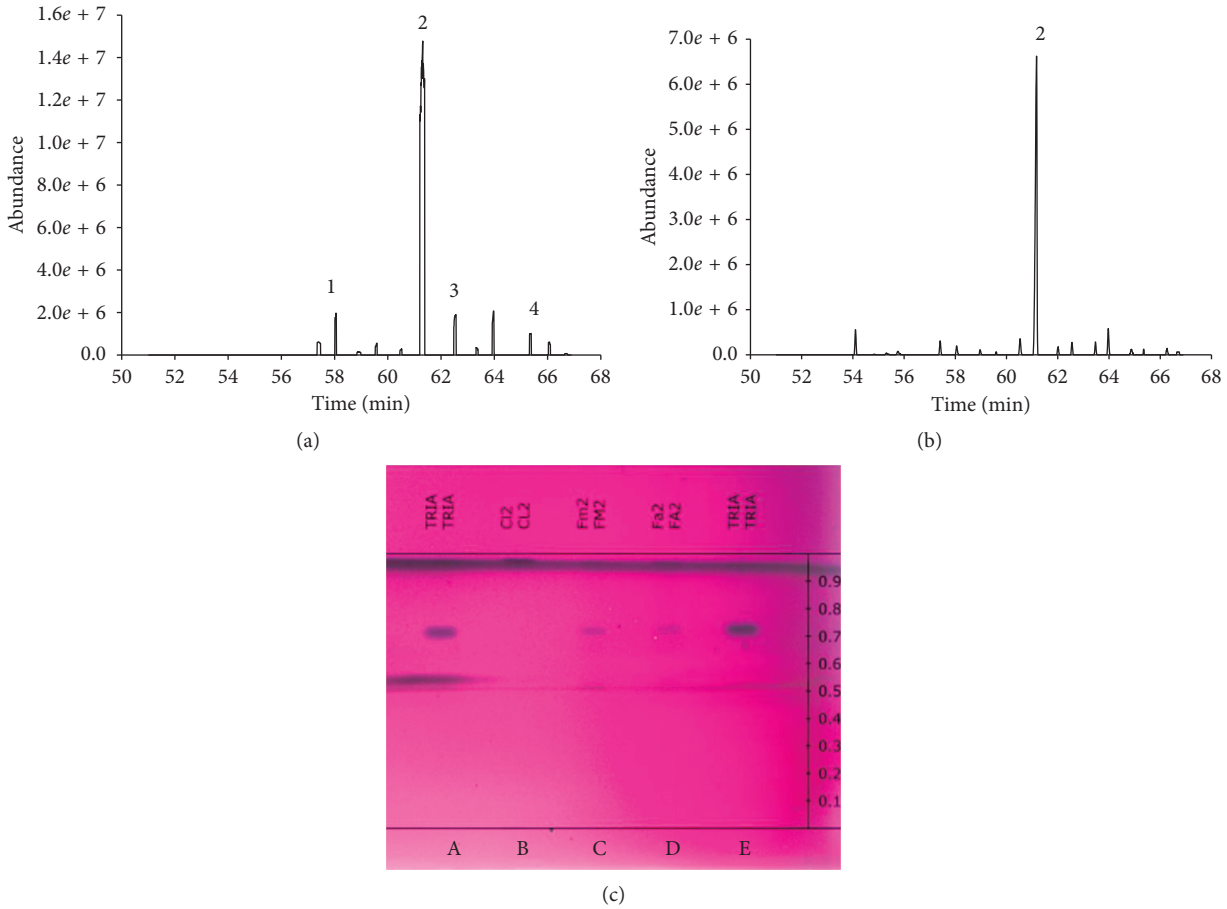

Figure 2: HPTLC chromatoplate: lanes A and E correspond to the triacontanol standard (Rf 0.73); lane B corresponds to the purified wax obtained by extraction with cyclohexane and cleaning with methanol and acetone; lane C is the methanolic fraction; and lane D is the acetonic fraction. Chromatograms of methanolic (a) and acetonic (b) fractions: peaks corresponding to 1, octacosanol; 2, triacontanol; 3, untriacontanol; and 4, tritriacontanol.

reaction to proceed, since it has been observed that inhibition by lower-chain alcohols is often due to alcohol insolubility [41]. Solvents are used to protect the enzyme from denaturation by alcohols by increasing alcohol solubility [41]. In this case, toluene as reaction medium in combination with isopropanol and butanol could improve solubility, favouring transesterification.

Regarding the composition of the policosanol obtained by the different reactions, this depended on the acyl receptor used. When propanol was added to the reaction medium, a policosanol consisting of tritriacontanol and triacontanol was obtained (Figure 3); when isopropanol was added, a policosanol comprising triacontanol, untriacontanol, and tritriacontanol was obtained (Figure 4).

Otherwise, it has been proved that sonication assists transesterification reactions by improving the yield within a shorter reaction time. It is an efficient mixing tool that provides sufficient activation energy to initiate the reaction [42], minimises the molar ratio of alcohol to oil, and reduces energy consumption compared to the conventional mechanical stirring method [43, 44].

A commercial lipase immobilised on acrylic resin, Novozym 435 from *C. Antarctica* lipase, was used as a biocatalyst in the system, and it was found that the enzymatic activity was enhanced with the assistance of low-frequency and mild-energy ultrasonic sound waves. In this case, enzymatic transesterification under sonication was carried out at 40 kHz, a lower frequency. The appearance of the reaction medium did not show good solubility. It was higher when butanol was added, causing problems in characterisation and quantification of the sample. Nevertheless, the activity of the enzyme was not diminished during the 2 h of reaction, as can be seen in the HPTLC plates. Orbital agitation reactions was performance so carry out an adequate quantification of triacontanol content.

3.2.3. Enzymatic Transesterification Reaction under Orbital Agitation. The reaction under orbital agitation (Figure 5) did not proceed as quickly as under sonication (Figures 3 and 4). The appearance of bands with similar Rf (0.53) to the triacontanol in the plates developed under sonication (Figures 3 and 4) can be observed from the first minutes, compared to the plates developed from transesterification reactions under orbital agitation (Figure 5). When propanol was used as the acyl receptor in enzymatic transesterification,

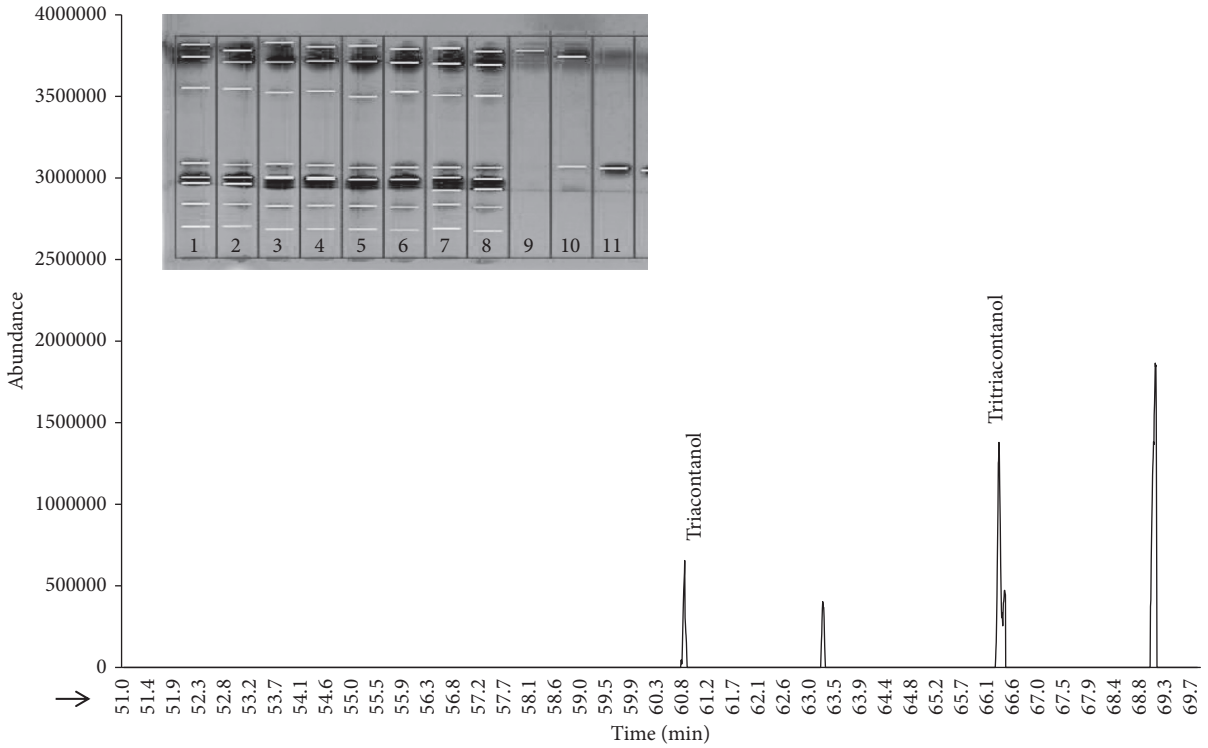

Figure 3: Policosanol composition in toluene medium, using propanol as the acyl receptor, in the enzymatic transesterification under sonication. HPTLC chromatoplate shows products of the reaction over time from lanes 1 to 8; lane 9 is the reaction target without enzyme; lane10 is the purified wax; and lane 11 is the triacontanol standard (30C).

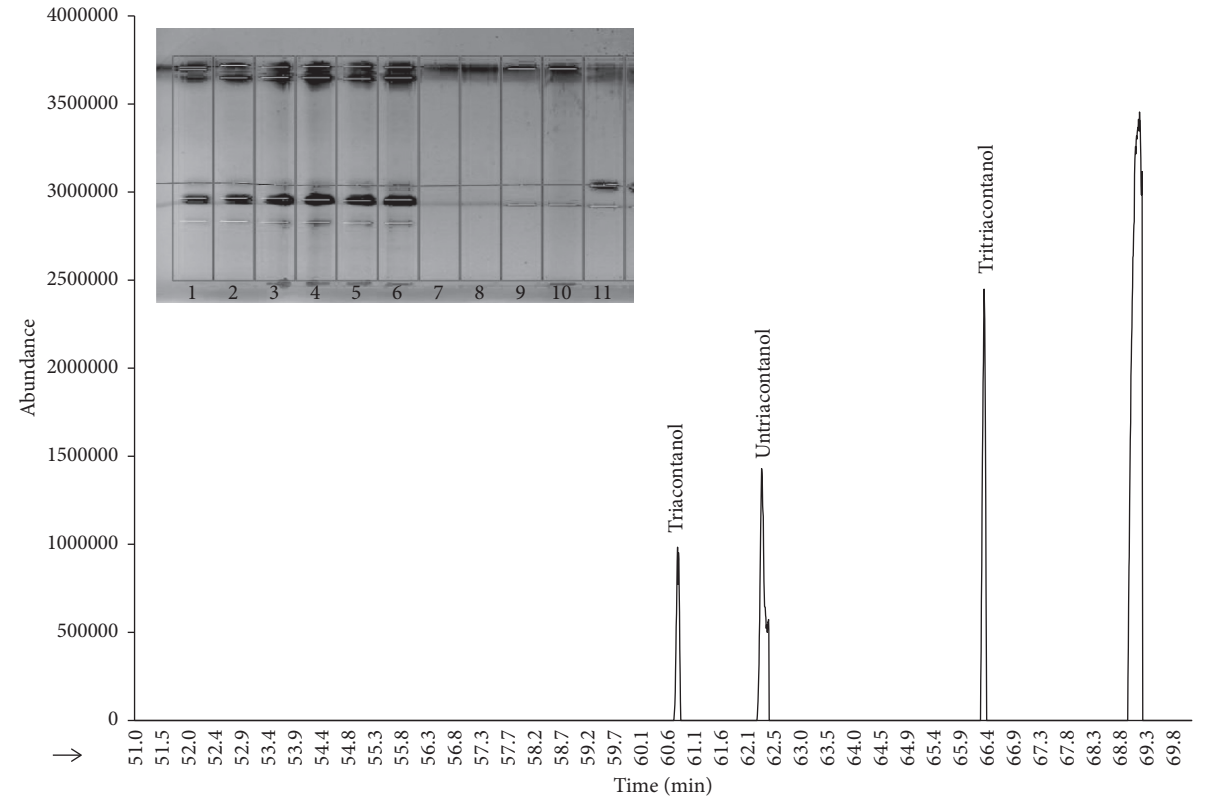

Figure 4: Policosanol composition using isopropanol as acyl receptor in toluene medium from enzymatic transesterification assisted by sonication. HPTLC chromatoplate shows products of the reaction over time from lane 1 to 6; lanes 7 and 8 are the reaction target without enzyme; lanes 9 and 10 are the purified wax; and lane 11 is the triacontanol standard (30C).

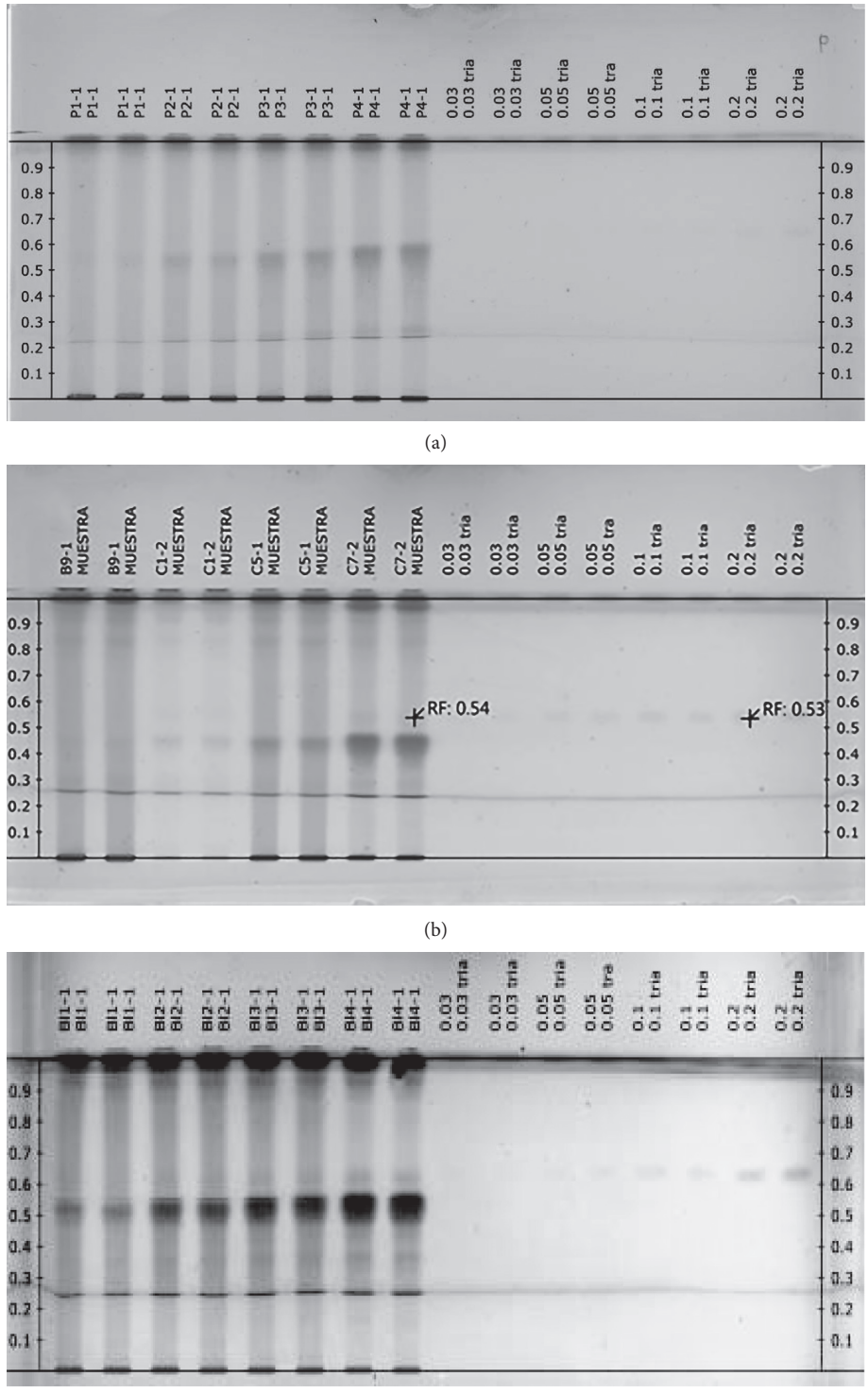

Figure 5: HPTLC chromatoplates. Products of the reaction with (a) propanol, (b) isopropanol, and (c) butanol as acyl receptors and toluene as a reaction medium under orbital agitation.

policosanol was not detected (Figure 5(a)), in comparison to reactions performed under sonication (Figure 3). Policosanol was obtained only after adding isopropanol and butanol as acyl receptors under orbital agitation (Figures 5(b) and 5(c)).

In the quantification carried out by GC-MS, it was possible to establish a relationship of triacontanol content with time. In Figure 6, it can be seen that in the transesterification reaction carried out with butanol as acyl receptor, the highest amount of triacontanol was found after

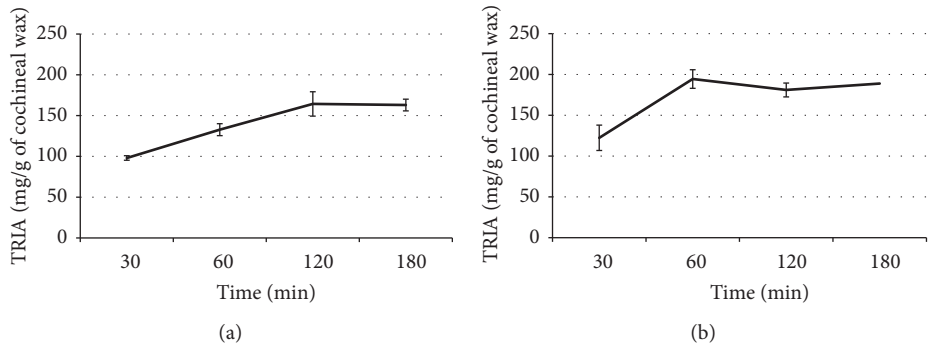

Figure 6: Enzymatic transesterification reaction assisted by orbital agitation with (a) butanol and (b) isopropanol as acyl receptor, in toluene reaction medium.

120 min (164.3 ± 14.9 mg/g of cochineal wax). However, when isopropanol was used as an acyl receptor, the maximum content of triacontanol was found after 60 min (194.4 ± 11.4 mg/g of cochineal wax).

Molecular sieves were used to create a water-free medium, especially in reactions where methanol was used as an acyl receptor, since this alcohol, in high doses, causes inhibition of the reaction. The effect of 3 Å and 4 Å molecular sieves on the enzymatic transesterification for policosanol procurement was analysed, and it was found that the use of molecular sieves had no significant effect on yields of triacontanol in any of the reactions (Figure 7). These results coincide with those of Hsu et al. [25], where the use of molecular sieves had a null effect on enzymes of *T. lanugilosa* and *C. antarctica* immobilised on silica granules; however, the use of molecular sieves favours the reuse of the enzyme in a semicontinuous process [45].

Triacontanol possesses commercial value due to its effect as growth promoter in plants. In this work, policosanol obtained from cochineal wax by both methods—alkaline hydrolysis and enzymatic transesterification—yielded triacontanol. Triacontanol yields in the enzymatic reactions were approximately 19%, compared to chemical hydrolysis, where the highest yields by method A were close to 13%. Although it would be worth conducting technical economic studies to evaluate the cost-benefit of each method, the proposed methods of alkaline hydrolysis do not require the chemical purification of cochineal wax, instead the enzymatic transesterification reactions raised in this work use an enzyme catalogued as a green product (CAL-B*n*), and in addition, solvents catalogued as type yellow are used.

The concentration of triacontanol obtained from cochineal wax is higher compared to that obtained from *Ericerus pela* insect wax, where yields ranged from 1.6 to 2.5% of triacontanol by chemical hydrolysis [15] and 4.9% by a method of solvent-free reduction using $LiAlH_4$ [17]. Other wax sources from agroindustrial waste, such as cuticle and leaves of cane, sesame seeds, and wheat, present triacontanol contents in values of mg per kilogram of wax (<1%) [4–6]. Irmak et al. [5] obtained a policosanol from beeswax, with a content of triacontanol of <1%, and there are reports of up to 200 g/kg of beeswax (20%) [15]. However, the disadvantage of policosanol from these sources is the octacosanol content,

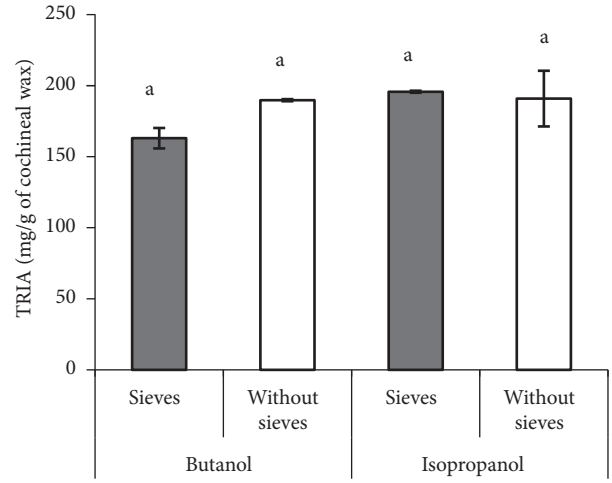

Figure 7: Effect of molecular sieves on triacontanol (TRIA) content obtained in transesterification reactions with butanol and isopropanol as acyl receptors in toluene medium using orbital agitation ($P < 0.05$; Tukey).

which is considered an inhibitor of the growth-promoting effect of triacontanol [46, 47]. Therefore, the use and application of triacontanol from these policosanol sources requires an additional process of purification. Triacontanol from cochineal wax could be applied directly to plants, since it is usually applied in the form of extracts in commercial products.

4. Conclusions

These results show an option to valorise the waste generated by the carmine industry. The policosanol obtained was composed mainly of triacontanol, an alcohol with great commercial value due to its properties as plant growth promoter. Triacontanol yields of up to 13% were attained through chemical hydrolysis and up to 19% by a novel method of enzymatic transesterification. Enzymatic transesterification was carried out with lipase *Candida antarctica* (CAL-B*n*) in a reaction medium with toluene, molecular sieves, and different acyl receptors. This ecofriendly method

can be applied to other wax sources to improve policosanol extraction.

The policosanol obtained presented high yields of triacontanol in relation to the most common sources used for this purpose, with the advantage that cochineal wax is a waste with no profitable application so far.

Data Availability

The data used to support the findings of this study are included within the article.

Conflicts of Interest

The authors declare that they have no conflicts of interest.

Acknowledgments

We acknowledge the Consejo Nacional de Ciencia y Tecnología (CONACyT) and Instituto Politécnico Nacional (IPN) for the scholarships during the course of this investigation and the IPN for financial support for the research. Martínez-Ayala A.L. and Antonio R. Jimenez-Aparicio are fellows of COFAA and EDI-IPN.

References

[1] A. C. Chibnall, A. L. Latner, E. F. Williams, and C. A. Ayre, "The constitution of coccerin," *Biochemical Journal*, vol. 28, no. 1, pp. 313–325, 1934.

[2] C. Hendrickson and D. Merkle, "Method for harvesting cochineal wax from cochineal insects grown on an artificial medium," Patent No. US 20130015397. United States, 2013.

[3] E. Méndez, M. Blanco, A. Laguna, and E. García, "Isolation and characterization of a mixture of higher primary alcohols of high molecular weight from henequen (*Agave furcroydes* L.) wax," *Revista CENIC Ciencias Químicas*, vol. 34, no. 1, pp. 35–38, 2003.

[4] S. Irmak and N. T. Dunford, "Policosanol contents and compositions of wheat varieties," *Journal of Agricultural and Food Chemistry*, vol. 53, no. 14, pp. 5583–5586, 2005.

[5] S. Irmak, N. T. Dunford, and J. Milligan, "Policosanol contents of beeswax, sugar cane and wheat extracts," *Food Chemistry*, vol. 95, no. 2, pp. 312–318, 2006.

[6] P. Adhikari, K. T. Hwang, J. N. Park, and C. K. Kim, "Policosanol content and composition in perilla seeds," *Journal of Agricultural and Food Chemistry*, vol. 54, no. 15, pp. 5359–5362, 2006.

[7] A. O. Cherif, M. Ben Messaouda, B. Kaabi, S. Boukhchina, C. Pepe, and H. Kallel, "Comparison of the concentrations of long-chain alcohols (policosanol) in three Tunisian peanut varieties (*Arachis hypogaea* L.)," *Journal of Agricultural and Food Chemistry*, vol. 58, no. 23, pp. 12143–12148, 2010.

[8] P. Kaewkool and K. Krisnangkura, "Transesterification/acetylation of long chain alcohols with alkyl acetate," *Chemistry and Physics of Lipids*, vol. 163, no. 7, pp. 685–688, 2010.

[9] M. L. Arruzazabala, D. Carbajal, R. Mas, M. Garcia, and V. Fraga, "Effects of policosanol on platelet aggregation in rats," *Thrombosis Research*, vol. 69, no. 3, pp. 321–327, 1993.

[10] D. Carbajal, M. L. Arruzazabala, S. Valdés, and R. Más, "Effect of policosanol on platelet aggregation and serum levels of arachidonic acid metabolites in healthy volunteers," *Prostaglandins, Leukotrienes and Essential Fatty Acids*, vol. 58, no. 1, pp. 61–64, 1998.

[11] R. Menéndez, V. Fraga, A. M. Amor, R. M. Gonzales, and R. Mas, "Oral administration of policosanol inhibits in vitro copper ion-induced rat lipoprotein peroxidation," *Physiology & Behavior*, vol. 67, no. 1, pp. 1–7, 1994.

[12] K. A. Varady, Y. Wang, and P. J. H. Jones, "Role of policosanols in the prevention and treatment of cardiovascular disease," *Nutrition Reviews*, vol. 61, no. 11, pp. 376–383, 2003.

[13] M. Naeem, M. M. A. Khan, and K. Moinuddin, "Triacontanol: a potent plant growth regulator in agriculture," *Journal of Plant Interactions*, vol. 7, no. 2, pp. 129–142, 2012.

[14] H. J. Magraner, G. A. Laguna, F. R. Mas et al., "Natural mixture composed of higher primary aliphatic alcohols obtained from bee wax for the treatment of gastric and duodenal ulcers that also present anti-inflammatory activity," Patent No. US 6235795. United States, 2001.

[15] Q. Jia and J.-F. Zhao, "Polycosanols from *Ericerus pela* wax," Patent No. US 7,034,060 B2. United States, 2006.

[16] M.-F. Wang, H.-Z. Lian, L. Mao et al., "Comparison of various extraction methods for policosanol from rice bran wax and establishment of chromatographic fingerprint of policosanol," *Journal of Agricultural and Food Chemistry*, vol. 55, no. 14, pp. 5552–5558, 2007.

[17] J. Ma, L. Ma, H. Zhang et al., "Policosanol fabrication from insect wax and optimization by response surface methodology," *PLoS One*, vol. 13, no. 5, Article ID e0197343, 2018.

[18] H. Fukuda, A. Kondo, and H. Noda, "Biodiesel fuel production by transesterification of oils," *Journal of Bioscience and Bioengineering*, vol. 92, no. 5, pp. 405–416, 2001.

[19] N. Syakirah and S. Sulaiman, "Overview of catalysts in biodiesel production," *ARPN Journal of Engineering and Applied Sciences*, vol. 11, no. 1, pp. 439–448, 2016.

[20] P. Trodler and J. Pleiss, "Modeling structure and flexibility of Candida Antarctica lipase B in organic solvents," *BMC Structural Biology*, vol. 8, no. 1, p. 9, 2008.

[21] G. S. Nunes and J. L. Marty, "Immobilization of enzymes on electrodes," in *Methods in Biotechnology: Immobilization of Enzymes and Cells*, J. M. Guisán, Ed., pp. 239–251, Humana Press, Totowa, NJ, USA, 2006.

[22] Z. Grosová, M. Rosenberg, and M. Rebroš, "Perspectives and applications of immobilised β-galactosidase in food industry-a review," *Czech Journal of Food Sciences*, vol. 26, no. 1, pp. 1–14, 2008.

[23] G. V. Chowdary and S. G. Prapulla, "The influence of water activity on the lipase catalyzed synthesis of butyl butyrate by transesterification," *Process Biochemistry*, vol. 38, no. 3, pp. 393–397, 2002.

[24] H. Noureddini, X. Gao, and R. S. Philkana, "Immobilized *Pseudomonas cepacia* lipase for biodiesel fuel production from soybean oil," *Bioresource Technology*, vol. 96, no. 7, pp. 769–777, 2005.

[25] A.-F. Hsu, K. Jones, T. A. Foglia, and W. N. Marmer, "Immobilized lipase-catalysed production of alkyl esters of restaurant grease as biodiesel," *Biotechnology and Applied Biochemistry*, vol. 36, no. 3, pp. 181–186, 2002.

[26] A. L. Serdakowski and J. S. Dordick, "Enzyme activation for organic solvents made easy," *Trends in Biotechnology*, vol. 26, no. 1, pp. 48–54, 2008.

[27] F. P. Byrne, S. Jin, G. Paggiola et al., "Tools and techniques for solvent selection: green solvent selection guides," *Sustainable Chemical Processes*, vol. 4, no. 1, p. 7, 2016.

[28] NIST/EPA/NIH, *Mass Spectral Library. Mass Spectral Library with Search Program (Data Version: NIST 05, Software Version 2.0)*, NIST, Gaithersburg, MD, USA, 2000.

[29] N. Srivastava, S. Khatoon, A. K. S. Rawat, V. Rai, and S. Mehrotra, "Chromatographic estimation of *p*-coumaric acid and triacontanol in an ayurvedic root drug patala (*Stereospermum suaveolens* Roxb.)," *Journal of Chromatographic Science*, vol. 47, no. 10, pp. 936–939, 2009.

[30] C. Matte, C. Bordinhão, J. Poppe et al., "Physical-chemical properties of the support Immobead 150 before and after the immobilization process of lipase," *Journal of the Brazilian Chemical Society*, vol. 28, no. 8, pp. 1430–1439, 2017.

[31] B. Chen, J. Hu, E. M. Miller, W. Xie, M. Cai, and R. A. Gross, "Candida antarcticaLipase B chemically immobilized on epoxy-activated micro- and nanobeads: catalysts for polyester synthesis," *Biomacromolecules*, vol. 9, no. 2, pp. 463–471, 2008.

[32] Y. Poojari and S. J. Clarson, "Thermal stability of Candida Antarctica lipase B immobilized on macroporous acrylic resin particles in organic media," *Biocatalysis and Agricultural Biotechnology*, vol. 2, no. 1, pp. 7–11, 2013.

[33] R. Blanco, P. Terreros, M. Fernández, C. Otero, and G. Díaz, "Functionalization of mesoporous silica for lipase immobilization characterization of the support and the catalysts," *Journal of Molecular Catalysis B: Enzymatic*, vol. 30, no. 2, pp. 83–93, 2004.

[34] Y. Li, F. Gao, W. Wei, J.-B. Qu, G.-H. Ma, and W.-Q. Zhou, "Pore size of macroporous polystyrene microspheres affects lipase immobilization," *Journal of Molecular Catalysis B: Enzymatic*, vol. 66, no. 1-2, pp. 182–189, 2010.

[35] N. Ognjanovic, S. Saponjic, D. Bezbradica, and Z. Knezevic, "Lipase-catalyzed biodiesel synthesis with different acyl acceptors," *Acta Periodica Technologica*, vol. 39, pp. 161–169, 2008.

[36] K. Nie, F. Xie, F. Wang, and T. Tan, "Lipase catalyzed methanolysis to produce biodiesel: optimization of the biodiesel production," *Journal of Molecular Catalysis B: Enzymatic*, vol. 43, no. 1–4, pp. 142–147, 2006.

[37] L. Azócar, R. Navia, L. Beroiz, D. Jeison, and G. Ciudad, "Enzymatic biodiesel production kinetics using co-solvent and an anhydrous medium: a strategy to improve lipase performance in a semi-continuous reactor," *New Biotechnology*, vol. 31, no. 5, pp. 422–429, 2014.

[38] L. A. Nelson, T. A. Foglia, and W. N. Marmer, "Lipase-catalyzed production of biodiesel," *Journal of the American Oil Chemists' Society*, vol. 73, no. 9, pp. 1191–1195, 1996.

[39] A. Kumar, K. Dhar, S. S. Kanwar, and P. K. Arora, "Lipase catalysis in organic solvents: advantages and applications," *Biological Procedures Online*, vol. 18, no. 1, p. 2, 2016.

[40] J. Kim, D. S. Clark, and J. S. Dordick, "Intrinsic effects of solvent polarity on enzymic activation energies," *Biotechnology and Bioengineering*, vol. 67, no. 1, pp. 112–116, 2000.

[41] A. Kumari, P. Mahapatra, V. Garlapati, and R. Banerjee, "Enzymatic transesterification of Jatropha oil," *Biotechnology for Biofuels*, vol. 2, no. 1, pp. 1–7, 2009.

[42] A. K. Singh, S. D. Fernando, and R. Hernandez, "Base-catalyzed fast transesterification of soybean oil using ultrasonication," *Energy & Fuels*, vol. 21, no. 2, p. 1161, 2007.

[43] J. Wang, Q. D. Huang, F. H. Huang, J. W. Wang, and Q. J. Huang, "Lipase-catalyzed production of biodiesel from high acid value waste oil using ultrasonic assistant," *Chinese Journal of Biotechnology*, vol. 23, no. 6, pp. 1121–1128, 2007.

[44] A. P. Vyas, J. L. Verma, and N. Subrahmanyam, "Effects of molar ratio, alkali catalyst concentration and temperature on transesterification of jatropha oil with methanol under ultrasonic irradiation," *Advances in Chemical Engineering and Science*, vol. 1, no. 2, pp. 45–50, 2011.

[45] L. Azócar, G. Ciudad, H. J. Heipieper, R. Muñoz, and R. Navia, "Lipase-catalyzed process in an anhydrous medium with enzyme reutilization to produce biodiesel with low acid value," *Journal of Bioscience and Bioengineering*, vol. 112, no. 6, pp. 583–589, 2011.

[46] J. Jones, V. Wert, and S. Ries, "Specificity of 1-triacontanol as a plant growth stimulator and inhibition of its effect by other long-chain compounds," *Planta*, vol. 144, no. 3, pp. 277–282, 1979.

[47] S. K. Ries and V. F. Wert, "Rapid elicitation of second messengers by nanomolar doses of triacontanol and octacosanol," *Planta*, vol. 173, no. 1, pp. 79–87, 1988.

Hindawi
Journal of Chemistry
Volume 2019, Article ID 5376452, 12 pages
https://doi.org/10.1155/2019/5376452

Research Article

Lauric Acid-Modified *Nitraria* Seed Meal Composite as Green Carrier Material for Pesticide Controlled Release

Bo Bai,[1,2,3,4] **Xiaohui Xu**,[2] **Jingjie Hai**,[2] **Na Hu**,[3,4] **Honglun Wang**,[3,4] **and Yourui Suo**[3,4]

[1]*Shaanxi Key Laboratory of Land Consolidation, Xi'an 710054, China*
[2]*Key Laboratory of Subsurface Hydrology and Ecological Effects in Arid Region, Ministry of Education, Chang'an University, Xi'an 710054, China*
[3]*Key Laboratory of Tibetan Medicine Research, Northwest Institute of Plateau Biology, Chinese Academy of Sciences, Xining 810016, China*
[4]*Qinghai Provincial Key Laboratory of Tibetan Medicine Research, Xining 810016, China*

Correspondence should be addressed to Bo Bai; baibochina@163.com

Received 25 October 2018; Revised 5 December 2018; Accepted 31 December 2018; Published 3 February 2019

Guest Editor: Alberto J. López

To alleviate the adverse effects of pesticide residues on the environment, development of a more safe, economical, and reliable usage approach of pesticides is critically urgent. In the present study, a novel pesticide carrier LA-NSM (lauric acid-modified *Nitraria* seed meal) with controlled release property was prepared through grafting esterification of lauric acid onto *Nitraria* seed meal substrates. The structure of the obtained samples was characterized by Fourier-transform infrared spectroscopy, scanning electron microscopy, and contact angle measurements. The results indicated that LA-NSM products had a well-defined hydrophobic surface and irregular holes for efficient loading of pesticide molecules. Deltamethrin (DEL), a representative insoluble pyrethroid insecticide in water, was deliberately selected as the index pesticide to evaluate the loading and releasing efficiency of LA-NSM. The loading capacity of LA-NSM for DEL can reach about 1068 mg/g. pH, humidity of soil, and temperature had a significant influence on controlled release performance of LA-NSM@DEL. Moreover, the releasing kinetics of LA-NSM@DEL composites could be fitted well with the Higuchi model. Overall, the highly hydrophobic property, excellent loading, and controlled release ability of LA-NSM made it a promising candidate in agricultural applications.

1. Introduction

Pesticide residues, caused by conventional usage routes like customarily spraying or mixing them with soil, undoubtedly have received considerable attention in recent years because of their high toxicity to the ecosystem and human health [1, 2]. To solve this problem, some remedial measures, including natural degradation [3], biotreatment [4], ion exchange [5], and electrochemical and physical methods [6], have been proposed. Unfortunately, these treatments are inefficient, time-consuming, or high in cost. In other words, such strategies cannot effectively, economically, and radically mitigate the abovementioned drawbacks [7]. Therefore, the development and design of environmental-friendly and safe usage approaches are becoming extremely urgent for reducing the risk of pesticide residues. Typically, controllable release of agrochemicals from various designed carriers has recently been put forward to replace the traditional treatment methods because of the facile preparation, low initial cost, and ease of operation. These strategies have been verified that they are able to serve as a superior technique for the remediation of environmental problems caused by pesticide residues [8, 9]. Up to date, various materials including clay minerals [10], montmorillonites [11], and starch [12–14] have been suggested to act as the scaffold for the controlled release of pesticides. In contrast, using alternative biomaterials as a vehicle has sparked another particular interest owing to their stable raw-material supply and low cost, renewable nature, nontoxicity, and biodegradable advantages [12, 15].

Nitraria, as an important economic crop belonging to the family Elaeagnaceae, is widely cultivated in East Asia,

North America, East Europe, and other areas in the world. Traditionally, the fruits of *Nitraria* are extensively used in pharmacy, brewing beer, and vinegar production [16]. In contrast, the residues of Nitraria, including seeds, pericarp, and roots, are often disposed as agricultural wastes. The common management options, such as discarding outside, burning, and burying, are harmful to groundwater resources, atmosphere, and the environment [17]. Therefore, effective utilization of discarded *Nitraria* residues still remains a challenge. *Nitraria* seed meals (NSMs) are the by-products of *Nitraria* seeds after oil extraction. Currently, a multitude of NSMs are used to be handled as agricultural wastes, which presents an obvious waste of resources. From the aspect of their microstructures, the residual NSMs are extremely rich in cellulose, oil body, and proteins since most of the oils of *Nitraria* seeds are mainly stored in tiny organelles (0.5–2.0 μm diameter) called oil body (OB) [17]. Hereby, it is inevitable that plenty of OB membranes and cellulosic substances would be left after oil expression. In terms of their chemical components, the oil-body membranes consist of approximately 50% phospholipids, 40% membrane proteins, and about 2–10% glycoproteins [18], which are abundant in various functional groups like acyl, long-chain alkyl, phosphate, carboxyl, and amidogen groups. The hydrophobic groups like long-chain alkyls endow NSMs with partial hydrophobicity and acquire the oily molecules voluntarily by absorptive function [19]. As a result, the NSMs display intrinsic positive sorption capacity for oily substances and consequently can be used as an ideal alternative base material for the fabrication of oleophilic carriers. However, to the best of our knowledge, there is no report on using NSMs as carriers for pesticide delivery.

Deltamethrin (DEL) is a water-fast pyrethroid insecticide that destroys the central nervous system of several insects [20, 21]. DEL pesticide has been extensively applied in the fields of agriculture, home pest control, and disease vector control [22] and achieves more effective insecticidal action compared with the common insecticides like dimethoate [23], carbofuran [24], and fenthion [25]. In practice, DEL is often utilized by spraying on the surface of emblements or mixing with soil into the roots of plants, which have brought about serious environmental issues. Hence, to alleviate the adverse effects of DEL residues on the environment, development of a more safe, economical, and reliable usage of DEL is critically urgent.

In the present study, a novel hydrophobic carrier LA-NSM, modified *Nitraria* seed meals with lauric acid, was fabricated through a facile chemical-surface modification route. The structure, surface wettability, and morphology of the obtained LA-NSM were characterized by Fourier-transform infrared spectroscopy (FT-IR), contact angle measurements (CAM), and scanning electron microscopy (SEM). Moreover, the degree of esterification and the influence of pH, temperature, and soil humidity on the release capacity of LA-NSM@DEL were also studied. Generally, the controlled DEL release of the LA-NSM platform not only enhanced the service efficiency of agrochemicals but also extended the utilization of waste *Nitraria* seeds.

2. Experimental Section

2.1. Materials. NSMs were obtained from the Delingha region (Qinghai, China). Lauric acid (LA) was obtained from Chengdu Kelong Chemical Reagent Factory (Chengdu, China). Deltamethrin (2.5 %) was supplied by Bayer Crop Science Co., Ltd. (Beijing, China). Absolute ethanol, hydrochloric acid (HCl), and sodium hydroxide (NaOH) were provided by Xian Chemical Reagent Corp. (Xian, China). The reagents used in this research were all of analytical grade and were used without further purification. Distilled water was used throughout the work.

2.2. Preparation of LA-NSM. NSMs were modified according to a previous method [26]. Raw waste *Nitraria* seeds were first dried and pulverized to obtain NSMs with suitable size for blending. Next, the pieces were washed with NaOH (2% w/w) as well as distilled water to remove the adhering substances and then dried at 60°C for 1.0 h. After that, 20.0 g of dried NSM powder was suspended in 400 mL of lauric acid solution (1.0 M). The mixture was stirred gently for 6 h at desired temperature (90°C–140°C). Finally, the reaction products were centrifuged, washed with *n*-hexane three times, and dried to yield LA-NSM carriers.

2.3. Characterization. Fourier-transform infrared spectroscopy (FT-IR) was performed using a Perkin Elmer FT-IR System 2000 from 400 to 4000 cm^{-1} range via KBr pellets. Scanning electron microscopy (SEM) images were recorded using a Hitachi S-4800 microscope. The contact angle measurement was evaluated by Dataphysics OCA15 (Germany) equipment at ambient temperature. Liquid droplets (~6 μL) were dropped carefully onto the surface of the products, and the average contact angle was determined by five parallel experiments at different positions on the same samples.

2.4. Determination of the Degree of Esterification. The degree of esterification (DE) was ascertained using the titration method reported by Chiou et al. [27]. Specifically, 1.0 g of LA-NSM was suspended in 50 mL of 75 % ethanol solution. The mixture was kept in a water bath (50°C) for 30 min under stirring, and 30 mL of NaOH solution (0.5 M) was then added to saponify the ester. The reaction was maintained for 72 h with continuous agitation at room temperature. The excess alkali was titrated by 0.5 M HCl using phenolphthalein as the indicator. Reference and duplicate samples were treated in a similar way. The DE was calculated according to the following equation [28, 29]:

$$\mathrm{DE}\,(\%) = \frac{(V_0 - V_n) \times N \times 199 \times 10^{-3} \times 100}{W}, \quad (1)$$

where V_0 and V_n (mL) are the volumes of HCl used to titrate the blank and the sample, respectively. N is the normality of used HCl. W (g) is the weight of the dry sample. 199 is the molecular weight of the lauric acid ester group.

2.5. Loading Capacity of LA-NSM. The loading capacity of LA-NSM was determined by a gravimetric method [30]. A small amount of weighed dried samples (m_0) was immersed into DEL (2.5%) and withdrawn at regular time intervals (t) and weighed (m_t). The loading capacity (q_e, mg·g^{-1}) of LA-NSM was calculated according to the equation [31]:

$$q_e = \frac{m_t - m_0}{m_0} \times 1000, \quad (2)$$

where m_t (g) is the quantity of carriers after loading and m_0 (g) is the initial weight of carriers, respectively.

2.6. Controlled Release Experiments. Controlled release of DEL-loaded LA-NSM was carried out in several 250 mL beakers containing different soils. The soils were employed as a medium to release DEL [32, 33]. The soil humidity and temperature were determined by soil moisture sensors (TRIME-PICO32, Germany). Specifically, 1.0 g LA-NSM@DEL was put into the dissolution medium under stirring (100 rpm). Every 10 min, 2.0 mL of the mixture was collected and assayed spectrophotometrically. After that, the analyzed samples were returned to the system to maintain a constant volume of the surrounding release medium. To verify the effect of pH on the release performance of LA-NSM@DEL, solutions with pH 3–10 were adjusted by dilution with HCl (pH 1.0) or NaOH (pH 13.0). The pH values were accurately measured with a pH meter (PHS-25, China). All experiments were conducted in triplicate, and the results were averaged. The accumulative release was calculated according to the following equation [33]:

$$\text{accumulative release } (\%) = \frac{(W_t)}{W_e} \times 100, \quad (3)$$

where W_e and W_t are the masses of the pesticide entrapped in LA-NSM carriers at the equilibrium state and released from pesticide-loaded LA-NSM at time t during the release process, respectively.

For further exploring the potential mechanism behind the slow release of LA-NSM@DEL, evaluating the release kinetics is particularly necessary. In this section, the experimental data were then fitted to the first-order, Higuchi, and Weibull models.

First order model:

$$\ln(Q_e - Q_t) = k_1 t + L. \quad (4)$$

Higuchi model:

$$\frac{Q_t}{Q_e} = k_2 t^{1/2}, \quad (5)$$

where Q_e and Q_t are the equilibrium loading amount (mg/g) and release amount at any time, respectively. k_1, and k_2 are the rate constants, t is the release time (h), and L is the intercept (mg/g).

3. Results and Discussion

3.1. Formation and Characterization of LA-NSM. The detailed functionalization and fabrication processes of LA-NSM composites are schematically illustrated in Scheme 1. As stated earlier, the surface of NSMs is covered by a number of inborn waxes, oils, and other impurities [19], making it difficult to be directly modified and to graft some new groups. Herein, we proposed a simple alkali-pretreatment method to remove these impurities and make the hydroxyl groups of NSMs exposed [34]. As a result, the surface of the alkali-pretreated NSM was inevitably equipped with abundant –OH groups in comparison with the naked NSM substrates, making the further surface functionalization of the NSM substrate easy to occur. Afterward, the pretreated NSMs were immersed into lauric acid methanol solutions, and the grafting esterification reaction between lauric acid molecules and the NSM substrate occurred, making a lauric acid layer attach to the surface of the NSM substrate tightly and uniformly (denoted here as LA-NSM) [35]. The details of the grafting esterification reaction are as follows: the carboxylic acid groups on two lauric acid molecules were first dehydrated to yield a longer chain anhydride under heating conditions [36] (step 2a). The reactive anhydride subsequently reacted with hydroxyl groups on the NSMs to form an ester linkage [37] (step 2b), resulting in the successful anchoring of the lauric acid layer on the NSM substrate. Owing to the oleophilic groups and hydrophobic active sites of the lauric acid layer, LA-NSM can provided more superior sites for higher loading of DEL molecules (step 3).

Predicting from their structure, the as-prepared LA-NSM with a denser hydrophobic lauric acid coating could be very valuable and notable for the development of biodegradable superabsorbent composites for water holding and sustained release of fertilizers in potential agriculture applications. First, the NSM particles have an outstanding adsorption ability for DEL molecules through a strong hydrogen bond interaction due to their plentiful long-chain alkyls and nonpolar hydrocarbon groups [38] arising from the phospholipid monolayers, membrane proteins, and glycoproteins in the oil-body membranes. What is more, the NSM substrates preserve lots of inherent pores in the oil body after oil extraction [39]. Just like a mini warehouse, these inner pores of the NSM matrix could efficiently improve the loading of the DEL pesticide, and the semipermeable property of tiny organelles in the oil body allows the loaded DEL molecules to slowly release into the environment. Second, the lauric acid molecules used as modifiers are natural and environmentally friendly. They offer a large number of active sites (long-chain alkyls and nonpolar hydrocarbon groups) for binding DEL molecules, which significantly improves the loading performance of the LA-NSM composite. Concurrently, the lauric acid layer was densely anchored on the NSM surface, which resembled a diffusion barrier to weaken the unexpected leakage of the agricultural insecticide, protect the insecticide loaded on the LA-NSM from burst release, and regulate the release behavior to a sustainable release. From these points of view, this intriguing and economical strategy opens up a suitable route to prepare a novel insecticide-loading system with an improved loading capacity and a sustainable release behavior by using the abundance, biodegradability, and renewability traits of the by-products of *Nitraria* seeds.

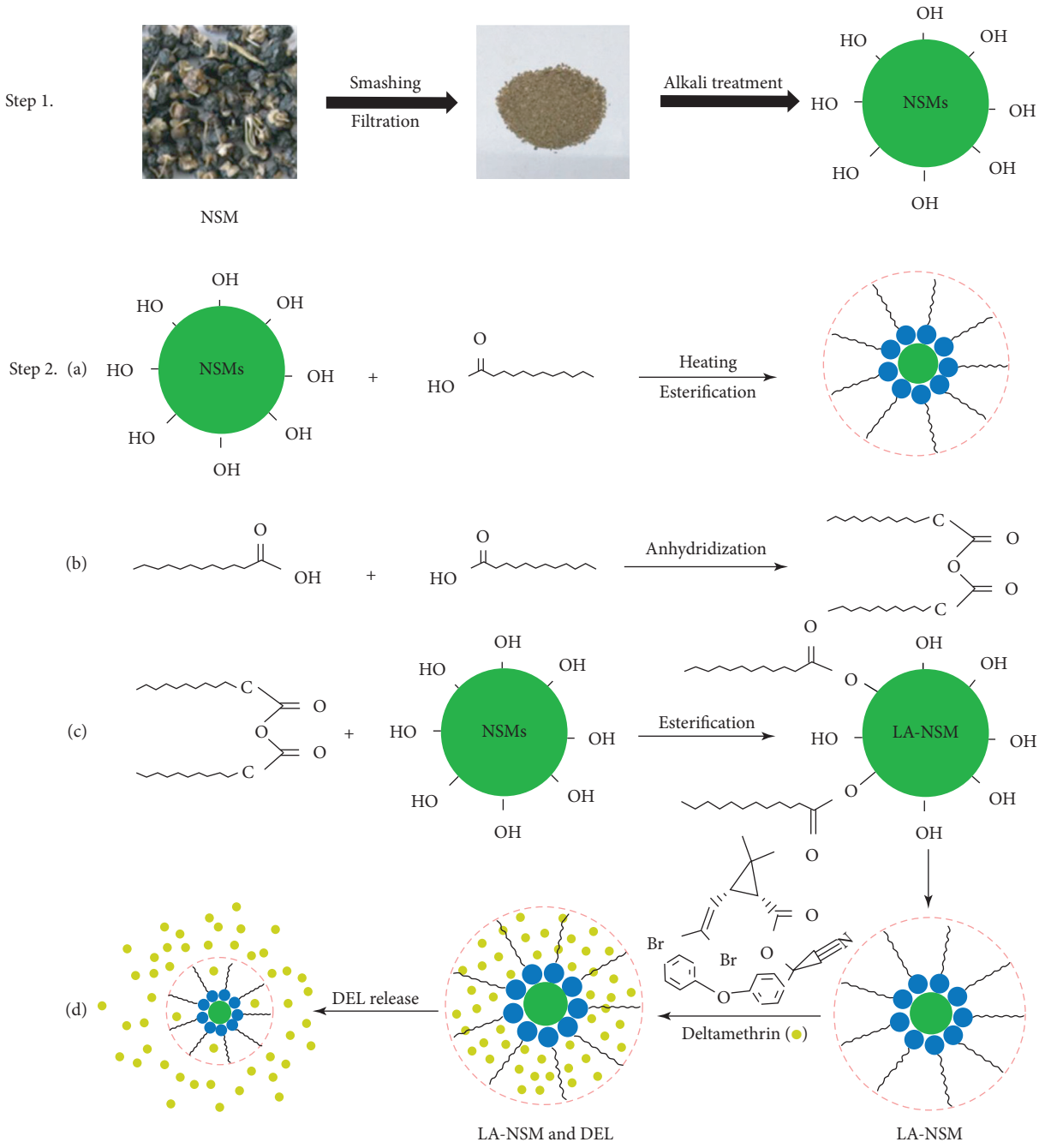

Scheme 1: The formation mechanism of LA-NSM and controlled release of DEL-loaded LA-NSM.

To verify the successful modification of NSMs, FT-IR was employed to monitor the chemical bond transformation of parallel NSMs and LA-NSMs (Figure 1). In Figure 1(a), the absorption peaks observed at 2927 and 2854 cm^{-1} are due to the asymmetric and symmetric methylene groups in lauric acid [40, 41], respectively. The peaks at 1722, 1415, 1313, and 995 cm^{-1} are assigned to C=O stretching vibrations in carboxylic acid groups, CH_2 bending vibrations caused by C=O, C–O in carboxylic acid groups, and ethyl group in alkyl chain, respectively [42–44]. The absorption band near 3440 cm^{-1} in the spectrum of NSMs (Figure 1(b)) is related to the stretching vibrations of the hydroxyl group [45, 46]: 2940 and 1535 cm^{-1} (C–H stretching vibrations in CH_2 and CH_3) [6, 47, 48], 1733 and 1649 cm^{-1} (C=O stretching vibrations in lignin), and 1242 cm^{-1} (ring vibrations in β-1, 4-glycosidic bonds) [49, 50], separately. These peaks belong to the characteristic absorption bands of the NSMs. After modifying NSM with lauric acid, significant changes occur in its FT-IR spectra (Figure 1(c)). For example, the peak at 3440 cm^{-1} shifts to 3300 cm^{-1} and exhibits a slight weaker intensity, proving the participation of hydroxyl groups of NSMs in the modification process. Furthermore, the intensive absorption bands appearing at 1655 and 1242 cm^{-1} were due to the C=O stretching

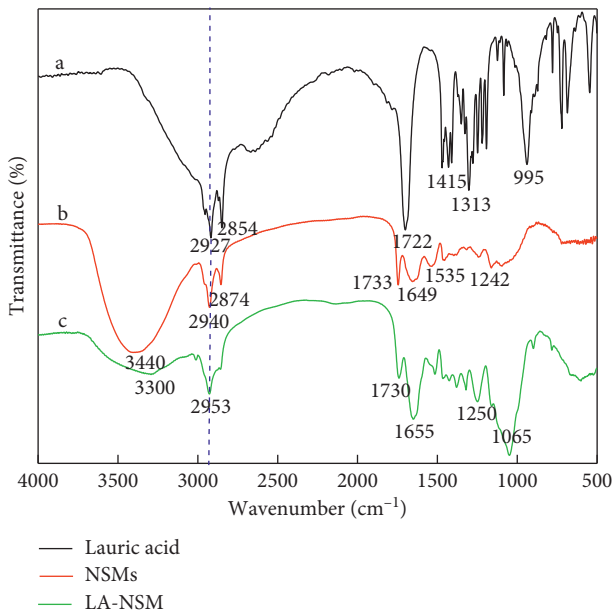

Figure 1: FT-IR spectra of lauric acid (a), NSMs (b), and LA-NSM (c).

vibrations in the ester group, further demonstrating the introduction of additional carbonyl groups onto the NSM surface during the esterification with lauric acid. Besides, a new absorption peak emerges at 1065 cm^{-1}, which corresponds to C–O–C vibrations, further verifying the successful modification of NSMs. On the whole, we conclude that the NSM surface has been successfully modified by lauric acid though reaction between hydroxyl and carboxyl groups, leading to the formation of a dense lauric acid coating outside the NSM surface.

SEM micrographs of the native NSM before and after modification with lauric acid (as illustrated in Figure 3) give further insight into NSM morphology and its modification during the treatment. In Figure 2(a), it was visible that there were lots of wrinkles and abundant pores with diverse diameters on the surface of the native NSM, which contributed to the relatively large specific surface area of the NSM substrate. Such surface morphology with a high surface area and irregular pores endowed the NSM material with abundant DEL-absorbing sites, and this was beneficial for pesticide molecules to penetrate into the internal oil-body structure. The inset image in the top right corner of Figure 2(a) is the optical photograph of the pure WH scaffold, exhibiting a distinct dark coffee-like skin. Furthermore, the light yellow LA-NSM powder in the inset image of Figure 2(b), in comparison with the dark green powder of the pure NSM substrate, provided assertive evidence that the LA layer had spontaneously deposited on the NSM scaffold, thereby leading to an alteration of appearance of color. Such differences of the color with and without modification further indicated that the –COOH groups of lauric acid had reacted with free –OH groups of the NSM matrix via esterification and that a denser lauric acid layer was formed on the surface to adsorb DEL molecules. Nevertheless, as seen from the surface morphology of LA-NSM, the porous structure and the rough surface of the parent NSM scaffold have still been maintained after LA modification, which should favor the adsorption of DEL molecules and enhance their loading capacity [33].

The surface modification of NSMs with lauric acid inevitably also led to a change in the surface wettability. To investigate the surface wettability of LA-NSM, contact angle measurements (CAM) were further performed on the substrate-air interface at ambient temperature, and the results are presented in Figure 3. Figures 3(a) and 3(b) show the images of water droplet (~6 μL) on NSMs and LA-NSM surfaces captured at predetermined time intervals. The contact angles of the water droplets placed on the surfaces of NSMs and LA-NSM are $120 \pm 2^{\circ}$ and $142 \pm 2^{\circ}$, respectively. After 6 s, the water drop sinks rapidly into the NSMs. But, the water droplet on the LA-NSM surface still maintains a larger contact angle of $104 \pm 2^{\circ}$ after 60 s, definitely indicating the low energy and hydrophobicity of the LA-NSM surface [51]. In contrast, a drop of ethyl acetate (~6 μL) can quickly spread over the LA-NSM surface and permeate thoroughly in less than 0.5 s (Figure 3(c)) [52]. Meanwhile, the contact angle of ethyl acetate is measured to be 0°, indicating the excellent lipophilicity of LA-NSM. This phenomenon can be attributed to the smaller surface tension of ethyl acetate (26.29 mN/m) in comparison with water (72.75 mN/m). Theoretically, when the surface tension of the substrate lies between water and oil, hydrophobicity and oleophilicity can be achieved [53]. Consequently, the synthesized LA-NSM carriers modified with lauric acid hold a highly hydrophobic and oleophilic property.

The esterification degree (DE) was the percentage of the reacted carboxyl groups relative to the total initial carboxyl groups of lauric acid, which can be determined by a titration method. We have ascertained that the loading of LA-NSM for DEL could be accurately controlled by the esterification degree (DE) between the hydroxyl groups in NSMs and carboxyl groups in lauric acid. Specifically, the degree of esterification can be adjusted by changing the reaction temperature on purpose, and the experimental results are shown in Figure 4.

It can be seen form Figure 4 (left axis) that the DE increases with increasing the temperature from 90°C to 110°C. The cause lies in that a high temperature provides a stronger driving force to the modification and cross-linking between NSMs and lauric acid. Nevertheless, as the temperature goes higher than 110°C, the DE between the hydroxyl group on NSMs and carboxyl groups of lauric acid exhibits a decreasing trend. This can be ascribed to that too higher temperatures produce a crucial restraining effect on the exothermal esterification [54], resulting in a lower DE. Due to the difference of the DE value of LA-NSM prepared at various temperatures, the LA-NSM showed different loading performances for DEL. Thus, the DEL-loading capacity at various temperatures was investigated. As depicted in Figure 4 (right axis), an increasing number of DEL molecules were loaded into the LA-NSM carriers with the temperature increasing from 90°C to 110°C, but an abrupt decrease occurs when the synthesis temperature goes higher from 110°C to 140°C. This decrease can be attributed to the decreasing DE between the hydroxyl group of NSMs and carboxyl groups of lauric acid. Considering its exothermic feature, esterification reaction can be promoted by increasing the reaction

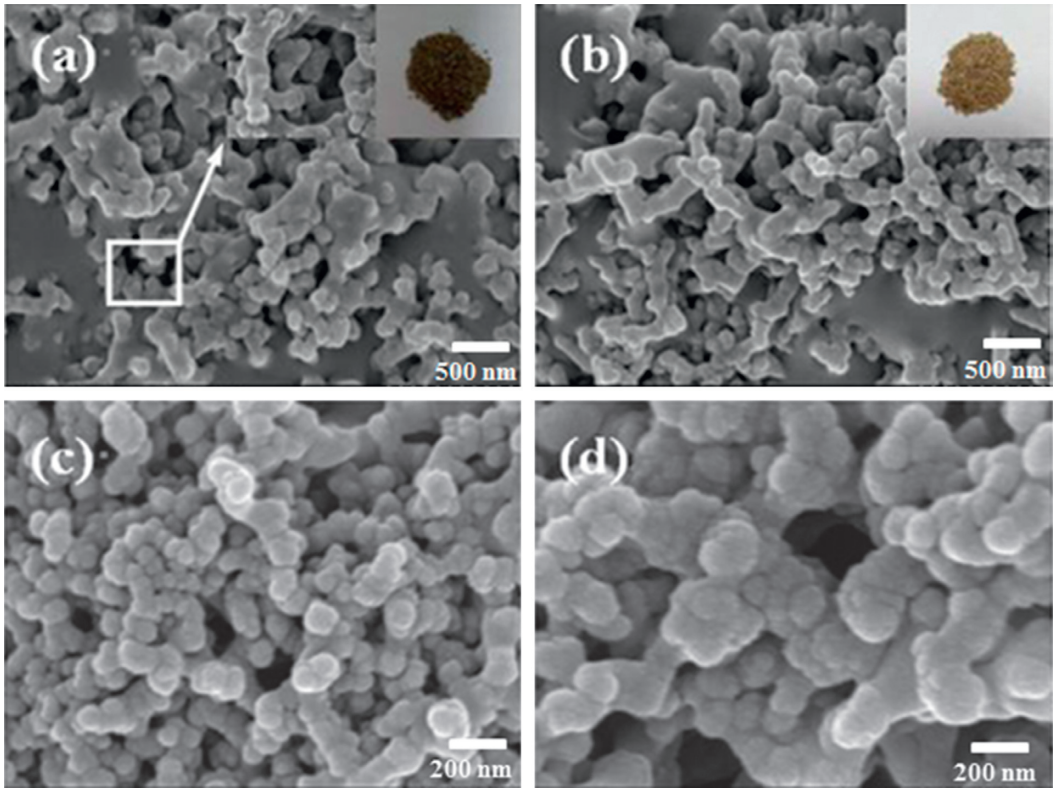

Figure 2: SEM images of NSM (a) and LA-NSM (b–d).

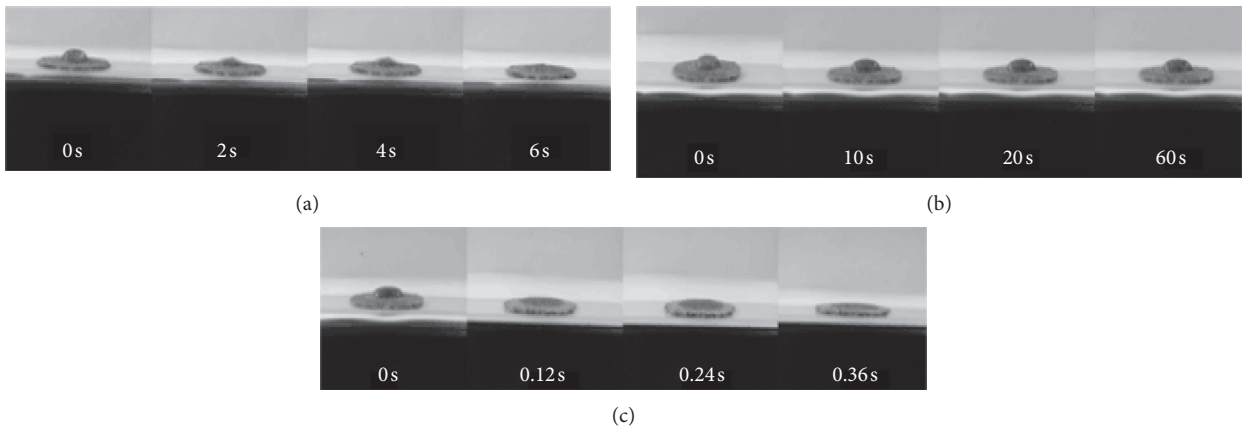

Figure 3: The images of a water droplet placed on NSMs (a) and water drop (b) and ethyl acetate (c) on LA-NSM.

temperature. But, too high temperatures may exert an intense restraining effect on the esterification, resulting in a lower degree of esterification [55]. Correspondingly, the loading amount of LA-NSM for DEL decreases.

3.2. Controlled Release Performance of the DEL Pesticide. DEL is one of the most widely used pesticides in agriculture. Unfortunately, approximately only 30–60% of DEL pesticides can be absorbed into plant bodies by spraying on the emblement surface or mixing with soil [22]. A vast majority of DEL molecules evaporate into atmosphere and get into groundwater and other botanic interiors. Therefore, to find an environmental-friendly and safe usage approach is extremely urgent for reducing the risk of DEL pesticide residues. Thus, the controlled release of DEL was proposed in the succeeding section. It is believed that such tactics through a controlled release approach not only can alleviate the adverse effects of DEL residues on the environment strongly but also can promote the assimilation of DEL

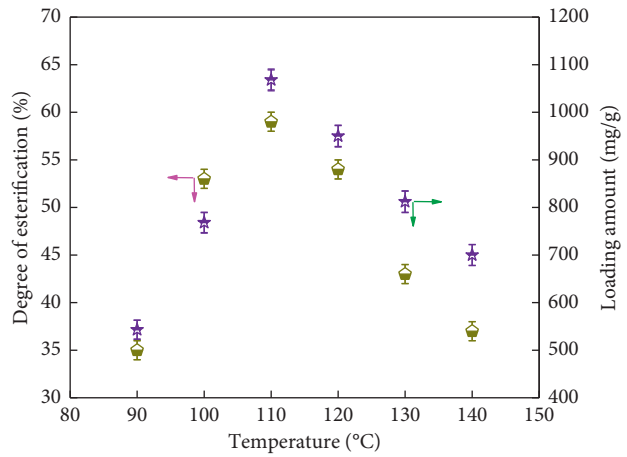

Figure 4: The effect of temperature on degree of esterification and loading amount of DEL.

pesticides by plants effectively [8, 9]. More importantly, the release behavior of DEL pesticides can be controlled by adjusting the environmental factors. Typically, the influence of pH, temperature, and soil humidity on controlled release of LA-NSM@DEL composites was evaluated.

3.2.1. pH-Dependent DEL Release. For pesticide delivery systems, the level of acidity or alkalinity of soil, which could have an impact on the degree of speciation of pesticide carriers, is one of the most significant factors influencing the whole release process. Thus, the effects of soil pH on the release behavior of NSMs and LA-NSM carriers were studied, as shown in Figure 5.

As seen in Figure 5, for NSMs without LA modification, an obvious burst release phenomenon was observed, and more than 80% of DEL diffuses quickly into the surrounding medium within 24 h. In contrast, the release amount of DEL from the LA-NSM@DEL was less than 12% within the same time under the same condition. The different release behaviors could be ascribed to the hydrophobic groups and diffusion barrier formed by lauric acid on the surface of LA-NSM particles. The intensive lauric acid layer could efficiently set up a barrier on the pathway of DEL diffusion from inside the LA-NSM@DEL to the soil, which could effectively reduce the diffusion rate and protect DEL molecules from unexpected leakage or burst release. Moreover, the release of DEL could be dramatically increased by adjusting pH values. For example, changing the acidification of soils from pH 8.5 to pH 6.0 and 3.8 gave rise to an increased release for DEL to 37.5% and 85.2%, respectively. The variation may be attributed to the degree of esterification on the LA-NSM surface. In theory, most ester groups fixed on the structure of LA-NSM carriers could combine with hydrogen ions (H^+) in strong acidic media ($3 < pH < 6$) to form hydrophilic carboxyl groups (–COOH) [56], decreasing the oleophilic and hydrophobic action. Thus, the attraction between the LA-NSM and DEL molecules would be weakened [15], strongly facilitating the DEL molecules to quickly diffuse into the surrounding medium. When the pH was higher ($pH > 6$), the carboxyl groups were deprotonated under alkaline conditions and a limited amount of DEL molecules was released from the LA-NSM composites. The higher the pH value of the incubation medium, the higher the number of carboxyl groups which were deprotonated, but the strong hydrogen bonds between the LA-NSM and DEL molecules would dominate the release efficiency, which largely restricted the release of DEL molecules into the external media. Therefore, the LA-NSM composites gave a major push to sustained release due to the pH-responsive property of carbonyl and ester groups [56], and the release behavior could be easily managed via controlling the environment pH values.

3.3. Temperature-Dependent DEL Release. The release profiles of DEL were exploited at various temperatures (10°C, 20°C, and 30°C) to evaluate the temperature stimuli responsiveness of the pesticide-loaded carrier. As we can see from Figure 6, the curves for the NSM@DEL without LA modification exhibited a classical cumulative release mode consisting of three stages, including an initial burst release (more than 77.4% at 10°C) followed by a slow release and a plateau in the range of temperature from 20°C to 30°C. In comparison, the DEL release from LA-NSM@DEL is dependent on the temperature of the surrounding environment. The release rate of DEL initially increased from ~13.5% at 10°C to ~40% at 20°C and then, a further increase in temperature from 20°C to 30°C caused a sharp increase in DEL release efficiency. This suggests that the DEL escape from LA-NSM@DEL is favored at higher temperatures within the appropriate temperature range and the release process is endothermic in nature. The causes of temperature-dependent release behavior lied in that, at lower temperatures, kinetic energy of the solid-liquid interface was relatively low and DEL molecules could not get enough driving force to quickly escape from the LA-NSM@DEL carriers, leading to a mild release of DEL. Also, the superoleophilic surface of LA-NSM acted as a positive diffusion barrier and suppressed the diffusion of DEL into the external medium. As the temperature increased, the mobility of DEL molecules is significantly enhanced and more energy was imparted into the system. Thus, the link between the DEL molecules and the hydrophobic groups in the LA-NSM composites was easy to break at higher temperatures, facilitating the DEL molecules to quickly diffuse into the surrounding medium [57]. It should be noted that the slow-release efficiency cannot reach 100% since some DEL molecules might be trapped in the pores of LA-NSM, and these remaining pesticides will be fully released with the continuous degradation of NSM matrices.

3.3.1. Soil Humidity-Dependent DEL Release. In addition to the temperature-sensitive property, the releasing capability of LA-NSM@DEL was also dependent on the soil humidity. To further confirm its soil humidity-sensitive property to trigger the DEL release, LA-NSM@DEL was immerged into soils of different humidity, and the results are depicted in Figure 7.

As can be perceived, at the initial stage, the releasing efficiency of NSMs@DEL presented a dramatic increase and up to 57.3% within 24 h, while the amount of DEL from LA-NSM was essentially negligible (~10% within 24 h). The reason

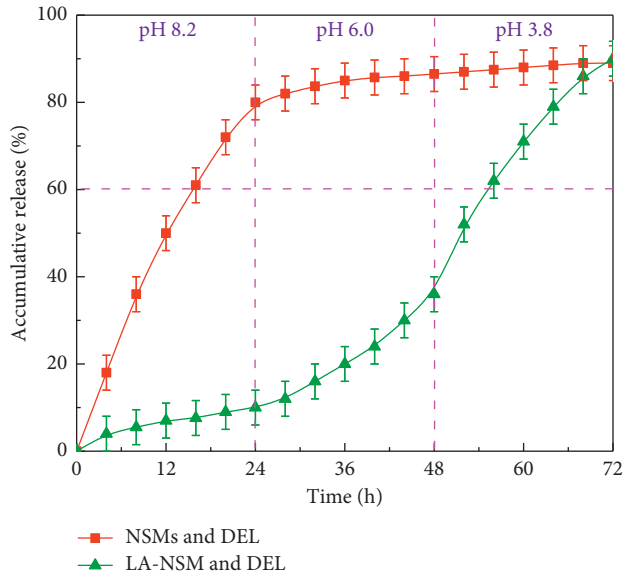

Figure 5: DEL-release profiles from LA-NSM and NSMs at different pH values in soils.

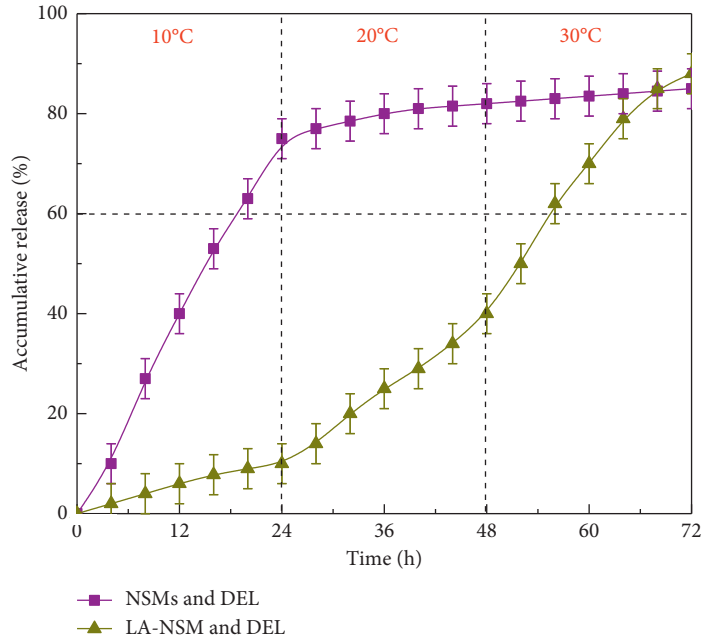

Figure 6: DEL release profiles from LA-NSM and NSMs at different temperatures in soils.

for this phenomenon was that the superhydrophobic surface on the LA-NSM carrier can indeed act as a diffusion barrier during the molecular diffusion between the LA-NSM domains and the soil environment. The superhydrophobic barriers will separate the internal domain of LA-NSM and the external soil environment, terminating transport of most of the molecules across the boundaries of the LA-NSM and thus significantly suppressing the diffusion rate of the DEL molecules. Nevertheless, NSMs would fail in preventing DEL molecules' diffusion at the beginning because of the weaker hydrophobicity of pristine-NSM surfaces, leading to a burst increase of releasing efficiency, up to 57.3% within 24 h. With the decrease of humidity, the amount of water molecules in the soil decreased, which could enhance the difference of osmotic pressure between the carrier interior and surrounding media, consequently expediting the release of DEL from LA-NSM. In contrast, there was a slight increase for NSMs@DEL, and it was attributed to the decrease of DEL entrapped inside the NSMs. It could be inferred hereby that the LA-NSM could be a valuable pesticide manager to efficaciously slow down the release of the pesticide into soil for plants and avoid excessive pesticide consumption in agriculture application.

3.3.2. Release Kinetics of DEL Pesticides through LA-NSM. Figure 8 shows the release profiles of DEL from LA-NSM@DEL with different esterification temperatures from 90°C to

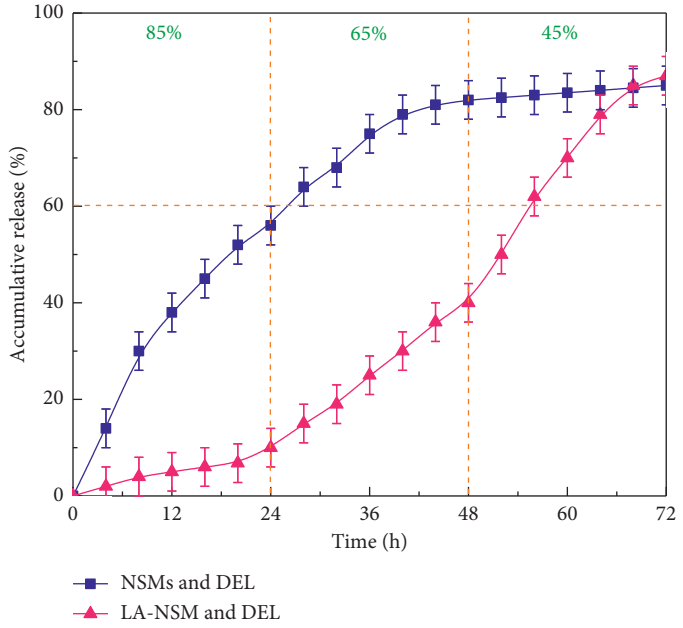

Figure 7: DEL release profiles from LA-NSM and NSMs at different humidity in soils.

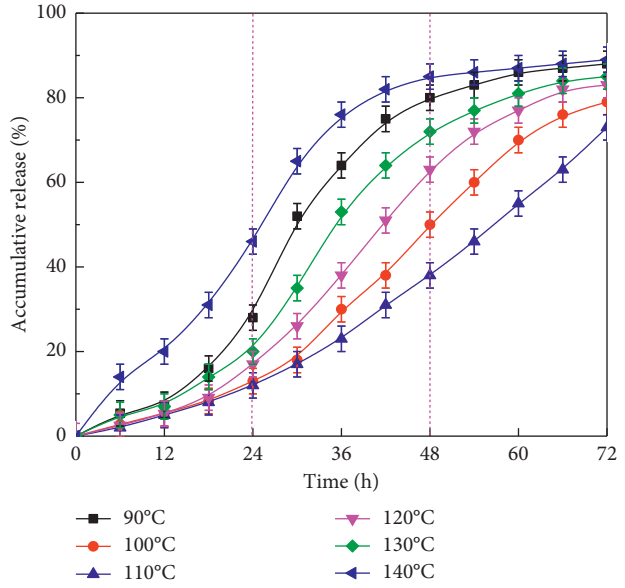

Figure 8: Release kinetic curves of LA-NSM@DEL with different esterification temperatures.

140°C. As seen in the picture, in all cases, there were no significant differences in the release tendency of DEL. At the beginning phase, the release efficiency increases gradually and then quickly after 24 h. This phenomenon could be ascribed to the esterification degree of LA-NSM. At lower and higher temperatures, the degree of esterification between hydroxyl functional groups on NSMs and carboxyl groups in lauric acid was lower, which could reduce loading active sites for binding DEL molecules via π-π stacking and electrostatic attraction, allowing DEL molecules to separate from LA-NSM@DEL. Nevertheless, at an excellent degree of esterification (~110°C), only a slow release rate of DEL was observed from the LA-NSM@DEL. The sluggish release capacity may be due to maximization of the degree of esterification, strengthening the attraction between the DEL molecules and LA-NSM. With time prolonging, there were less DEL molecules entrapped inside the LA-NSM, resulting in a slight increase of DEL release.

Data obtained from the release studies were calculated by the first-order and Higuchi models [58, 59], and the corresponding parameter values are listed in Table 1. From Figure 9 and the obtained correlation coefficients (R_2) in Table 1, it is evident that the release of DEL from LA-NSM@DEL composites could be better described by the Higuchi model than the first-order model. It signified that the DEL release from LA-NSM@DEL was controlled by a relatively strong physical

Table 1: DEL-releasing coefficients calculated with the two models.

	Temperature (°C)	Equations		R^2	
		First order	Higuchi	First order	Higuchi
LA-NSM@DEL	90	$y = -0.058x + 5.072$	$y = 1.22x - 0.358$	0.958	0.981
	100	$y = -0.0295x + 4.87$	$y = 1.23x - 9.769$	0.883	0.988
	110	$y = -0.0205x + 4.75$	$y = 1.03x - 8.329$	0.858	0.992
	120	$y = -0.0383x + 4.97$	$y = 1.36x - 8.601$	0.913	0.984
	130	$y = -0.0442x + 4.96$	$y = 1.39x - 4.285$	0.944	0.997
	140	$y = -0.0653x + 4.94$	$y = 1.31x - 11.945$	0.975	0.987

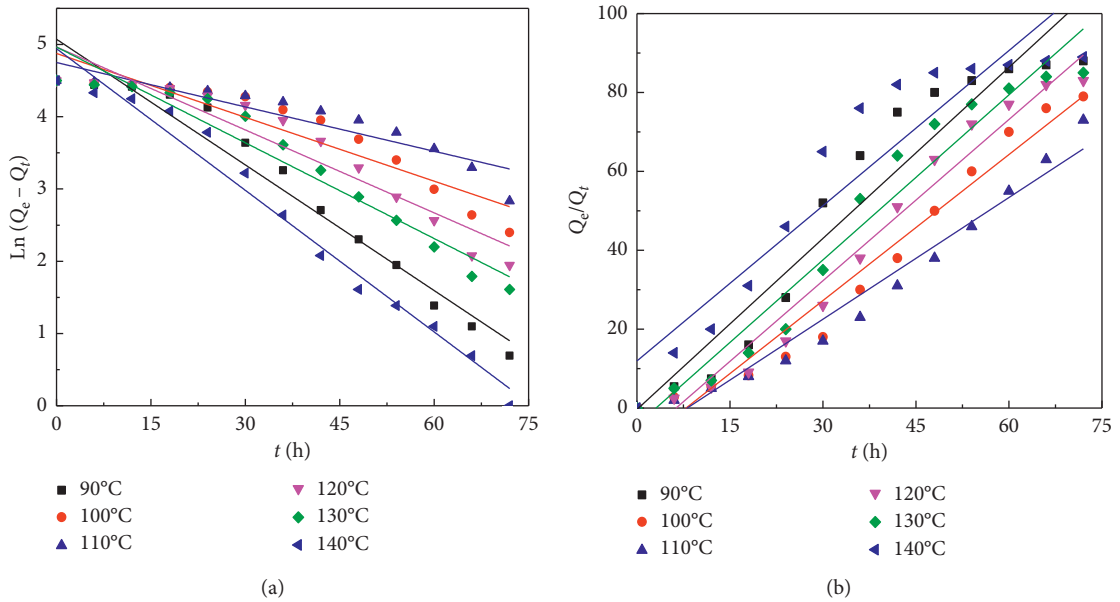

Figure 9: Release profiles of LA-NSM@DEL with different esterification temperatures: (a) first-order model and (b) Higuchi model.

process instead of a common chemical one. Also, the model revealed the release boundaries of LA-NSM@DEL carriers moved inward as the DEL was gradually released into the surrounding medium [60]. In other words, the release process of LA-NSM@DEL had a "moving boundary". Moreover, the regression of Q_t/Q_e versus $t_{1/2}$ for the intraparticle diffusion model is found to be linear, and the linear plots do not pass through the origin point (Figure 9(b)). This phenomenon demonstrated that the pore diffusion was also a rate-controlling step during the pesticide-releasing process.

4. Conclusions

In summary, an environmentally friendly LA-NSM carrier was successfully prepared through modifying waste NSMs with lauric acid. FT-IR, SEM, and CAM analyses confirmed the reaction between hydroxyl groups of NSMs and carboxyl groups of lauric acid. The loading experimental results indicate that the equilibrium loading capacity of DEL into the LA-NSM carrier can reach about 1068 mg/g. The pH of soil, environmental temperature, and soil humidity have an obvious influence on the releasing property of LA-NSM@DEL. Moreover, the release process was fitted well to the Higuchi model. Of particular interest regarding this technology that deserves to be mentioned is that the present route not only makes good use of natural waste resources but also can significantly address and reduce multiple issues created by pesticides, in view of their handy, convenient, and inexpensive fabrication method.

Data Availability

The data used to support the findings of this study are available from the corresponding author upon request.

Conflicts of Interest

The authors declare that they have no conflicts of interest.

Acknowledgments

This work was supported by the Fund Project of the Shaanxi Key Laboratory of Land Consolidation, Innovation Platform for the Development and Construction of Special Project of Key Laboratory of Tibetan Medicine Research of Qinghai Province (No. 2017-ZJ-Y11), Qinghai Provincial Science Foundation (2017-SF-A8), and Yulin Municipal Science and Technology Bureau Science Foundation.

References

[1] A. S. Grewal, A. Singla, P. Kamboj, and J. S. Dua, "Pesticide residues in food grains, vegetables and fruits: a hazard to human health," *Journal of Medicinal Chemistry and Toxicology*, vol. 2, no. 1, pp. 40–46, 2017.

[2] H. Ouyang, X. Tu, Z. Fu et al., "Colorimetric and chemiluminescent dual-readout immunochromatographic assay for detection of pesticide residues utilizing g-C3N4/BiFeO3 nanocomposites," *Biosensors and Bioelectronics*, vol. 106, pp. 43–49, 2017.

[3] T. B. Moorman, "Pesticide degradation by soil microorganisms: environmental, ecological, and management effects," in *Soil Biology*, CRC Press, Boca Raton, FL, USA, 2017.

[4] B. Karishma and S. H. Prasad, "Isolation, characterization and growth studies of malathion insecticide degrading bacteria," *International Journal of Environmental Sciences*, vol. 6, pp. 697–706, 2016.

[5] C. Fan, Y. Liang, H. Dong et al., "In-situ ionic liquid dispersive liquid-liquid microextraction using a new anion-exchange reagent combined Fe3O4 magnetic nanoparticles for determination of pyrethroid pesticides in water samples," *Analytica Chimica Acta*, vol. 975, pp. 20–29, 2017.

[6] M. B. Brahim, H. B. Ammar, R. Abdelhédi, and Y. Samet, "Electrochemical removal of the insecticide imidacloprid from water on a boron-doped diamond and Ta/PbO2 anodes using anodic oxidation process," *Korean Journal of Chemical Engineering*, vol. 33, pp. 2602–2609, 2016.

[7] M. Rani, U. Shanker, and V. Jassal, "Recent strategies for removal and degradation of persistent toxic organochlorine pesticides using nanoparticles: a review," *Journal of Environmental Management*, vol. 190, pp. 208–222, 2017.

[8] B. D. Mattos, B. L. Tardy, W. L. E. Magalhães, and O. J. Rojas, "Controlled release for crop and wood protection: recent progress toward sustainable and safe nanostructured biocidal systems," *Journal of Controlled Release*, vol. 262, pp. 139–150, 2017.

[9] G. Babaladimath and B. Vishalakshi, "Silver nanoparticles embedded gum ghatti-graft-poly (N, N-dimethylacrylamide) biodegradable hydrogel: evaluation as matrix for controlled release of 2, 4-dichlorophenoxyacetic acid," *Journal of Polymer Research*, vol. 24, no. 10, p. 155, 2017.

[10] Y. Xiang, G. Zhang, Y. Chi, D. Cai, and Z. Wu, "Fabrication of a controllable nanopesticide system with magnetic collectability," *Chemical Engineering Journal*, vol. 328, pp. 320–330, 2017.

[11] H. Yan, X. Chen, Y. Feng et al., "Modification of montmorillonite by ball-milling method for immobilization and delivery of acetamiprid based on alginate/exfoliated montmorillonite nanocomposite," *Polymer Bulletin*, vol. 73, no. 4, pp. 1185–1206, 2016.

[12] D. Li, B. Liu, F. Yang, X. Wang, H. Shen, and D. Wu, "Preparation of uniform starch microcapsules by premix membrane emulsion for controlled release of avermectin," *Carbohydrate Polymers*, vol. 136, pp. 341–349, 2016.

[13] S. Wang, Z. Jia, X. Zhou et al., "Preparation of a biodegradable poly (vinyl alcohol)–starch composite film and its application in pesticide controlled release," *Journal of Applied Polymer Science*, vol. 134, no. 28, article 45051, 2017.

[14] B. Zhong, S. Wang, H. Dong et al., "Halloysite tubes as nanocontainers for herbicide and its controlled release in biodegradable poly(vinyl alcohol)/starch film," *Journal of Agricultural and Food Chemistry*, vol. 65, no. 48, pp. 10445–10451, 2017.

[15] A. Rashidzadeh, A. Olad, and M. J. Hejazi, "Controlled release systems based on intercalated paraquat onto montmorillonite and clinoptilolite clays encapsulated with sodium alginate," *Advances in Polymer Technology*, vol. 36, no. 2, pp. 177–185, 2017.

[16] J. Q. Zhao, Y. M. Wang, Y. L. Yang et al., "Isolation and identification of antioxidant and α-glucosidase inhibitory compounds from fruit juice of *Nitraria* tangutorum," *Food Chemistry*, vol. 227, pp. 93–101, 2017.

[17] X. H. Xu, B. Bai, C. X. Ding, H. L. Wang, and Y. R. Suo, "Synthesis and properties of an ecofriendly superabsorbent composite by grafting the poly(acrylic acid) onto the surface of dopamine coated sea buckthorn branches," *Industrial & Engineering Chemistry Research*, vol. 54, no. 13, pp. 3269–3277, 2015.

[18] Z. Purkrtova, P. Jolivet, M. Miquel, and T. Chardot, "Structure and function of seed lipid-body-associated proteins," *Comptes Rendus Biologies*, vol. 331, no. 10, pp. 746–754, 2008.

[19] I. López-Ribera, J. L. La Paz, C. Repiso et al., "The evolutionary conserved oil body associated protein OBAP1 participates in the regulation of oil body size," *Plant Physiology*, vol. 164, pp. 1237–1245, 2014.

[20] C. Ngufor, A. Fongnikin, M. Rowland, and R. N'Guessan, "Indoor residual spraying with a mixture of clothianidin (a neonicotinoid insecticide) and deltamethrin provides improved control and long residual activity against pyrethroid resistant Anopheles gambiae sl in Southern Benin," *PLoS ONE*, vol. 12, Article ID e0189575, , 2017.

[21] E. I. Cengiz, A. S. Bayar, V. Kızmaz, M. Başhan, and A. Satar, "Acute toxicity of deltamethrin on the fatty acid composition of phospholipid classes in liver and gill tissues of nile tilapia," *International Journal of Environmental Research*, vol. 11, no. 3, pp. 377–385, 2017.

[22] T. P. Kuhar, B. D. Short, G. Krawczyk, and T. C. Leskey, "Deltamethrin-incorporated nets as an integrated pest management tool for the invasive *Halyomorpha halys* (Hemiptera: pentatomidae)," *Journal of Economic Entomology*, vol. 110, no. 2, pp. 543–545, 2017.

[23] M. R. Shadegan and M. Banaee, "Effects of dimethoate alone and in combination with Bacilar fertilizer on oxidative stress in common carp, *Cyprinus carpio*," *Chemosphere*, vol. 208, pp. 101–107, 2018.

[24] T. Khan, S. Shadab, R. Afroz, M. A. Aziz, and M. Farooqui, "Study of suppressive effect of biological agent fungus, natural organic compound and carbofuran on root knot nematode of tomato (*Lycopersicon esculentum*)," *Journal of Microbiology and Biotechnology Research*, vol. 1, pp. 7–11, 2017.

[25] M. C. Vagi, A. S. Petsas, M. D. Pavlaki, N. M. Smaragdaki, and M. N. Kostopoulou, "Toxic effects of the organophosphorus insecticide fenthion on growth and chlorophyll production activity of unicellular marine microalgae tetraselmis suecica: comparison between observed and predicted endpoint toxicity data," *Insecticides-Agriculture and Toxicology*, vol. 7, pp. 118–136, 2017.

[26] M. Sidik, A. A. Jalil, S. Triwahyono, S. H. Adam, M. A. H. Satar, and B. H. Hameed, "Modified oil palm leaves adsorbent with enhanced hydrophobicity for crude oil removal," *Chemical Engineering Journal*, vol. 203, pp. 9–18, 2012.

[27] B. S. Chiou, H. Jafri, T. Cao et al., "Modification of wheat gluten with citric acid to produce superabsorbent materials," *Journal of Applied Polymer Science*, vol. 129, no. 6, pp. 3192–3197, 2013.

[28] F. E. Soetaredjo, S. Ismadji, L. H. Huynh et al., "Facile preparation of sago starch esters using full factorial design of experiment," *Starch/Staerke*, vol. 64, no. 8, pp. 590–597, 2012.

[29] M. Elomaa, T. Asplund, P. Soininen et al., "Determination of the degree of substitution of acetylated starch by hydrolysis, 1H NMR and TGA/IR," *Carbohydrate Polymers*, vol. 57, no. 3, pp. 261–267, 2004.

[30] D. J. Feng, B. Bai, C. X. Ding, H. L. Wang, and Y. R. Suo, "Synthesis and swelling behaviors of yeast-g-poly(acrylic acid) superabsorbent co-polymer," *Industrial & Engineering Chemistry Research*, vol. 53, no. 32, pp. 12760–12768, 2014.

[31] J. T. Zhang, S. Petersen, M. Thunga et al., "Micro-structured smart hydrogels with enhanced protein loading and release efficiency," *Acta Biomaterialia*, vol. 6, no. 4, pp. 1297–1305, 2009.

[32] L. Z. Huang, H. X. Wang, B. Li et al., "Hos-guest complexes of various cucurbit[n]urils with the hydrochloride salt of 2, 4-diaminoazobenzene," *Journal of Inclusion Phenomena and Macrocyclic Chemistry*, vol. 80, pp. 209–215, 2014.

[33] X. H. Xu, X. Y. Su, B. Bai, H. L. Wang, and Y. R. Suo, "Controlled pesticide release of a novel superabsorbent by grafting citric acid onto water hyacinth powders with the assistance of dopamine," *RSC Advances*, vol. 6, no. 36, pp. 29880–29888, 2016.

[34] T. Takei, M. Ataku, T. Konishi, M. Fuji, and T. Watanabe, "Investigation of the structure of surface hydroxyl groups on silica. Chemical reaction and molecular adsorption method," *Biochemical Society Transactions*, vol. 36, pp. 180–183, 1999.

[35] B. Morein, K. Lovgren, K. Dalsgaard, J. Thurin, and B. Sundquist, "Matrix with immunomodulating activity," pp. 10–21, 1997, U.S. Patent 5,679,354.

[36] S. Ramesh and M. L. Green, "Process for dehydration of condensation reaction mixtures obtained by azeotropic distillation," pp. 8–11, 1992, US. Patent 5,137,605.

[37] Z. Wu, S. Yang, Q. Xin, and C. Li, "In situ IR spectroscopic studies on molybdenum nitride catalysts: active sites and surface reactions," *Catalysis Surveys from Asia*, vol. 7, pp. 103–108, 2003.

[38] J. T. Tzen, G. C. Lie, and A. H. Huang, "Characterization of the charged components and their topology on the surface of plant seed oil bodies," *Journal of Biological Chemistry*, vol. 267, pp. 15626–15634, 1992.

[39] J. T. Wang, Y. Zheng, and A. Q. Wang, "Preparation and properties of kapok fiber enhanced oil sorption resins by suspended emulsion polymerization," *Journal of Applied Polymer Science*, vol. 127, no. 3, pp. 2184–2191, 2013.

[40] K. Yamakawa, Y. Sato, and K. Fukutani, "Asymmetric and symmetric absorption peaks observed in infrared spectra of CO_2 adsorbed on TiO_2 nanotubes," *Journal of Chemical Physics*, vol. 144, no. 15, article 154703, 2016.

[41] W. J. Zhou, W. He, X. D. Zhang et al., "Biosynthesis and characterization of mesoporous organic–inorganic hybrid iron phosphate," *Materials Chemistry and Physics*, vol. 116, no. 2-3, pp. 319–322, 2009.

[42] M. Beekes, P. Lasch, and D. Naumann, "Analytical applications of Fourier transform-infrared (FT-IR) spectroscopy in microbiology and prion research," *Veterinary Microbiology*, vol. 123, no. 4, pp. 305–319, 2007.

[43] J. J. Cui, W. He, H. T. Liu, S. J. Liao, and Y. Z. Yue, "Ordered hierarchical mesoporous anatase TiO_2 from yeast biotemplates," *Colloids and Surfaces B: Biointerfaces*, vol. 74, no. 1, pp. 274–278, 2009.

[44] J. Z. Gao, X. F. Li, Q. F. Lu, Y. Li, D. L. Ma, and W. Yang, "Synthesis and characterization of poly(methyl methacrylate-butyl acrylate) by using glow-discharge electrolysis plasma," *Polymer Bulletin*, vol. 68, no. 1, pp. 38–48, 2012.

[45] W. He, Z. M. Li, Y. J. Wang et al., "Synthesis of mesoporous structured hydroxyapatite particles using yeast cells as the template," *Journal of Materials Science: Materials in Medicine*, vol. 21, no. 1, pp. 155–159, 2010.

[46] R. Gnanasambandam and A. Protor, "Determination of pectin degree of esterification by diffuse reflectance fourier transform infrared spectroscopy," *Food Chemistry*, vol. 68, no. 3, pp. 327–332, 2000.

[47] X. M. Zhou and C. Z. Chuai, "Synthesis and properties of novel high oil-absorbing resin based on poly (ethylene-propylene-diene/α-methylstyrene/itaconic acid)," *Polymer Engineering & Science*, vol. 53, no. 3, pp. 540–545, 2013.

[48] M. H. Zhou and W. J. Cho, "Synthesis and properties of high oil-absorbent 4-tert- butylstyrene-EPDM-divinylbenzene graft terpolymer," *Journal of Applied Polymer Science*, vol. 85, no. 10, pp. 2119–2125, 2002.

[49] M. A. Abdullah, A. U. Rahmah, and Z. Man, "Physico-chemical and sorption characteristics of Malaysian *Ceiba pentandra* (L.) Gaertn. as a natural oil sorbent," *Journal of Hazardous Materials*, vol. 177, no. 1-3, pp. 683–691, 2010.

[50] A. K. Chaudhary, E. J. Beckman, and A. J. Russell, "Rapid biocatalytic polytransesterification: reaction kinetics in an exothermic reaction," *Biotechnology and Bioengineering*, vol. 59, no. 4, pp. 428–437, 1998.

[51] J. J. Gu, W. Jiang, F. H. Wang, M. D. Chen, J. Y. Mao, and T. Xie, "Facile removal of oils from water surfaces through highly hydrophobic and magnetic polymer nanocomposites," *Applied Surface Science*, vol. 301, pp. 492–498, 2014.

[52] B. Ge, Z. Z. Zhang, X. T. Zhu, X. H. Men, X. Y. Zhou, and Q. J. Xue, "A graphene coated cotton for oil/water separation," *Composites Science and Technology*, vol. 102, pp. 100–105, 2014.

[53] T. Wan, R. Huang, Q. Zhao, L. Xiong, and L. Qin, "Synthesis of wheat straw composite superabsorbent," *Journal of Applied Polymer Science*, vol. 130, no. 5, pp. 3404–3410, 2013.

[54] T. J. Snee, C. Barcons, H. Hernandez, and J. M. Zaldivar, "Characterisation of an exothermic reaction using adiabatic and isothermal calorimetry," *Journal of Thermal Analysis*, vol. 38, no. 12, pp. 2729–2747, 1992.

[55] X. Zhou, Z. Zhang, X. Xu et al., "Robust and durable superhydrophobic cotton fabrics for oil/water separation," *ACS Applied Materials & Interfaces*, vol. 5, no. 15, pp. 7208–7214, 2013.

[56] D. J. Feng, B. Bai, H. L. Wang, and Y. R. Suo, "Thermo-chemical modification to produce citric acid–yeast superabsorbent composites for ketoprofen delivery," *RSC Advances*, vol. 5, no. 127, pp. 104756–104768, 2015.

[57] H. A. A. El-Rehim, E. S. A. Hegazy, and H. L. A. El-Mohdy, "Radiation synthesis of hydrogels to enhance sandy soils water retention and increase plant performance," *Journal of Applied Polymer Science*, vol. 93, no. 3, pp. 1361–1368, 2004.

[58] V. Vobalaboina and M. Kopparam, "Preparation, characterization and in vitro release kinetics of clozapine solid lipid nanoparticles," *J Controlled Release*, vol. 95, no. 3, pp. 628–637, 2004.

[59] D. B. Chen, T. Z. Yang, W. L. Lu, and Q. Zhang, "In Vitro and in vivo study of two types of long-circulating solid lipid nanoparticles containing paclitaxel," *Chemical & Pharmaceutical Bulletin*, vol. 49, no. 11, pp. 1444–1447, 2011.

[60] D. R. Paul, "Elaborations on the Higuchi model for drug delivery," *International Journal of Pharmaceutics*, vol. 418, no. 1, pp. 13–16, 2011.

Hindawi
Journal of Chemistry
Volume 2019, Article ID 4329609, 11 pages
https://doi.org/10.1155/2019/4329609

Research Article

Preparation of Pore-Size Controllable Activated Carbon from Rice Husk Using Dual Activating Agent and Its Application in Supercapacitor

Khu Le Van and Thuy Luong Thi Thu

Faculty of Chemistry, Hanoi National University of Education, Hanoi 1000, Vietnam

Correspondence should be addressed to Khu Le Van; khulv@hnue.edu.vn

Received 17 August 2018; Revised 27 November 2018; Accepted 6 December 2018; Published 15 January 2019

Guest Editor: Gassan Hodaifa

Activated carbons prepared from rice husk by chemical activation with dual activation agents, KOH and NaOH, have been studied and characterized by BET, SEM, EDX, FTIR, Boehm titration, Raman, and TGA. It was found that the KOH/NaOH impregnation ratio plays an important role on textural properties of AC. At the same amount of total alkali hydroxide, the KOH/NaOH ratio higher than 1.33 resulted in larger specific surface area (2990~3043 $m^2 \cdot g^{-1}$), microporous surface area (2747~2831 $m^2 \cdot g^{-1}$), and higher micropore volume (1.4250~1.4316 $cm^3 \cdot g^{-1}$). The as-prepared samples exist in the form of spherical-shaped particles with the size ranging from 20 to 60 nm and contain numerous surface functional groups. The as-prepared activated carbons were then assessed as an electrode material of supercapacitor operating in the 0.5 M K_2SO_4 electrolyte in potential windows of −1.0~0.0 V. The highest capacitance obtained was 205 $F \cdot g^{-1}$ at the scan rate of 2 $mV \cdot s^{-1}$ and 225 $F \cdot g^{-1}$ at a current density of 0.2 $A \cdot g^{-1}$. At the scan rate as high as 50 $mV \cdot s^{-1}$, all the as-prepared activated carbons in this study have the specific capacitance greater than 100 $F \cdot g^{-1}$.

1. Introduction

It is well known that activated carbon (AC) is a material with a porous structure and high specific surface area and is widely used as an adsorbent in water/air treatment, catalyst supporter, or electrical energy/gas storage material. By utilizing agricultural wastes, the synthesis of AC becomes more cost-effective which helps us to speed up the commercialization process measurably.

The preparation of AC consists of two stages: the carbonization stage at lower temperature and the activation stage at elevated temperature. Due to the advantage of lower temperature, shorter time, and developed porous structure, chemical activation is usually chosen over physical activation. In the chemical activation process, the chars (carbonized materials) are impregnated in activation agents such as potassium hydroxide (KOH), sodium hydroxide (NaOH), zinc chloride ($ZnCl_2$), and phosphoric acid (H_3PO_4) followed by activation at temperature in the range between 600 and 900°C under nitrogen flow. The characteristics of the resulting AC are very sensitive to preparing conditions, especially types of activating agents. The activated carbons prepared from lapsi seed (Nepal) are highly porous when activated by KOH or $CaCl_2$ than nonactivating agent pyrolyzed char; on the other hand, the activated carbons impregnated with $MgCl_2$, $FeCl_3$, and H_2SO_4 do not show porous structure [1]. Activated carbons prepared from macadamia nutshells have more microporous structure when activated by KOH while have more mesoporous structure when activated by $ZnCl_2$ [2]. With agricultural waste precursors, the alkali hydroxide activating agent produces more developed surface area than other salts, oxides, or acids. For example, *Enteromorpha prolifera* (China) based activated carbon activated by KOH resulted in higher surface area and larger total pore volume than that activated by $H_4P_2O_7$ [3]; tomato paste processing industry waste (Turkey) established highest surface area that was activated by KOH, much larger than by K_2CO_3 or HCl [4].

Furthermore, for rice husk, because of its high silica content, alkali hydroxide leaching is a preferable method for AC preparation. Comparative researches between KOH and NaOH have been conducted and showed that NaOH activation can satisfactorily control the mesopore volume of the activated carbons [5]. The KOH ACs had higher micropore volumes, whereas NaOH ACs had relatively higher densities [6]. Another difference between the activation process by KOH and NaOH is that KOH can be used effectively with any types of materials while NaOH only with disorder materials. This is ascribed to the intercalating ability of metallic K compared to metallic Na produced during the redox reactions. Metallic Na can only intercalate into the highly disorganized materials [7]. Nevertheless, no study has been conducted to use both KOH and NaOH as well as the effect of the KOH/NaOH ratio on the properties of activated carbon.

The main objective of this work is to prepare AC from rice husk with high porosity and large specific surface area using dual activating agent (KOH and NaOH) and investigate the effect of the NaOH/KOH ratio on the specific surface area, pore structure, morphology, and thermal stability of the AC samples. Moreover, the obtained materials were characterized and evaluated for potential application as supercapacitor electrode materials.

2. Materials and Methods

2.1. Materials and Chemicals. Rice husk was collected from Vinh Phuc Province, Vietnam. The raw precursor was washed, oven-dried at 110°C for 12 h, grounded, and then sieved to obtain uniform particle with a diameter of 1.0 mm. All chemicals used were of analytical reagent grade, and distilled water was used to prepare all solutions.

2.2. Preparation of Activated Carbon. The prepared husks were first carbonized at 500°C for 90 min in nitrogen atmosphere. The resulting chars were then impregnated with KOH and NaOH under various impregnation weight ratios as indicated in Table 1. For comparison, the chars were also impregnated with only KOH or NaOH (with the same molar ratio). The activation process was carried out in a tube furnace under nitrogen flow of 300 mL·min^{-1} and at heating rate of 10°C·min^{-1}. The samples were heated to 400°C and left for 20 min, and then afterwards, the temperature was raised to 850°C and maintained for 90 min (following our previous research [8] and other literatures [9]). The activated products were washed sequentially with 0.1 M HCl solution and hot distilled water to the neutral pH range (6.6–7.0). Finally, the activated carbon samples were dried at 120°C for 24 h and stored for use. The as-prepared samples were labeled as presented in Table 1.

2.3. Characterization of Activated Carbons. Textural properties of the ACs were measured from N_2 adsorption/desorption isotherms at 77 K (Micromeritics, TriStar 3020). The specific surface area (S_{BET}) was calculated by the Brunauer–Emmet–Teller (BET) equation [10]; the microporous surface area (S_{mic}), external surface area (S_{ext}), and micropore volume (V_{mic}) were evaluated by the *t*-plot method [11]; and the mesopore volume (V_{mes}) was obtained by the Barrett–Joyner–Halenda (BJH) method [12]. The total pore volume (V_{tot}) was evaluated by the sum of microporous and mesoporous volumes. The pore-size distribution of AC samples was calculated using density functional theory (DFT) [13] with the assumption that the pores of the sample have slit shape.

Table 1: AC samples prepared under various impregnation ratios.

Sample	Impregnation ratio KOH : NaOH : char (wt. ratio)
RH-K4N0	4 : 0 :1
RH-K0N3	0 : 3 : 1
RH-K1N2	1 : 2 : 1
RH-K1.5N2	1.5 : 2 : 1
RH-K2N2	2 : 2 : 1
RH-K2N1.5	2 : 1.5 : 1
RH-K2N1	2 : 1 : 1

The morphology of the activated carbons was observed using a field-emission scanning electron microscope S4800 (Hitachi). The element analysis was determined using SM-6510LV (Jeol).

The surface chemistry characteristics were identified by Fourier-transform infrared spectroscopy (Nicolet, Nexus 670) operating in a wave number range of 500–4000 cm^{-1} and employing the potassium bromide pellet method.

The concentrations of surface acidic/basic functional groups were determined by following the Boehm titration method [14] and were calculated under the assumption that NaOH neutralizes carboxylic, phenolic, and lactonic groups; Na_2CO_3 neutralizes both carboxylic and lactonic groups; and $NaHCO_3$ neutralizes only carboxylic groups. The amount of basic groups was calculated from the amount of hydrochloric acid consumed by the ACs.

Raman spectra were obtained with the Renishaw Raman microscope using an excitation wavelength at 250 nm.

The thermal behavior was performed with the thermogravimetric analyzer (DTG-60H, Shimazu). Before measurement, the AC samples were dried in air at 120°C in 2 h to remove adsorbed water. Then, the AC samples were heated from 120 to 650°C in pure air (flow rate 50 mL·min^{-1}) at a ramping rate of 10°C min^{-1}. Measurements were made using calcined alumina as reference material.

2.4. Electrode Preparation and Electrochemical Measurement. A mixture of activated carbon, conductive additive (carbon black), and binder (polytetrafluoroethylene) with weight ratio 8 : 1 : 1 was dispersed in ethanol. The slurry was laminated on each side of the current collector (nickel foam) and dried in oven at 120°C for 15 h. The resulting electrode was then pressed under 20 MPa and cut into 1 cm × 1 cm geometry shape. Electrochemical measurements were conducted in a three-electrode cell using an Autolab 302N instrument. The as-prepared activated carbon electrode was used as the working electrode, with saturated calomel

electrode (SCE) as the reference electrode, platinum sheet as the counterelectrode, and 0.5 M K_2SO_4 as well as 0.5 M Na_2SO_4 aqueous solutions as the neutral electrolytes. Cyclic voltammetry (CV) measurements were performed with a potential window from −1.0 to 0.0 V vs. SCE at scan rates from 2 to 100 mV·s^{-1}. Galvanostatic charge/discharge was carried out with the same potential window at current densities from 500 to 2000 mA·g^{-1}.

Specific capacitance based on CV measurements was calculated by the following equation:

$$C_{CV} = \frac{\sum |I| \Delta t}{2m\Delta V}, \quad (1)$$

while the gravimetric specific capacitance based on charge/discharge curves was evaluated by the following equation:

$$C_{CP} = \frac{I_d \Delta t_d}{m\Delta V}, \quad (2)$$

where $\sum |I| \Delta t$ is the area of the current (A) against the time (s) curve, m is the mass of the active material in the electrode (g), I_d is the discharge current (A), Δt_d is the discharge time (s), and ΔV is the potential interval (V).

3. Results and Discussion

3.1. Activated Carbon Characterization

3.1.1. Porous Texture. Nitrogen adsorption/desorption isotherms at 77K of AC samples prepared at different KOH/NaOH impregnation ratios are shown in Figure 1. All the isotherms are a combination of type I at low relative pressures (p/p°) and type IV at intermediate and high relative pressures according to IUPAC classification [15] with hysteresis loops, indicating the coexistence of micropores and mesopores.

Physical properties of AC samples obtained from N_2 adsorption isotherms are summarized in Table 2. It can be observed that the samples activated with single activation agent, RH-K4N0 and RH-K0N3, have different pore structures despite having the same amount of alkaline molecules. RH-K4N0 has higher specific surface area (2696 $m^2 \cdot g^{-1}$) consisting mainly of micropores while RH-K0N3 is detected with about 20% percent of mesopores (0.4396 $cm^3 \cdot g^{-1}$). This result is in good agreement with other research studies [16]. Nevertheless, the BET surface of single agent activated samples is smaller than that of all the samples activated with dual activation agents (S_{BET} is in the range of 2365~3043 $m^2 \cdot g^{-1}$). Therefore, it could be deduced that using dual activation agents enhances the development of the surface area of the activated carbon.

The effect of employing the dual activation agent KOH and NaOH on porous characteristic of the obtained activated carbon can also be seen from Table 2. The specific surface areas and the total pore volume were lowest when the alkali hydroxide/char impregnation ratio is 3.0 (2365 $m^2 \cdot g^{-1}$ and 1.2002 $cm^3 \cdot g^{-1}$ for RH-K1N2; 2829 $m^2 \cdot g^{-1}$ and 1.3636 $cm^3 \cdot g^{-1}$ for RH-K2N1). When the alkali hydroxide/char impregnation ratio is higher than 3.0, specific surface area and total pore volume increased to a certain degree (2945~3043 $m^2 \cdot g^{-1}$ and 1.7212~1.8084 $cm^3 \cdot g^{-1}$, respectively), which indicate that surface pyrolysis and interior etching processes happened concurrently.

While the amount of impregnated alkali hydroxide tends to affect the pore texture of the AC samples, the KOH/NaOH ratio however seems to have more influence. The S_{BET} was significantly increased from 2365 to 3043 $m^2 \cdot g^{-1}$ at KOH/NaOH ratios from 0.50 to 1.33. Nevertheless, as the KOH/NaOH ratio further increased to 2.00, S_{BET} decreased to 2990 $m^2 \cdot g^{-1}$. Additionally, the following points were observed from Table 2:

(i) At the same amount of alkali hydroxide, higher KOH content gave larger specific surface area, microporous surface area, and higher micropore volume. RH-K1N2 has S_{BET} = 2365 $m^2 \cdot g^{-1}$, S_{mic} = 2258 $m^2 \cdot g^{-1}$, and V_{mic} = 1.0156 $cm^3 \cdot g^{-1}$, while RH-K2N1, at the same amount of alkali hydroxide (alkali hydroxide/char = 3.0), led to S_{BET} = 2829 $m^2 \cdot g^{-1}$, S_{mic} = 2736 $m^2 \cdot g^{-1}$, and V_{mic} = 1.2267 $cm^3 \cdot g^{-1}$. The same situation happened with RH-K1.5N2 and RH-K2N1.5 (alkali hydroxide/char = 3.5), and S_{BET}, S_{mic}, and V_{mic} of RH-K1.5N2 (2945, 2745 $m^2 \cdot g^{-1}$, and 1.3811 $cm^3 \cdot g^{-1}$) are always lower than that of RH-K2N1.5 (3043, 2831 $m^2 \cdot g^{-1}$, and 1.4250 $cm^3 \cdot g^{-1}$).

(ii) At the same amount of the KOH/char ratio, as the NaOH/char ratio increased from 1.0 to 1.5 (RH-K2N1 and RH-K2N1.5), specific surface area and micropore surface area increased from 2829 and 2736 $m^2 \cdot g^{-1}$ to 3043 and 2831 $m^2 \cdot g^{-1}$. When the NaOH ratio further increased to 2.0 (RH-K2N2), specific surface area and micropore surface area decreased slightly to 2990 and 2747 $m^2 \cdot g^{-1}$. However, external surface area, mesopore volume, and total pore volume increased with the increase of the NaOH ratio from 1 to 2 (S_{ext}, V_{mes}, and V_{tot} increase from 93 $m^2 \cdot g^{-1}$, 0.1369, and 1.3636 $cm^3 \cdot g^{-1}$ to 243 $m^2 \cdot g^{-1}$, 0.3768, and 1.8084 $cm^3 \cdot g^{-1}$, respectively).

(iii) At the same amount of the NaOH/char ratio, when the KOH/char ratio increased gradually from 1 (RH-K1N2) to 1.5 (RH-K2N1.5) and 2 (RH-K2N2), specific surface area as well as total pore volume increased, reaching the highest value of 2990 $m^2 \cdot g^{-1}$ and 1.8084 $cm^3 \cdot g^{-1}$. This raise is resulted from the increase of micropore and mesopore, which were from 2258 and 107 $m^2 \cdot g^{-1}$ to 2747 and 243 $m^2 \cdot g^{-1}$.

The change in specific surface area and pore characteristic of AC samples with KOH/char and NaOH/char ratios might be explained by the formation of alkali metal through the reaction of hydroxide and carbon in the process of preparation of AC [17, 18] and by the lower boiling point of KOH (758°C) than NaOH (883°C [19]). It is easier for potassium to diffuse into the layer of carbon, causing the enhancement of pores (especially micropore), which in turn increases the specific and microporous surface area as well as the microporous volume of AC samples. As a result, the variation of Na content only causes the change in external site and mesopore of AC samples.

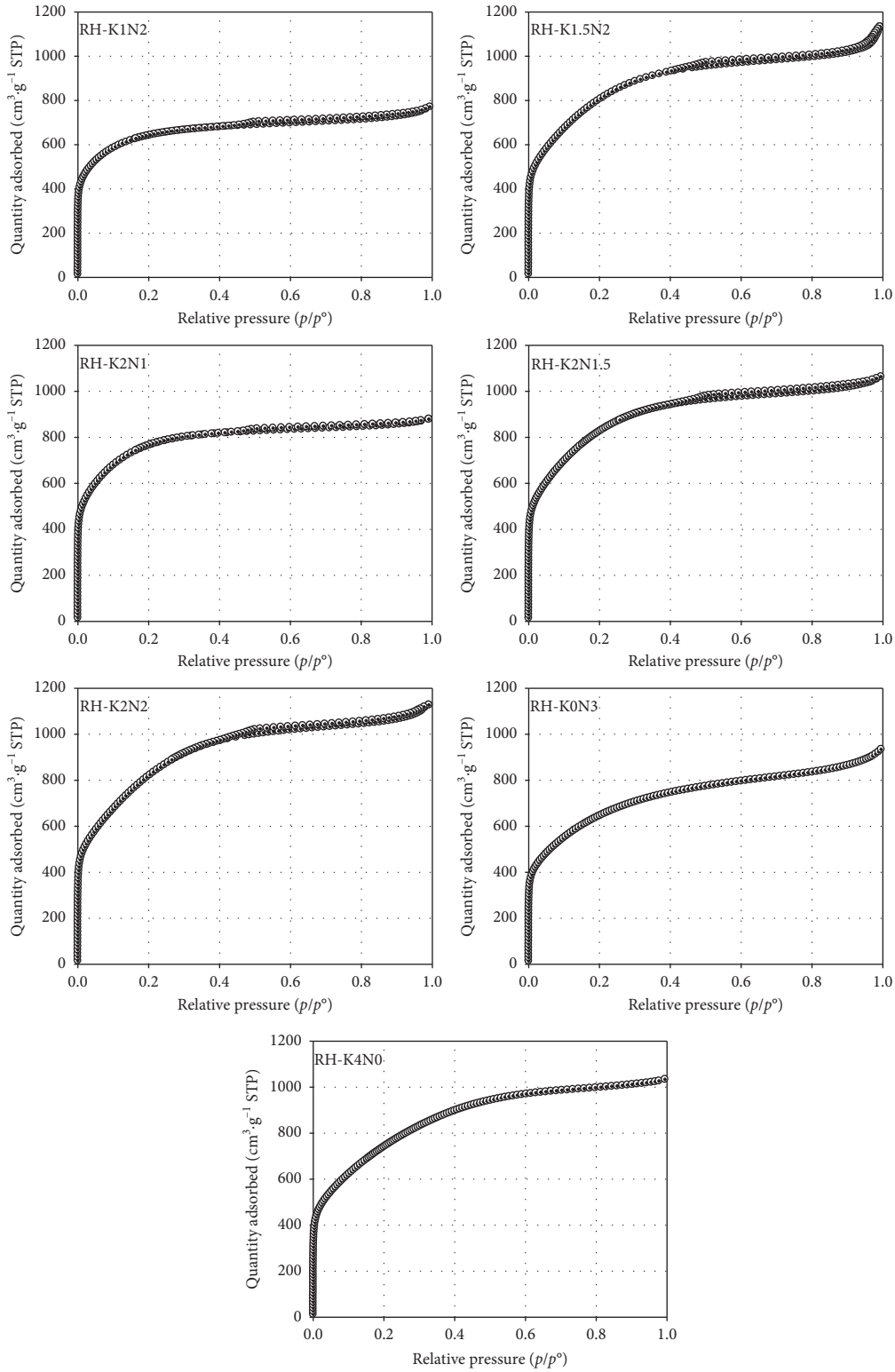

Figure 1: Adsorption-desorption isotherms of N_2 at 77K for AC samples (the same scale on the quantity adsorbed axes was maintained to enable better comparison between graphs).

Figure 2 shows the pore-size distributions (PSDs) calculated from the N_2 adsorption isotherm by applying the DFT method. It can be noticed that a considerable amount of pores is distributed in the range from 0.8 to 1.8 nm, and from 1.8 to 5 nm, further indicating the concurrence of micropores and mesopores, which corresponds well with the observation from N_2 adsorption/desorption at 77K in Figure 1. Combined with the summarized data in Table 1, it

Table 2: Physical properties deduced from N_2 adsorption at 77K of AC samples.

Sample	S_{BET} ($m^2 \cdot g^{-1}$)	S_{mic} ($m^2 \cdot g^{-1}$)	S_{ext} ($m^2 \cdot g^{-1}$)	V_{mic} ($cm^3 \cdot g^{-1}$)	V_{mes} ($cm^3 \cdot g^{-1}$)	V_{tot} ($cm^3 \cdot g^{-1}$)	V_{mic}/V_{tot} (%)
RH-K4	2696	2470	226	1.4258	0.3111	1.7369	82.1
RH-N3	2360	2065	295	1.0927	0.4396	1.5323	71.3
RH-K1N2	2365	2258	107	1.0156	0.1846	1.2002	84.6
RH-K1.5N2	2945	2745	200	1.3811	0.4200	1.8011	76.7
RH-K2N1	2829	2736	93	1.2267	0.1369	1.3636	90.0
RH-K2N1.5	3043	2831	211	1.4250	0.2962	1.7212	82.8
RH-K2N2	2990	2747	243	1.4316	0.3768	1.8084	79.2

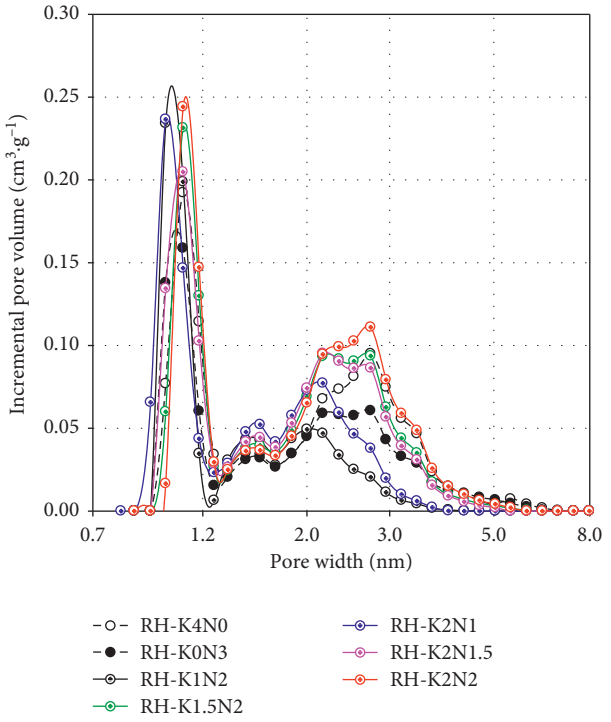

Figure 2: Pore-size distribution of AC samples.

can be seen that the total volume is increasing with the increase of alkali hydroxide/char ratios and V_{tot} is highest with alkali hydroxide/char = 4.0 (RH-K2N2). At the same amount of alkali hydroxide/char, the higher KOH content resulted in the development of microporosity. V_{mi}/V_{tot} of RH-K2N1.5 and RH-K2N1 (82.8% and 90.0%) are higher than those of RH-K1.5N2 and RH-K1N2 (84.6% and 76.7%). According to Alcaniz-Monge and Illan-Gomez [20], the development of microporosity is due to carbon gasification and the metal intercalation, and only KOH generates supermicroporosity.

With the significantly improvement of porous characteristic of activated carbons by employing dual activation agents and by varying the KOH/NaOH ratio, we focus on dual activation agents in further studies.

3.1.2. SEM Analysis. The SEM micrographs of AC samples are shown in Figure 3. All samples exist in the form of spherical-shaped particles with the size ranging from 20 to 60 nm. The impregnation ratios only have slight effect on the compact of the samples. There are more cracks and crevices as the KOH/NaOH ratios increase, and the samples with higher amount of impregnated KOH are more porous than the other.

3.1.3. Element Analysis. The element analysis of AC samples was determined by EDX measurement and is given in Table 3. All the samples have relatively high carbon content (94.38~95.23%) and no or less than 0.09% silica content. This is due to the use of the alkali hydroxide activation agent which reacts with silica (relatively rich in rice husk) to form alkali silicate and be removed in the washing process [21]. The presence of oxygen (4.54~5.35%) is owing to the adsorbed water and surface functional groups. The existence of Cl, Cr, and Fe might be caused by the reactor container during the activation process and by HCl washing thereafter. Neither K nor Na has been detected, which demonstrates the effectiveness of the washing process.

3.1.4. FTIR Analysis. The FTIR spectra of all the AC samples are shown in Figure 4, which have similar shapes with most of the peaks located at the same wave number. The wide bands located at 3450 cm^{-1} can be attributed to the presence of –OH vibration [22]. The band at 2920 and 2860 cm^{-1} may be assigned to the presence of aliphatic C–H vibration [23]. The strong band at 1630 nm represents the C=O vibration [24]. The peak at 1384 cm^{-1} is ascribed to CH_2 and CH_3 groups [23]. There is no SiO_2 absorption peaks (at 1101, 944, and 789 cm^{-1} [25]), indicating that silica has been successfully removed from the samples. The obtained result is consistent with earlier EDX studies, in which Si content of all AC samples is less than 0.1%.

3.1.5. Boehm Titration. The acid/base properties of the AC samples are evaluated by Boehm titration and shown in Table 4. From the results in Table 4, it can be observed that the acidic sites are dominant over basic sites. Total amount of acidic groups is in the range of 1.387~1.771 $mmol \cdot g^{-1}$ whereas the amount of basic groups is only from 0.346 to 0.704 $mmol \cdot g^{-1}$. The smallest amount of total acidic groups is found at the RH-K1.5N2 sample (1.387 $mmol \cdot g^{-1}$) and the highest at the RH-K2N1.5 sample (1.771 $mmol \cdot g^{-1}$). This result is in good agreement with the EDX measurement that oxygen content is lowest and highest in RH-K1.5N2 (4.54%) and

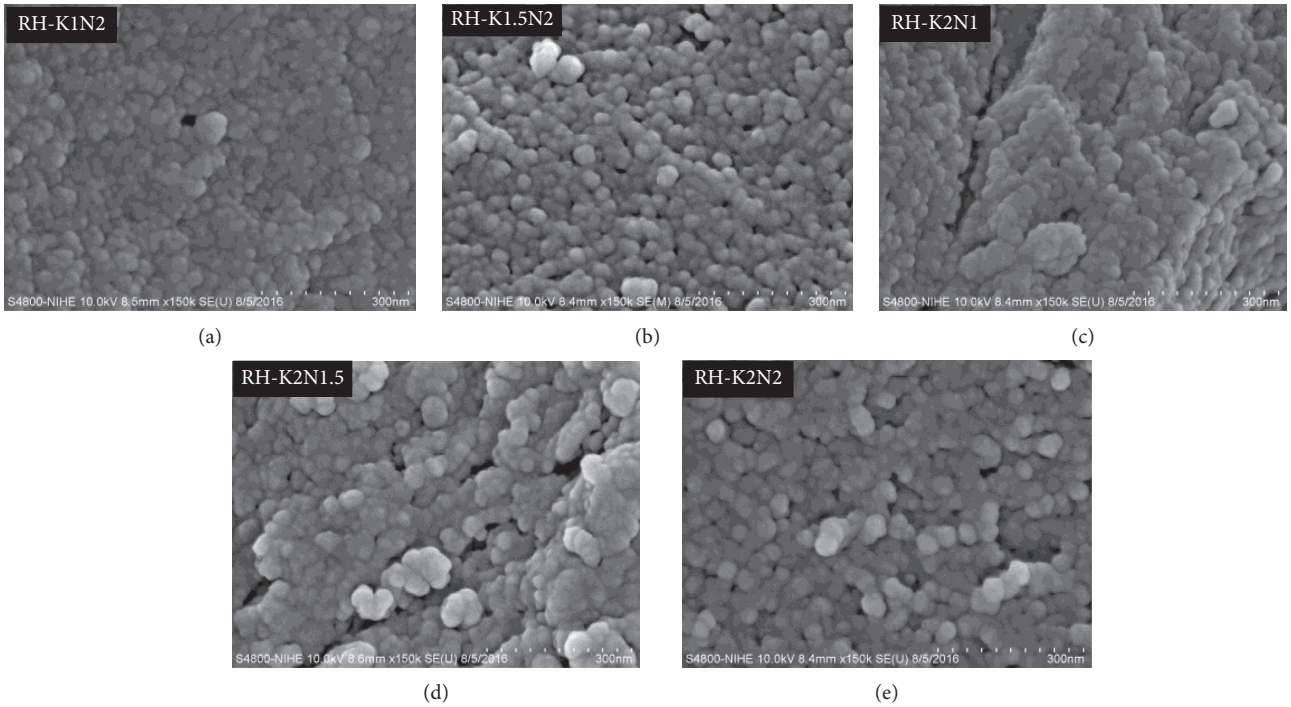

Figure 3: SEM images of AC samples.

Table 3: EDX analysis of AC samples.

Sample	Mass percentage						
	C	O	Si	Cl	Cr	Fe	Total
RH-K1N2	94.67	5.13	0	0.09	0.05	0.06	100
RH-K1.5N2	95.23	4.54	0.08	0.04	0.06	0.05	100
RH-K2N1	94.91	4.92	0.07	—	0.04	0.06	100
RH-K2N1.5	94.38	5.35	0.09	0.08	0.05	0.05	100
RH-K2N2	94.79	5.09	—	—	0.06	0.06	100

in RH-K2N1.5 (5.35%), respectively. It can also be noticed from Table 4 that the numbers of carboxylic, phenolic, and lactonic groups as well as total basic groups are almost unrelated to the amount of alkali hydroxide used or the KOH/NaOH impregnation ratio.

3.1.6. Raman Analysis. The degree of surface disorder and defect of the as-prepared AC samples were evaluated by Raman spectra and are illustrated in Figure 5 and Table 5. There are graphite (G) peak at 1580 cm^{-1} and the defect-disorder (D) peak at 1350 cm^{-1}. The G-peak is associated with E_{2g}, and the D-peak is corresponded to A_{1g}. The ratio of the integrated intensities of D-band and G-band (I_D/I_G) is consistent with the degree of graphitization of carbonaceous materials, and I_D/I_G increases with the decreasing in crystallinity [26]. The results from Table 5 reveal that RH-K2N1.5 has the highest I_D/I_G value which indicates the highest surface disorder degree of this sample. The I_D/I_G values of RH-K1.5N2 and RH-K2N2 are 1.361 and 1.291, suggesting that these two samples have higher degree of graphite organization. This outcome confirms the Boehm titration results, since the surface disorder degree is

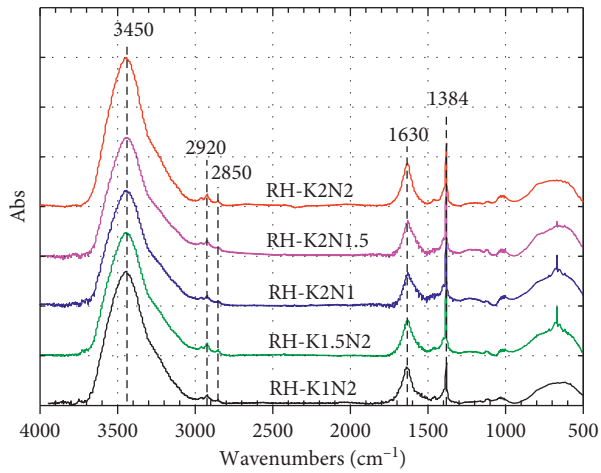

Figure 4: FTIR spectra of AC samples.

resulting from high amount of surface functional groups. The crystalline size along the basal plane (L_a) in Table 5 was calculated by the following equation [27]: $L_a\,(nm) = (4.35 \times I_G)/I_D$ (3). RH-K1.5N2 and RH-K2N2 have low value of I_D/I_G; consequently, their calculated crystallite sizes are towering over other samples.

3.1.7. TGA Analysis. Figure 6 shows the TGA-DTA curves of AC samples prepared at different KOH/NaOH/char ratios. All samples show a similar behavior in the temperature range under study, which occurs in two weight-loss stages: 120~350°C and 350~600°C. The weight loss in the temperature range of 120~350°C is summarized in

Table 4: Functional groups on the surface of AC samples by Boehm titration.

Sample	Functional groups (mmol g^{-1})				
	Carboxylic	Phenolic	Lactonic	Acidic site	Basic site
RH-K1N2	0.500	0.850	0.250	1.600	0.630
RH-K1.5N2	0.495	0.397	0.495	1.387	0.693
RH-K2N1	0.350	0.550	0.600	1.500	0.690
RH-K2N1.5	0.260	0.990	0.521	1.771	0.704
RH-K2N2	0.445	0.595	0.545	1.585	0.346

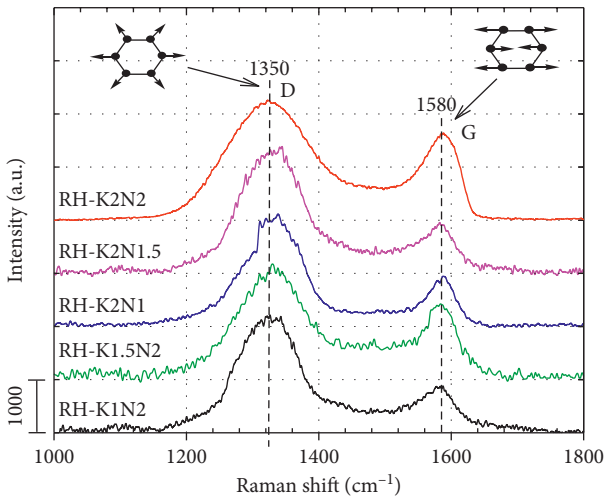

Figure 5: Raman analysis of AC samples.

Table 5: I_D, I_G, I_D/I_G, and L_a.

Sample	I_D (a.u.)	I_G (a.u.)	I_D/I_G	L_a (nm)
RH-K1N2	1875	838	2.237	1.94
RH-K1.5N2	1870	1374	1.361	3.20
RH-K2N1	1889	859	2.199	1.98
RH-K2N1.5	2205	918	2.402	1.81
RH-K2N2	2021	1566	1.291	3.37

Table 6. The weight loss of all the samples in this range is lower than 5.09% and is due to the decomposition of some oxygen containing groups (carboxylic 100–250°C and lactonic 200–400°C [28]). Hence, for the convenience of comparison, the amount of carboxylic and lactonic groups evaluated from Boehm titration is also presented in Table 6. Table 6 shows that there is a consistency between the weight loss and the total amount of carboxylic and lactonic groups, which further confirms the Boehm titration results above.

It also has to be pointed out that the main difference between TGA-DTA curves is only shown in the exothermic peaks of the second weight loss range. At the same impregnated alkali hydroxide amount, the exothermic peak temperature is lower for higher KOH content (between RH-K2N1.5 and RH-K1.5N2 or between RH-K2N1 and RH-K1N2) confirming that KOH is a more reactive agent, in comparison with NaOH [29].

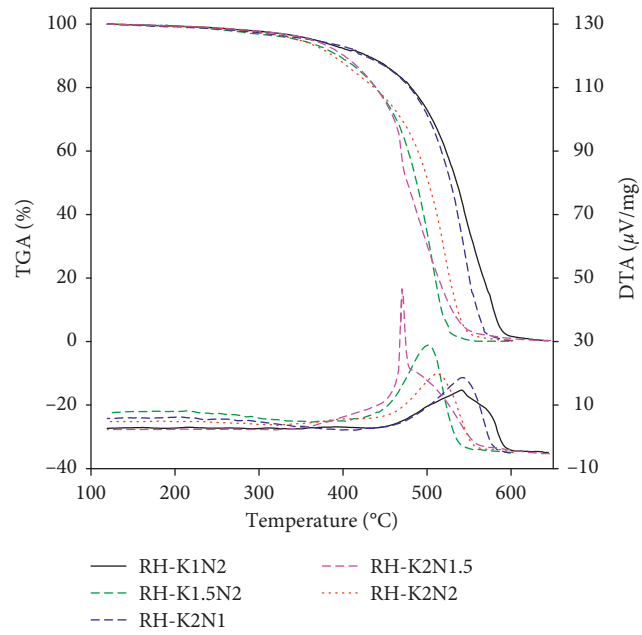

Figure 6: TGA-DTA curves of AC samples.

Table 6: Weight loss of AC samples and total carboxylic and lactonic groups.

Sample	Weight loss (%) in the temperature range of 120~350 (°C)	Total carboxylic and lactonic groups (mmol g^{-1})
RH-K1N2	4.01	0.750
RH-K1.5N2	5.09	0.990
RH-K2N1	4.45	0.950
RH-K2N1.5	4.10	0.781
RH-K2N2	5.02	0.990

3.2. Electrochemical Features. The electrochemical performance of electrodes made of the as-prepared AC samples was evaluated using cyclic voltammetry and galvanostatic charge/discharge. Figure 7 depicts cyclic voltammograms of AC electrodes in 0.5 M K_2SO_4 electrolyte at four typical scan rates 2, 10, 30, and 50 m·V s^{-1} in the potential windows of −1.0~0.0 V vs. SCE. At 2 mV·s^{-1}, CV curves exhibit a symmetric rectangular shape with a slight distortion, indicating an ideal electrochemical double-layer capacitor behavior. The little hump appeared in CV curves of AC electrodes can be accounted for the reaction of surface functional groups [30].

In detail, as the scan was initiated at 0.0 V in negative direction to −1.0 V, the K^+ ions immigrated to the activated carbon surface, diffused into the pores, and adsorbed onto the surface as well as inside the pores to form an electrical double layer. The specific capacitance of activated carbon is caused by the double-layer capacitance of the adsorbed K^+ ions (positive charge) and the electrons accumulated on the carbon surface (negative charge) as well as the pseudocapacitance provided by the reduction of surface functional

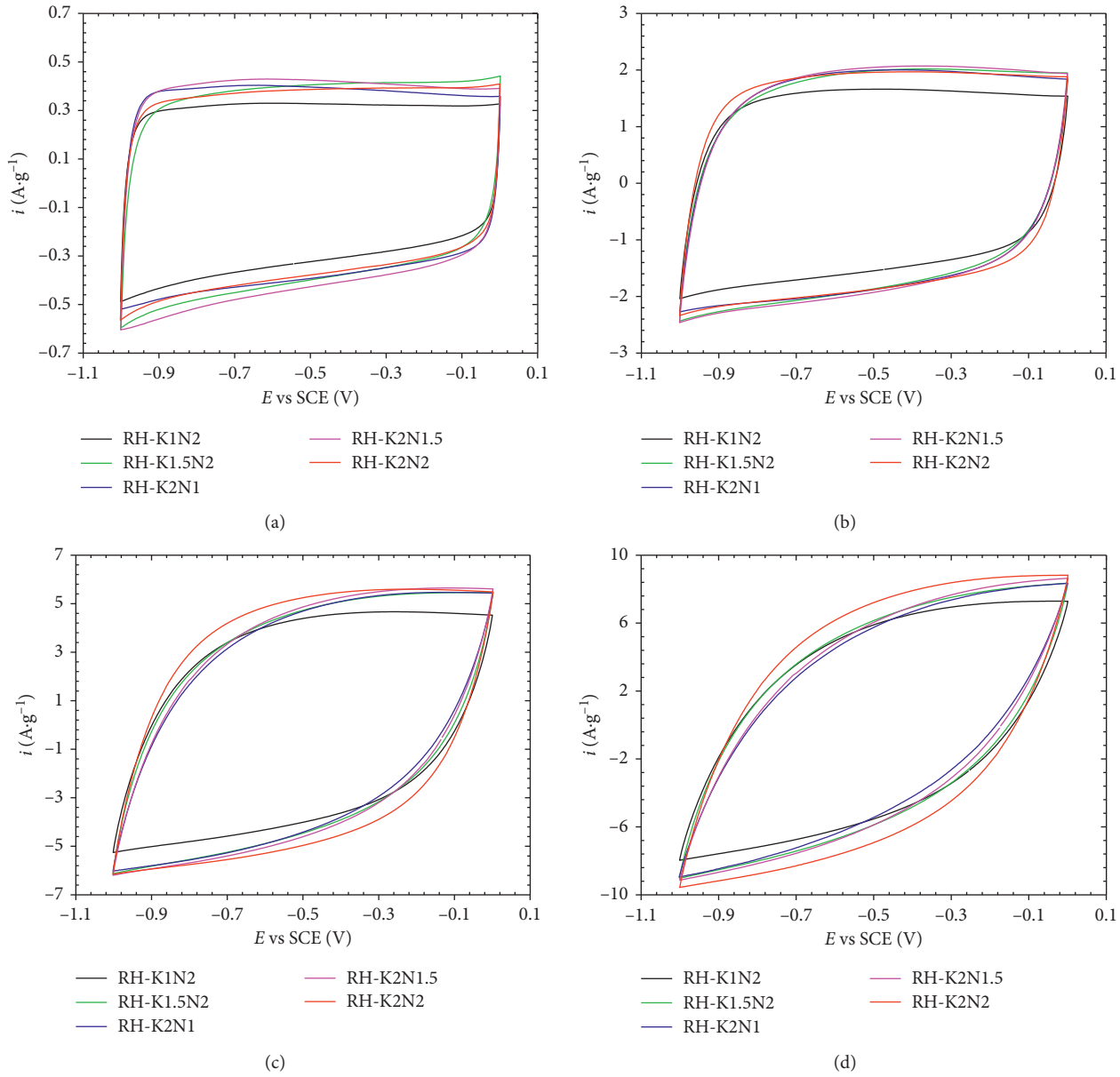

Figure 7: Cyclic voltammograms of AC samples in 0.5 M K_2SO_4 at different scan rates from 2 to 50 mV·s^{-1}. (a) $v = 2$ mV·s^{-1}, (b) $v = 10$ mV·s^{-1}, (c) $v = 30$ mV·s^{-1}, and (d) $v = 50$ mV·s^{-1}.

groups. By reverse scan from −1.0 to 0.0 V, the K^+ ions are desorbed and diffused out of the pores. Simultaneously with this process, there exists the oxidation of surface functional groups. According to Frackowiak and Béguin [31], the redox reaction can be described as follows:

$$\begin{aligned} &>C-OH \rightleftarrows >C=O+H^+ + e \\ &-COOH \rightleftarrows -COO + H^+ + e \\ &>C=O + e \rightleftarrows >C-O^- \end{aligned} \quad (3)$$

As the scan rate increases from 2 to 10, 30, and further to 50 mV·s^{-1}, the CV curves are deformed. The deviations from the rectangular shape are more pronounced with increasing scan rate and in the order RH-K2N2 < RH-K2N1.5 < RH-K1.5N2 < RH-K1N2 < RH-K2N1. This is due to the kinetic limitation of the adsorption/desorption rate of K^+ ions which is directly affected by the diffusion of K^+ ions into and out of the micropores of AC electrodes. This, in turn, will increase the resistance of AC materials, leading to a deformed rectangle [32]. RH-K2N2 has the largest external surface (243 m^2·g^{-1}); thus, it is the least affected by the scan rate. By contrast, as the external surface of RH-K2N1 (93 m^2·g^{-1}) is smallest, its CV curve is the most deviated from the ideal shape.

The specific capacitances calculated from CV curves at different scan rates are summarized in Table 7. All the calculated C_{CV} are in the range of 160~205 F·g^{-1} at the scan rate of 2 mV·s^{-1}. These values are about 1.6~2 times of the

Table 7: C_{CV} at different scan rates.

Sample	C_{CV} (F g^{-1}) at different scan rates						
	2 mV·s^{-1}	5 mV·s^{-1}	10 mV·s^{-1}	20 mV·s^{-1}	30 mV·s^{-1}	50 mV·s^{-1}	100 mV·s^{-1}
RH-K1N2	160	155	147	134	123	103	72
RH-K1.5N2	197	182	167	144	128	111	83
RH-K2N1	191	179	169	149	134	102	69
RH-K2N1.5	205	193	179	157	140	114	74
RH-K2N2	193	184	176	162	149	127	90

PICATIF activated carbon in the same testing conditions [33]. This is owing to the high specific surface area of the as-prepared activated carbons. RH-K2N1.5 and RH-K1N2 has the highest and lowest specific surface area (3043 vs. 2365 $m^2 \cdot g^{-1}$); for that reason, the C_{cv} of RH-K2N1.5 is the highest (205 $F \cdot g^{-1}$) and of RH-K1N2 is the lowest (160 $F \cdot g^{-1}$). Besides, the contribution of surface functional groups should be taken into account, especially at the low scan rate. The highest amount of acidic and basic groups of RH-K2N1.5 (2.475 mmol·g^{-1}) also help raising its specific capacitance.

As the scan rate increases, the specific capacitance of the sample decreases. However, at the scan rate heighten up to 50 mV·s^{-1}, specific capacitances of all samples are still greater than 100 $F \cdot g^{-1}$, which implies the good capacitance of the as-prepared activated carbon in the K_2SO_4 electrolyte. With the increasing scan rate, the specific capacitance decreases gradually, which could be due to the limited diffusion of K^+ ions. At the scan rate as high as 100 mV·s^{-1}, the highest specific capacitance of 90 $F \cdot g^{-1}$ was observed with the RH-K2N2 sample while the lowest of 69 $F \cdot g^{-1}$ was seen in the RH-K2N1 sample. This result might be explained by the effect of the external area of the samples as described above.

Figure 8 displays the charge/discharge curves of AC electrodes at two typical current densities 0.5 and 3.0 $A \cdot g^{-1}$ in 0.5 M K_2SO_4 electrolyte. A good linear variation of potential vs. time is observed for all curves, and the charge curves are symmetric to the corresponding discharge counterparts. There are only small Ohmic drops at high current density, implying the small resistivity of the cell. The Ohmic drops increase with but not proportional to the increasing of current density. At current density of 0.5 $A \cdot g^{-1}$, the Ohmic drops increase in the order RH-K2N2 RH-K1.5N2 < RH-K2N1 RH-K1N2 < RH-K2N1.5. At current density of 3.0 $A \cdot g^{-1}$, however, the order changes to RH-K2N2 < RH-K2N1.5 < RH-K1.5N2 < RH-K1N2 < RH-K2N1.

The difference in the Ohmic drop is owing to the internal resistance of materials, and the less mesopores (lower external surface), the higher the internal resistance. However, the surface disorder of the material also adds up to the increase of internal resistance. The Raman results in Table 5 show that the surface disorder increase in the following order: RH-K2N2 < RH-K1.5N2 < RH-K2N1 < RH-K1N2 < RH-K2N1.5. This means that the surface conductivity of the samples decreases in order RH-K2N2 > RH-K1.5N2 > RH-K2N1 > RH-K1N2 > RH-K2N1.5, which is consistent with the magnitude of Ohmic drops at low current density (0.5 $A \cdot g^{-1}$). At high current density, the Ohmic drop strongly depends on the mesopores amount. RH-K2N2 has the highest mesopores amount (BET result in Table 2); therefore, it has the smallest Ohmic drop. In contrast, the Ohmic drop of RH-K2N1 is highest owing to its low mesopores amount.

The gravimetric specific capacitances at different current densities calculated from equation (2) are illustrated in Figure 9. It can be seen from Figure 9 that the specific capacitance decreases with the increasing of current density. As current density increases from 0.2 to 3.0 $A \cdot g^{-1}$, the specific capacitance of RH-K2N1.5 decreases from 225 to 154 $F \cdot g^{-1}$. It also can be seen from Figure 9 that the change in the specific capacitance of AC samples with current density is similar to the change with the scan rate (described above). This result confirms the CV result and can also be explained due to Raman as well as BET result.

4. Conclusions

High surface area activated carbons from rice husk have been prepared by chemical activation with dual activation agents, KOH and NaOH. The activation condition, namely, total alkali hydroxide/char and KOH/NaOH ratio can affect the pore structure of the activated carbons. The as-prepared activated carbon samples have a porous structure with developed specific surface area (2365~3043 $m^2 \cdot g^{-1}$) and high pore volume (1.2002~1.8084 $cm^3 \cdot g^{-1}$). The alkali hydroxide/char and KOH/NaOH ratio have a significant effect on the pore texture of AC samples. The AC sample prepared with alkali hydroxide/char = 3.0 and KOH/NaOH = 0.5 has specific surface area and pore volume as 2365 $m^2 \cdot g^{-1}$ and 1.2002 $cm^3 \cdot g^{-1}$, respectively. Alkali hydroxide/char = 3.5 and KOH/NaOH = 1.33 give the highest specific surface area of 3043 $m^2 \cdot g^{-1}$ and pore volume of 1.7212 $cm^3 \cdot g^{-1}$. The as-prepared AC samples have particle size in the range of 20~60 nm and were estimated to have more than 94% carbon, about 5% oxygen, and a trace amount of other elements (Si, Cl, Cr, and Fe). The presence of oxygen is due to the adsorbed water and surface functional groups (1.931~2.475 mmol·g^{-1}). All the AC samples exhibit a good capacitive behavior when used as an electrode material of supercapacitors. In the 0.5 M K_2SO_4 electrolyte, the highest capacitance obtained is 205 $F \cdot g^{-1}$ at the scan rate of 2 mV·s^{-1} and is 225 $F \cdot g^{-1}$ at the current density of 0.2 $A \cdot g^{-1}$. This result shows the potential for valorization of rice husk waste by

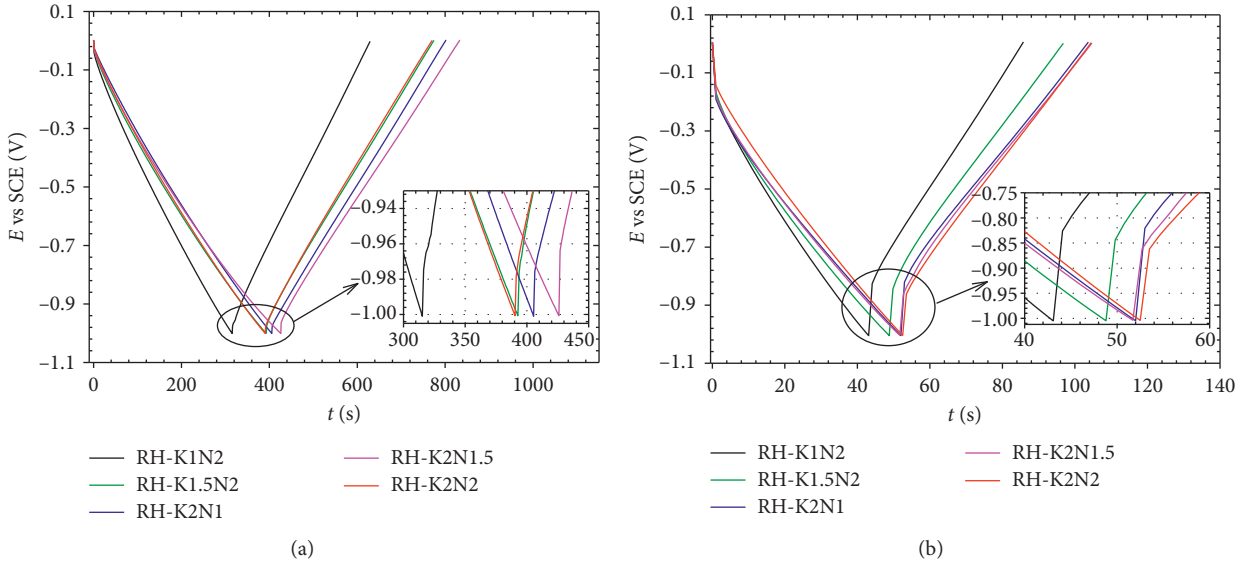

Figure 8: Charge-discharge curves of AC electrode at two different current densities. (a) $i = 0.5\ A{\cdot}g^{-1}$ and (b) $i = 3.0\ A{\cdot}g^{-1}$.

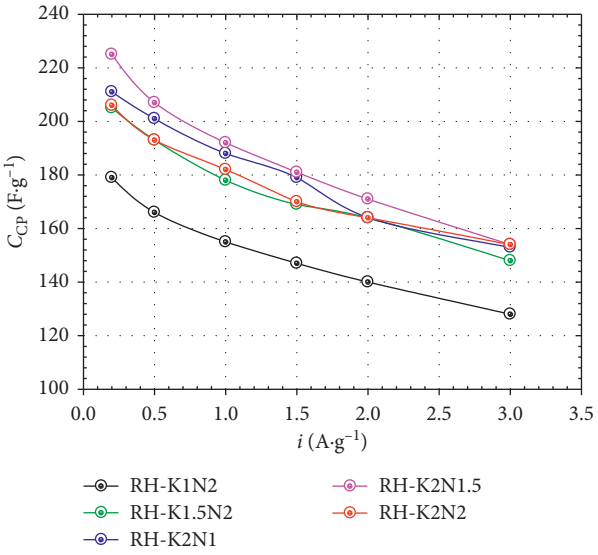

Figure 9: Gravimetric specific capacitances of AC electrodes at different current densities.

controlling the specific surface area and pore structure of the prepared activated carbon toward the application as a supercapacitor electrode.

Data Availability

The datasets used to support the findings of this study are available from the corresponding author upon request.

Conflicts of Interest

The authors declare that there are no conflicts of interest regarding the publication of this paper.

Acknowledgments

This research has received funding from the Vietnamese Ministry of Education and Training under grant number B2016-SPH-20.

References

[1] S. J. Sahira, A. Mandira, P. B. Prasad, and P. R. Ram, "Effects of activating agents on the activated carbons prepared from Lapsi seed," *Research Journal of Chemical Sciences*, vol. 3, no. 5, pp. 19–24, 2013.

[2] A. Ahmadpour, B. A. King, and D. D. Do, "Comparison of equilibria and kinetics of high surface area activated carbon produced from different precursors and by different chemical treatments," *Industrial and Engineering Chemistry Research*, vol. 37, no. 4, pp. 1329–1334, 1998.

[3] Y. Gao, Q. Yue, B. Gao et al., "Comparisons of porous, surface chemistry and adsorption properties of carbon derived from Enteromorpha prolifera activated by $H_4P_2O_7$ and KOH," *Chemical Engineering Journal*, vol. 232, pp. 582–590, 2013.

[4] N. Ozbay and A. S. Yargic, "Comparison of surface and structural properties of carbonaceous materials prepared by chemical activation of tomato paste waste: the effects of activator type and impregnation ratio," *Journal of Applied Chemistry*, vol. 2016, Article ID 8236238, 10 pages, 2016.

[5] R.-L. Tseng, "Mesopore control of high surface area NaOH-activated carbon," *Journal of Colloid and Interface Science*, vol. 303, no. 2, pp. 494–502, 2006.

[6] A. Ahmadpour, H. Rashidi, M. J. D. Mahboub, and M. R. Farmad, "Comparing the performance of KOH with NaOH-activated anthracites in terms of methane storage," *Adsorption Science and Technology*, vol. 31, no. 8, pp. 729–745, 2013.

[7] E. Raymundo-Piñero, P. Azaïs, T. Cacciaguerra, D. Cazorla-Amorós, A. Linares-Solano, and F. Béguin, "KOH and NaOH activation mechanisms of multiwalled carbon nanotubes with

different structural organisation," *Carbon*, vol. 43, no. 4, pp. 786–795, 2005.

[8] K. Le Van and T. T. Luong Thi, "Activated carbon derived from rice husk by NaOH activation and its application in supercapacitor," *Progress in Natural Science: Materials International*, vol. 24, no. 3, pp. 191–198, 2014.

[9] L. Muniandy, F. Adam, A. R. Mohamed, and E.-P. Ng, "The synthesis and characterization of high purity mixed microporous/mesoporous activated carbon from rice husk using chemical activation with NaOH and KOH," *Microporous and Mesoporous Materials*, vol. 197, pp. 316–323, 2014.

[10] S. Brunauer, P. H. Emmett, and E. Teller, "Adsorption of gases in multimolecular layers," *Journal of the American Chemical Society*, vol. 60, pp. 309–319, 1938.

[11] B. Lippens and J. H. de Boer, "Studies on pore systems in catalysts V. The t method," *Journal of Catalysis*, vol. 4, no. 3, pp. 319–323, 1965.

[12] E. P. Barrett, L. G. Joyner, and P. P. Halenda, "The determination of pore volume and area distributions in porous substances. I. Computations from nitrogen isotherms," *Journal of the American Chemical Society*, vol. 73, pp. 373–380, 1951.

[13] P. A. Webb and C. Orr, *Analytical Methods in Fine Particle Technology*, Micromeritics Instrument Corporation, Norcross, GA, USA, 1997.

[14] N. Rambabu, R. Azargohar, A. K. Dalai, and J. Adjaye, "Evaluation and comparison of enrichment efficiency of physical/chemical activations and functionalized activated carbons derived from fluid petroleum coke for environmental applications," *Fuel Processing Technology*, vol. 106, pp. 501–510, 2013.

[15] K. S. W. Sing, D. H. Everett, R. A. W. Haul et al., "Reporting physisorption data for gas/solid systems with special reference to the determination of surface area and porosity (Recommendations 1984)," *Pure and Applied Chemistry*, vol. 57, no. 4, pp. 603–619, 1985.

[16] H. Marsh and F. R. Reinoso, *Activated Carbon*, Elsevier, Amsterdam, Netherlands, 2006.

[17] A. Sirimuangjinda, K. Hemra, D. Atong, and C. Pechyen, "Comparison on pore development of activated carbon produced from scrap tire by potassium hydroxide and sodium hydroxide for active packaging materials," *Key Engineering Materials*, vol. 545, pp. 129–133, 2013.

[18] M. A. Lillo-Ródenas, D. Cazorla-Amorós, and A. Linares-Solano, "Understanding chemical reactions between carbons and NaOH and KOH," *Carbon*, vol. 41, no. 2, pp. 267–275, 2003.

[19] A. Linares-Solano, M. A. Lillo-Rodenas, J. P. Marco-Lozar, M. Kunowsky, and A. J. Romero-Anaya, "NaOH and KOH for preparing activated carbons used in energy and environmental application," *International Journal of Energy, Environment and Economics*, vol. 20, no. 4, pp. 59–91, 2012.

[20] J. Alcañiz-Monge and M. J. Illán-Gómez, "Insight into hydroxides-activated coals: chemical or physical activation?," *Journal of Colloid and Interface Science*, vol. 318, no. 1, pp. 35–41, 2008.

[21] Y. Guo, J. Qi, Y. Jiang, S. Yang, Z. Wang, and H. Xu, "Performance of electrical double layer capacitors with porous carbons derived from rice husk," *Materials Chemistry and Physics*, vol. 80, no. 3, pp. 704–709, 2003.

[22] S. Valizadeh, H. Younesi, and N. Bahramifar, "Highly mesoporous K_2CO_3 and KOH/activated carbon for SDBS removal from water samples: batch and fixed-bed column adsorption process," *Environmental Nanotechnology, Monitoring and Management*, vol. 6, pp. 1–13, 2016.

[23] A. Reffas, V. Bernardet, B. David et al., "Carbon prepared from coffee grounds by H_3PO_4 activation: characterization and adsorption of methylene blue and Nylosan Red N-2RBL," *Journal of Hazardous Materials*, vol. 175, no. 1-3, pp. 779–788, 2010.

[24] A. R. S. Neto, M. A. M. Araujo, F. V. D. Souza, L. H. C. Mattoso, and J. M. Marconcini, "Characterization and comparative evaluation of thermal, structural, chemical, mechanical and morphological properties of six pineapple leaf fiber varieties for use in composites," *Industrial Crops and Products*, vol. 43, pp. 529–537, 2013.

[25] D. An, Y. Guo, B. Zou, Y. Zhu, and Z. Wang, "A study on the consecutive preparation of silica powders and active carbon from rice husk ash," *Biomass and Bioenergy*, vol. 35, no. 3, pp. 1227–1234, 2011.

[26] M. A. Amaral Junior, J. T. Matsushima, M. C. Rezende, E. S. Gonçalves, J. S. Marcuzzo, and M. R. Baldan, "Production and characterization of activated carbon fiber from textile PAN fiber," *Journal of Aerospace Technology and Management*, vol. 9, no. 4, pp. 423–430, 2017.

[27] F. Tuinstra and J. L. Koenig, "Raman spectrum of graphite," *Journal of Chemical Physics*, vol. 53, no. 3, pp. 1126–1130, 1970.

[28] J. L. Figueiredo, M. F. R. Pereira, M. M. A. Freitas, and J. J. M. Órfão, "Modification of the surface chemistry of activated carbons," *Carbon*, vol. 37, no. 9, pp. 1379–1389, 1999.

[29] M. Lillorodenas, J. Juan-Juan, D. Cazorla-Amoros, and A. Linares-Solano, "About reactions occurring during chemical activation with hydroxides," *Carbon*, vol. 42, no. 7, pp. 1371–1375, 2004.

[30] M. Zhang, Y. Li, H. Si, B. Wang, and T. Song, "Preparation and electrochemical performance of coconut shell activated carbon produced by the H_3PO_4 activation with rapid cooling method," *International Journal of Electrochemical Science*, vol. 12, pp. 7844–7852, 2017.

[31] E. Frackowiak and F. Béguin, "Carbon materials for the electrochemical storage of energy in capacitors," *Carbon*, vol. 39, no. 6, pp. 937–950, 2001.

[32] S. Sarangapani, B. V. Tilak, and C.-P. Chen, "Materials for electrochemical capacitors," *Journal of The Electrochemical Society*, vol. 143, no. 11, pp. 3791–3799, 1996.

[33] T. Brouse, P.-L. Taberna, O. Crosnier et al., "Long-term cycling behavior of asymmetric activated carbon/MnO_2 aqueous electrochemical supercapacitor," *J. Power Sources*, vol. 173, no. 1, pp. 633–641, 2007.

Hindawi
Journal of Chemistry
Volume 2018, Article ID 3951540, 9 pages
https://doi.org/10.1155/2018/3951540

Research Article

Potential of Duckweed (*Lemna minor*) for the Phytoremediation of Landfill Leachate

M. K. Daud,[1,2] **Shafaqat Ali**,[3] **Zohaib Abbas**,[3] **Ihsan Elahi Zaheer**,[3] **Muhammad Ahsan Riaz**,[3] **Afifa Malik**,[4] **Afzal Hussain**,[3] **Muhammad Rizwan**,[3] **Muhammad Zia-ur-Rehman**,[5] **and Shui Jin Zhu**[1]

[1]*Department of Agronomy, College of Agriculture and Biotechnology, Zhejiang University, Zijingang Campus, Hangzhou 310058, China*
[2]*Department of Biotechnology and Genetic Engineering, Kohat University of Science and Technology, Kohat 26000, Pakistan*
[3]*Department of Environmental Sciences and Engineering, Government College University, Allama Iqbal Road, Faisalabad 38000, Pakistan*
[4]*Sustainable Development Study Center, Government College University, Lahore, Pakistan*
[5]*Institute of Soil & Environmental Sciences, University of Agriculture, Faisalabad, Pakistan*

Correspondence should be addressed to Shafaqat Ali; shafaqataligill@gcuf.edu.pk and Shui Jin Zhu; shjzhu@zju.edu.cn

Received 9 May 2018; Revised 8 October 2018; Accepted 22 October 2018; Published 2 December 2018

Guest Editor: Gassan Hodaifa

Phytoextraction of zinc, copper, lead, iron, and nickel from landfill leachate by duckweed (*L. minor*) was investigated every 3 days over a period of 2 weeks. Bioconcentration factor and removal efficiency were also calculated. Results of this study proved that *L. minor* significantly reduced the concentration of heavy metals in landfill leachate. Removal efficiency of *L. minor*, for all the metals, from landfill leachate was more than 70% with the maximum value for copper (91%). Reduction in chemical oxygen demand (COD) and biological oxygen demand (BOD) was observed by 39% and 47%, respectively. However, other physiochemical parameters like pH, total suspended solids, (TSS) and total dissolved solids (TDS) were reduced by 13%, 33%, and 41%, respectively. The value of bioconcentration factor (BCF) was less than 1 with the maximum figure for copper (0.84) and lead (0.81), showing that the plant is a moderate accumulator for these heavy metals. Duckweed (*L. minor*) appeared as a sustainable alternative candidate and is recommended for the treatment of landfill leachate waste water contaminants.

1. Introduction

Ever-increasing population and expansion of industrial activities along with changing lifestyle gave rise to exponential generation of solid waste over the last few years [1]. Therefore, management of municipal solid waste is of utmost importance under current scenario [2]. Feasible and ideal options for the management of municipal solid waste (MSW) at low cost are hard to decide because of diverse considerations [3]. Landfilling is the most acceptable management option for waste disposal in Third World countries. Technical feasibility, low operational cost, less supervision, and simplicity make landfilling the most preferred method for the management of MSW [4]. Degradation of solid waste takes place due to physicochemical changes occurring in the solid waste and matrix of the landfill soil. Landfill leachate, assisted by rainwater and biochemical, physical, and chemical reactions, percolates all the way through the matrix of solid waste. Quality and quantity of leachate depends upon the weather discrepancies, age of landfill, precipitation, and amount/type of solid waste composition [5]. While passing through the waste mass, leachate is polluted with toxic substances and heavy metals [6]. In leachate, the major sources of toxic metals are electronic waste, dyes, pesticides, batteries, and fluorescent lamps [7].

Heavy metal solubility and mobility is highly dependent on the age of landfill, pH, and ratio of organic and inorganic substances [8]. Acid formation at low pH is considered as the most deliberate phase which boosts up the occurrence of

high concentration of toxic metals in landfill leachate [9]. Heavy metals are among the major environmental contaminants because of their toxic effects, ability to accumulate in the aquatic system, and nonbiodegradable nature [10]. Landfill leachate is thus regarded as a major environmental hazard which pollutes the surrounding environment affecting local biota, groundwater, and other aquatic systems [5]. Similarly presence of organic parameters like BOD, COD, and pH are also among complicated parameters in landfill leachate. Higher fractions of these organics are primarily more challenging as they are less biodegradable in nature and have selective toxicity for biological process [11]. Hence, selection of suitable methods for the treatment of the landfill leachate, before its final disposal into any water body, is an important step to avoid the environmental degradation.

Traditional heavy metals remediation techniques like ion exchange, filtration, and adsorption are not cost effective and may adversely affect the aquatic ecosystem [12]. Use of plants in purification process is called phytoremediation, and it has gained attention as a suitable option for the treatment of landfill leachate [6, 13]. In case of heavy metals, phytoremediation is a self-sustaining and economical alternative treatment technology [14]. During the last two decades, phytoremediation has attained substantial significance and the discovery of hyperaccumulator plants made it more promising because of their ability to accumulate high amount of heavy metals in aerial parts of the body [15, 16]. Ideally, the plants used for phytoremediation should have the ability to produce high biomass, survive in extremely toxic environment, and accumulate the contaminants in high concentration. Degradation of different contaminants depends upon the selection of phytoremediation technique and type of the particular contaminants [17]. Plants act as host for endophytic bacteria by providing nutrients and offering protection against physical environment. These symbiotic relations promote the growth and competitiveness of plants to respond to the external stresses such as nutrients and heavy metals [18].

Recent studies have described some aquatic plant species best suited for the remediation of heavy metals like Cu, Zn, Fe, Cd, Pb, Cr, Hg, and Ni [19, 20]. Aquatic plants like *Eichhornia crassipes*, *Azolla filiculoides*, *Pistia stratiotes*, *Hydrilla verticillata*, *Typha domingensis*, *Salvinia Cucullata*, *Azolla caroliniana*, *Azolla pinnata*, *Lemna minor*, *Lemna aequinoctialis*, *Lemna gibba*, and *Spirodela polyrhiza* are suitable aquatic plants for the removal of heavy metals as reported by several researchers [21–27]. Aquatic plants play a vital role in harmonizing the water bodies. They naturally have the tendency to treat different wastewater streams including landfill leachate [28]. Duckweed (*L. minor*) is an aquatic plant that belongs to the family Lemnaceae. Owing to rapid growth rate, cold tolerance, ease of harvesting, and cost effectiveness, *Lemna minor* is a much better candidate than other aquatic plants for phytoextraction of heavy metals [29]. Duckweed has been reported to be very effective in the phytoextraction of organic matter, suspended solids, heavy metals, and soluble salts from wastewater [30]. In wastewater treatment studies, *L. minor* is used for the monitoring of heavy metals [31]. In this study, phytoremediation potential of duckweed (*L. minor*), for the treatment of landfill leachate, was evaluated for 15 days. Heavy metal content and physiochemical parameters of landfill leachate were investigated.

2. Materials and Methods

2.1. Collection of Leachate. Raw samples of landfill leachate (LL) were randomly collected from three different points under normal weather conditions from Mehmood Booti landfill site. Mehmood Booti landfill site (Lahore, Pakistan) is located in the north side of Bund road (latitude: 31.610°N, longitude: 74.382°E) approximately 1 kilometer away from river Ravi. Leachate was collected and stored in 1000 ml plastic cans. Temperature and pH of the samples were recorded in situ with the help of a portable pH meter (Hanna HI 2210). Samples of landfill leachate were then immediately transferred to the laboratory and stored at 4°C before going for further analysis. Physiochemical parameters and heavy metal contents were analyzed according to the standard methods for the examination of water and wastewater, unless otherwise stated [32].

2.2. Collection of Plant Sample. Samples of duckweed (*L. minor*) were collected from fresh water ponds at the Fisheries Research and Training Institute, Lahore (31.5890°N, 74.4642°E). Plants were carefully washed with water to remove the insect larvae and epiphytes. Plant samples were put into the plastic jar, filled with water, for one week to acclimatize with the existing environment. After that, plants of the same size were collected for the research experimentation. Samples of landfill leachate and *Lemna minor* were collected in the month of July 2016.

2.3. Experimental Setup. One set of experimental containers, having three tubs, was arranged. Each experimental container was filled with 20 L landfill leachate and 200 g fresh weight of duckweed. Experiment was conducted in triplicate to attain the average efficiency of the plant, and the study was performed in the month of November. The mean daily temperature during the study was 23 ± 5°C, while daily average humidity was 72 ± 15% at the experimental site. Test duration was 0, 3, 6, 9, 12, and 15 days (total 6 observations with pretreatment data).

2.4. Heavy Metal Estimation in Leachate and Plant Samples. Plant samples were washed thoroughly before they were oven dried at 70°C. After complete drying, plant samples were crushed and sieved to < 1 mm. Plant samples (0.25 g each) were digested with diacid (HNO_3-$HCLO_4$) by gradually increasing the temperature. After complete digestion, distilled water was added in the sample to make the final volume up to 50 ml. Heavy metal (Zn, Pb, Fe, Cu, and Ni) contents were determined in both plant and leachate samples using the atomic absorption spectrophotometer (AAS) (Z-8230).

2.5. Calculation. Uptake of heavy metals by the plant was calculated using the dilution factor as follows:

$$\text{dilution factor} = \frac{\text{total volume of sample (ml)}}{\text{weight of the plant (g)}}. \quad (1)$$

Percentage efficiency was calculated by determining the initial (C0) and final concentration (C1) of metals in the sample as described previously [33]:

$$\text{Removal percentage} = \frac{C0 - C1}{C0} * 100, \quad (2)$$

where C0 and C1 are the initial and final concentration of the metal in the medium $(\text{mg} \cdot \text{L}^{-1})$.

The bioconcentration factor was calculated as described previously [34]:

$$\text{BCF} = \frac{\text{metal concentration in plant } \left(\text{mg} \cdot \text{kg}^{-1}\right)}{\text{metal concentration in medium } \left(\text{mg} \cdot \text{L}^{-1}\right)}. \quad (3)$$

2.6. Statistical Analysis. Data presented in this paper are the mean of three replicates ± SD. Analysis of variance (ANOVA) and graphical representation were performed with GraphPad prism5 software followed by Tukey's test to get the significant difference between different mean values.

3. Results and Discussion

3.1. Physiochemical Parameters. Results of the phytoremediation potential study on *Lemna minor* are given in Table 1. pH of landfill leachate reduced from its initial value (7.9) to the final value of (6.8) by the end of 15-day experiment as depicted in Table 1. Duckweed (*L. minor*) has the potential to survive under a wide range of pH, i.e., 4.5 to 7.5 [35]. Values of TSS and TDS were 63.5 $\text{mg} \cdot \text{L}^{-1}$ and 1695 $\text{mg} \cdot \text{L}^{-1}$, respectively, in landfill leachate. As demonstrated in Table 1, concentration of TSS was reduced with the passage of time, reaching the minimum level of 42 $\text{mg} \cdot \text{L}^{-1}$ at the end of the experiment. Results regarding the reduction of TSS were in line with a previous study that reported a noticeable decline in resuspension of TSS in Taiho lake, covered with aquatic plants during the experimental period of 41 days [35]. Meanwhile, the least value of TDS, i.e., 986 $\text{mg} \cdot \text{L}^{-1}$, was recorded after the 15-day experimental period. This reduction in the TDS is attributed to the plants' capacity to absorb inorganic and organic ions. The values of COD and BOD in landfill leachate were also higher than the permissible limit set by NEQS [36]. The high level of COD reveals the presence of organic contaminants and intense load of heavy metals. Both, COD and BOD showed a gradual decrease during the experiment. Results revealed that *L. minor* successfully reduced COD by 39% (from 1899 to 756 $\text{mg} \cdot \text{L}^{-1}$) and BOD by 47% (from 889 to 423 $\text{mg} \cdot \text{L}^{-1}$). In agreement with the results of present research, Azeez and Sabbar [37] also reported a 32.7% and 49.6% decline in COD and BOD, respectively, during a 4-week phytoremediation study on oil refinery by *Lemna minor*. Similarly, Zimmo et al. [38] reported a more efficient reduction in BOD of duckweed-based ponds than that of algal-based ones.

3.2. Heavy Metal Removal from Leachate. Results on removal of heavy metals (Zn, Pb, Fe, Cu, and Ni) through phytoremediation of landfill leachate by *Lemna minor* at different time periods of exposure are shown in Figures 1–5. Reduction in concentration of heavy metals in landfill leachate depends upon the duration of exposure to *L. minor*. Zinc concentration of leachate was reduced from 1.47 $\text{mg} \cdot \text{L}^{-1}$ to 0.024 $\text{mg} \cdot \text{L}^{-1}$ during 15-day experiment. Initial concentration of lead was 0.83 $\text{mg} \cdot \text{L}^{-1}$ in the landfill leachate in which significant decrease ($p < 0.05$) was observed during the first 9 days, following a negligible change thereafter till the end of the experiment. A similar response of iron was observed as its initial concentration (1.17 $\text{mg} \cdot \text{L}^{-1}$) was significantly reduced to 0.26 $\text{mg} \cdot \text{L}^{-1}$ at the end of the experiment. Concentration of copper considerably declined from 0.69 to 0.06 $\text{mg} \cdot \text{L}^{-1}$ in landfill leachate ($p < 0.01$). Concentration of nickel also significantly reduced ($p < 0.05$) from 1.21 $\text{mg} \cdot \text{L}^{-1}$ to 0.29 $\text{mg} \cdot \text{L}^{-1}$ after phytoremediation through *Lemna minor* as described in Figure 5. Overall, *Lemna minor* exhibited a great ability to remove all the heavy metals under study from the landfill leachate. The higher potential of *L. minor* to remove metals from leachate is attributed to huge biomass production and efficient growth in the highly metal-polluted environment [39].

3.3. Removal Efficiency. The present study demonstrates that metal removal efficiency of *L. minor* from landfill leachate was more than 70 to 90% (Figure 6). The maximum efficiency (91 %) of *L. minor* was observed for the removal of copper from leachate. Removal efficiency for Pb, Zn, Fe, and Ni was 78, 83, 77, and 76%, respectively. A previous study reported that *L. minor* removed 76% lead and 82% nickel from the contaminated solution under laboratory conditions [25]. Metal removal efficiency of *L. minor* was in the following order: Cu (91%) > Zn (83%) > Pb (78%) > Fe (77%) > Ni (76%). Similar results for heavy-metal removal efficiency were also reported by other researchers [21, 40]. Results of a previous study reported that that removal efficiency of *L. minor* was 58%, 62%, and 68% for copper, lead, and nickel, respectively [41]. Similarly, *L. minor* removes nickel by 74 % and lead by 79% from the industrial wastewater stream [42].

3.4. Accumulation of Heavy Metals. Heavy metal accumulation in dry biomass of plants is dependent on concentration of metals and duration of the experiment [43]. Accumulation of zinc was highest on the 6th day, following a gradual decrease with time (Figure 1). Concentration of zinc in *L. minor* was recorded as 1.15, 1.17, 0.99, 0.95, and 0.93 $\text{mg} \cdot \text{kg}^{-1}$ after 3, 6, 9, 12, and 15 days of exposure, respectively. Similarly, in a previous study, *L. minor* was reported to accumulate higher amount of zinc as compared to *L. gibba* [44]. Zinc is an essential trace element which plays an important role in the growth and development of plants. Zinc is a most commonly found element in several enzymes

Table 1: Physicochemical characteristics of landfill leachate before and after phytoremediation experiment.

Parameters	Before phytoremediation	After phytoremediation *Lemna minor* L.	Percentage reduction	NEQS permissible limit
pH mg·L^{-1}	7.9	6.8 ± 0.24 ns	13%	6–10
TSS mg·L^{-1}	63.4	42.2 ± 3.56 ns	33%	150
TDS mg·L^{-1}	1695	986 ± 7.68 ns	41%	3500
COD mg·L^{-1}	1899	756 ± 4.32 ns	39%	150
BOD mg·L^{-1}	889	423 ± 4.69*	47%	80
Zn mg·L^{-1}	1.47	0.24 ± 0.02*	83%	5
Pb mg·L^{-1}	0.83	0.18 ± 0.04*	78%	0.5
Cu mg·L^{-1}	0.69	0.06 ± 0.02**	91%	1
Fe mg·L^{-1}	1.17	0.26 ± 0.03*	77%	2
Ni mg·L^{-1}	1.21	0.29 ± 0.02*	76%	1

Values are the mean of three replicates. NIQS, National Environment Quality Standards, Pakistan; ND, not detected; ns, nonsignificant. *,**significantly different at $p < 0.05$ or $p < 0.01$ level of ANOVA, respectively (mean ± SD, $n = 3$).

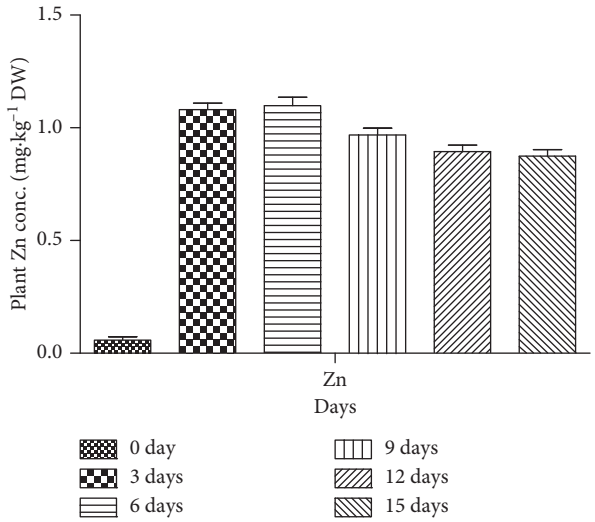

Figure 1: Zinc concentration in *L. minor* at different exposure time (days) from leachate. Bars represent standard deviation. Values are mean ± SD of three replicates.

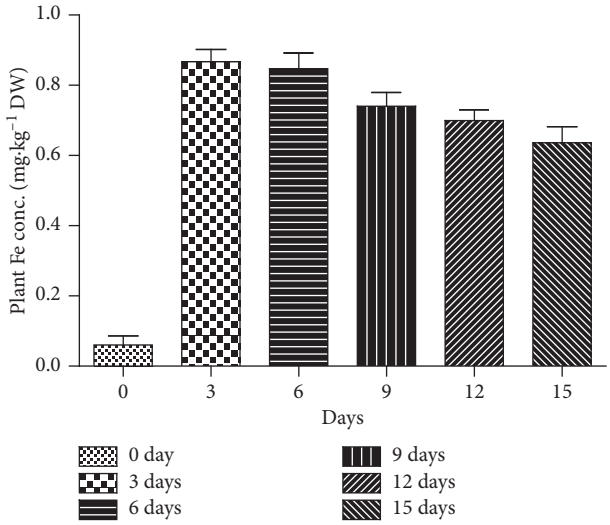

Figure 3: Iron concentration in *L. minor* at different exposure time (days) from leachate. Bars represent standard deviation. Values are mean ± SD of three replicates.

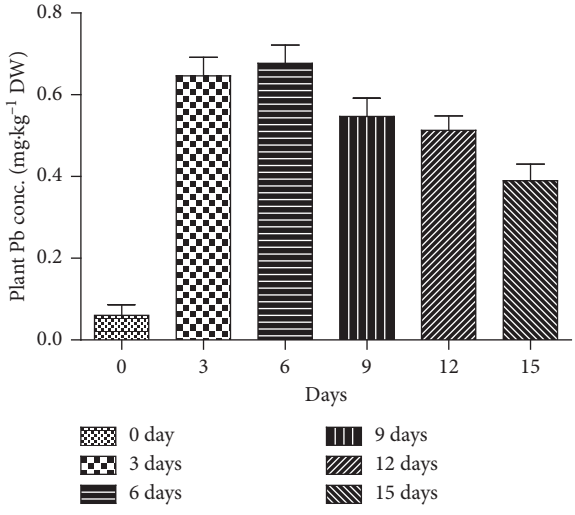

Figure 2: Lead concentration in *L. minor* at different exposure time (days) from leachate. Bars represent standard deviation. Values are mean ± SD of three replicates.

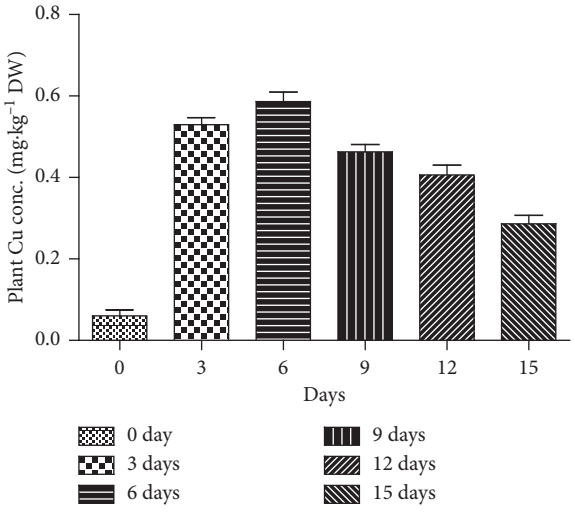

Figure 4: Copper concentration in *L. minor* at different exposure time (days) from leachate. Bars represent standard deviation. Values are mean ± SD of three replicates.

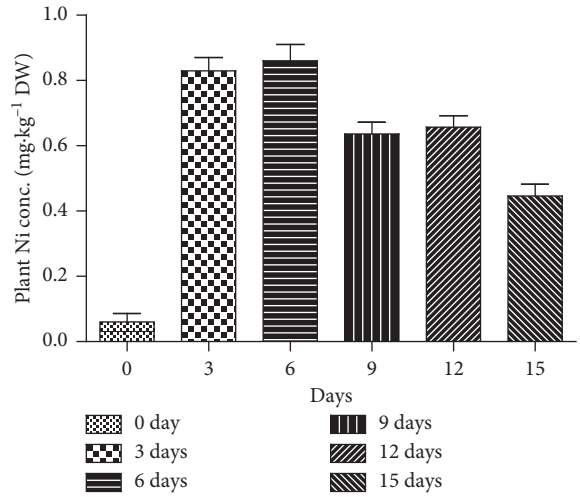

Figure 5: Nickel concentration in *L. minor* at different exposure time (days) from leachate. Bars represent standard deviation. Values are mean ± SD of three replicates.

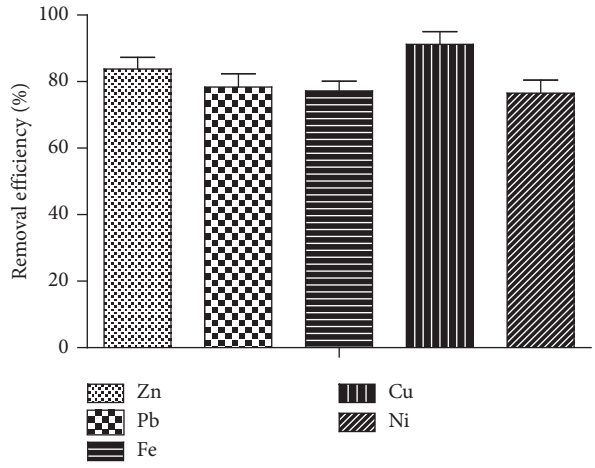

Figure 6: Percentage removal efficiency by *L. minor* for landfill leachate wastewater. Bars represent standard deviation. Values are mean ± SD of three replicates.

such as cytochrome oxides, polyphenol oxides, and ascorbic acid oxides [45, 46]. Upon absorption by plants, Zn is transformed from insoluble to soluble state (Zn^{2+}) which ultimately enhances the capacity of the aquatic plant to accumulate higher amount of Zn in their body [47]. Plants accumulated maximum concentration of lead on the 6th day of the experiment, after which minor changes occurred till the end of the experiment. Highest lead accumulation was 0.68 mg·kg^{-1} on day 6, while the least 0.39 mg·kg^{-1} was observed on day 15 (Figure 2). Similar observations for the accumulation of lead by *L. minor* were also recorded by Singh et al. [19]. *L. minor* also accumulated Pb at the rate of 561 mg·kg^{-1} dry weight (dw) on day 7 of the experiment at 50 mg·L^{-1} concentration in the growth medium [48].

The results of this study demonstrated that accumulation of Pb increased with the increase in concentration and duration of exposure. Results for accumulation of Pb are in line with the earlier studies on different aquatic plants like *Wolffia arrhiza*, [49] *Najas indica*, [50] *C. demersum*, [51] *Lemna minor*, and *Lemna gibba* [52]. Uptake of iron by *L. minor* was increased gradually till the 12th day of experiment and exhibited a declining trend thereafter. Accumulation of iron on days 3 and 9 of the experiment was 0.87 and 0.74 mg·kg^{-1}, respectively. It was reduced to 0.64 mg·kg^{-1} by the end of the treatment (Figure 3). Iron, at the same time, is equally important for the growth and development of plants. Uptake of Fe is crucial for the metabolism of chloroplast and mitochondria. Mostly iron exists in the form of less soluble ferric oxides, which becomes free of oxides at low pH and is converted to readily available form of Fe for the plants to uptake [53].

From the leachate, plants accumulated highest concentration of copper at the start of the experiment till day 9, followed by no significant increase in its accumulation. Maximum accumulation (0.58 mg·kg^{-1}) was recorded on day 6 of the experiment (Figure 4). Copper is an essential micronutrient and plays a vital role in the growth and development of plants [54, 55]. Plants regulate the intercellular copper level by rectifying its uptake and declining the free intercellular copper concentrations by metallochaperones. These are Cu-binding soluble proteins which transport it to the sections of the plant cells where they are needed the most [56]. During the study, maximum concentration of nickel accumulated on days 3 and 6 of the experiment. Its concentration was 0.83 and 0.86 and 0.64 mg·kg^{-1} on days 3, 6, and 9, respectively. Nickel promoted the growth and development of *Lemna minor* fronds when applied at the rate of 0.5 mg·L^{-1} [57]. *Lemna minor* absorbed nickel more proficiently as compared with lead [24]. *L. minor* removed 65, 72 and 87% Ni at different initial concentrations during a twenty-two-day experimental study [58]. Similar result was also reported where *L. Minor* accumulated more Ni as compared to *L. gibba* after 80 days of exposure [59]. Results of the present study, for the accumulation of nickel, are in agreement with the earlier reports [60–62]. The accumulation of heavy metals by *L. minor* was in order of Cu (0.84 mg·kg^{-1}) > Pb (0.68 mg·kg^{-1}) > Zn (1.17 mg·kg^{-1}) > Fe (0.87 mg·kg^{-1}) > Ni (0.86 mg·kg^{-1}) from the landfill leachate.

Accumulation of heavy metals by the whole plant is depicted in Figure 7. Results obtained from the present study revealed that the uptake of metal by plants was dependent upon their initial concentration in the wastewater. Findings of this study were in line with those of Axtell et al. [24]. Similarly, *L. minor* showed a significant phytoremediation potential by accumulating more than 90% of Fe, Zn, and Cu with different concentrations at different time periods [63]. Analysis of variance showed significant uptake ($p < 0.05$) of all heavy metals from landfill leachate during the experimental study.

3.5. Bioconcentration Factor for Heavy Metals. Bioconcentration factor is expressed as the ratio of the concentration of heavy metals absorbed by plant tissues to that in the medium [34]. Bioconcentration factor (BCF) is considered as a blueprint for the determination of metal uptake effectiveness by aquatic plants [64]. Bioconcentration

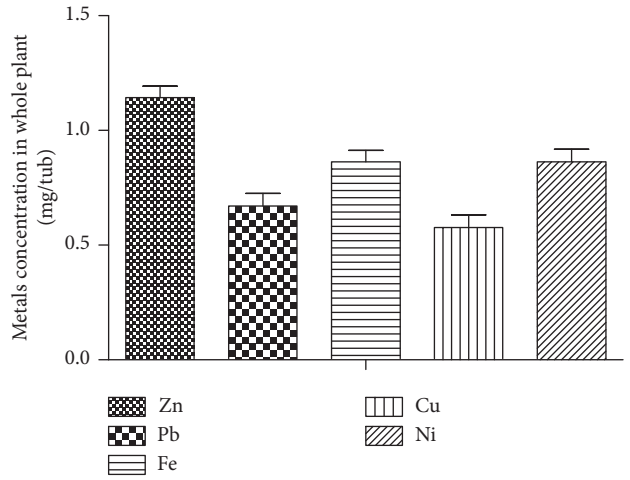

Figure 7: Metal concentration in whole plant (mg/tub). Bars represent standard deviation. Values are mean ± SD of three replicates.

factor values, for the accumulation of heavy metals by *L. minor* at different exposure time periods, are given in Table 2. The maximum BCF value for zinc was 0.78 and 0.81 on the 3rd and 6th day of the experiment, respectively. The bioconcentration value for lead increased progressively and attained the maximum level (0.81) on the 6th day of the experiment. From landfill leachate, BCF value for iron was the highest one on the 3rd and 6th day of experiment. BCF value for copper was 0.76, 0.84, 0.68, 0.65, and 0.42 on day 3, 6, 9, 12, and 15 of the experiment, respectively. Maximum BCF value (0.71) for nickel was observed on 6th day of the experiment. Results indicate that *L. minor*, grown on the landfill leachate, showed maximum BCF values for copper, lead, and zinc. BCF values of heavy metals by *L. minor* were in the order of Cu (0.84) > Pb (0.81), Zn (0.81) > Fe (0.74) > Ni (0.71). Similarly, BCF values for Cu, Ni, Pb, and Cd were also found to be less than one by *L. minor* from two different kinds of effluents in a hydroponic experiment for 31 days [61]. In another study, *L. minor* came out as an excellent accumulator for Fe, Zn, and Cu having the BCF value more than 1 from different lakes in south Urals region, Russia [65].

According to previous studies, different floating aquatic plants demonstrated much higher accumulation for these heavy metals with higher bioconcentration factor. Roots of *Eichhornia crassipes* and *Pistia stratiotes* showed much better metal accumulation potential as compared to the upper parts of the plants. In this study, values of bioconcentration factor for Zn, Cu, and Pb were more than 1 in both aquatic plants [66]. Physiological demand of plant tissues for certain heavy metals and their accumulation kinetics directly or indirectly affects their absorption from the growth medium [67]. The value of BCF more than 1 indicates the suitability of certain aquatic plants (i.e., hyperaccumulators) for phytoextraction of heavy metals. In the current study, the BCF values of *L. minor* for all the heavy metals were found to be lower than 1. The results suggest that *L. minor* is a moderate accumulator for Zn, Cu, Pb, Ni, and Cu under given circumstances of the present study.

Table 2: Bioconcentration factor for *L. minor* for heavy metals at different exposure time periods from landfill leachate.

Sample metal	Exposure time (days)				
	3	6	9	12	15
Zn	0.78	0.81	0.46	0.29	0.27
Pb	0.46	0.81	0.41	0.37	0.29
Fe	0.63	0.60	0.44	0.41	0.30
Cu	0.76	0.84	0.68	0.65	0.42
Ni	0.58	0.71	0.37	0.34	0.25

4. Conclusion

The present study concluded that landfill leachate was loaded with both organic and inorganic pollutants. Phytoremediation experiment of landfill leachate using *L. minor* was found to be efficient for the reduction of both organic and inorganic pollutants. The reduction in pH, TSS, TDS, COD, BOD, Zn, Pb, Fe, Cu, and Ni was recorded during 15 days phytoremediation experiment using *L. minor*. The rate of removal was accelerated from the 3rd to 9th day of the experiment. Accumulation of heavy metals was directly proportional to their initial concentration in landfill leachate. Removal efficiency for all the metals was higher than 70%. Among 5 metals under study, the accumulation of copper in *L. minor* was the highest one. The highest BCF values were shown by copper (0.84) and lead (0.81). Plants demonstrate extensive ability to remove heavy metals from landfill leachate. High removal efficiency and accumulation capacity of *L. minor* for heavy metals indicate its phytoremediation potential. This study provides a deep insight into the potential of duckweed (*L. minor*) to be used as a convenient and economically feasible method for the phytoremediation of metal-polluted aquatic environment on large-scale basis.

Data Availability

The data used to support the findings of this study are included within the article.

Conflicts of Interest

The authors declare that they have no conflicts of interest regarding the publication of this article.

Acknowledgments

This work was funded by the National Key Technology R&D program of China (2016YFD0101404), the National Natural Science Fund (31501342), China Agriculture Research System (CARS-18-25), and Jiangsu Collaborative Innovation Center for Modern Crop Production.

References

[1] F. N. Ahmed and C. Q. Lan, "Treatment of landfill leachate using membrane bioreactors: a review," *Desalination*, vol. 287, pp. 41–54, 2012.

[2] C. O. Akinbile, M. S. Yusoff, and A. Z. Ahmad Zuki, "Landfill leachate treatment using sub-surface flow constructed wetland by *Cyperus haspan*," *Waste Management*, vol. 32, no. 7, pp. 1387–1393, 2012.

[3] M. Umar, H. Aziz, and M. S. Yusoff, "Trends in the use of Fenton, electro-Fenton and photo-Fenton for the treatment of landfill leachate," *Waste Management*, vol. 30, no. 11, pp. 2113–2121, 2010.

[4] S. Renou, J. Givaudan, S. Poulain, and M. P. Dirassouyan, "Landfill leachate treatment: review and opportunity," *Journal of Hazardous Material*, vol. 150, no. 3, pp. 468–493, 2008.

[5] A. A. Abbas, G. Jingsong, L. Z. Ping, Y. Y. Pan, and W. S. Al-Rekabi, "Review on landfill leachate treatments," *American Journal of Applied Sciences*, vol. 6, no. 4, pp. 672–684, 2009.

[6] D. L. Jones, K. L. Williamson, and A. G. Owen, "Phytoremediation of landfill leachate," *Waste Management*, vol. 26, no. 8, pp. 825–837, 2006.

[7] M. L. Ward, G. Bitton, and T. Townsend, "Heavy metal binding capacity (HMBC) of municipal solid waste landfill leachate," *Chemosphere*, vol. 60, no. 2, pp. 206–215, 2005.

[8] S. Bozkurt, L. Moreno, and I. Neretnieks, "Long term processes in waste deposits," *Science of the Total Environment*, vol. 250, no. 1–3, pp. 101–121, 2000.

[9] A. S. Erses and T. T. Onay, "In situ heavy metal attenuation in landfills under methanogenic conditions," *Journal of Hazardous Marterial, Part B*, vol. 99, no. 2, pp. 159–175, 2003.

[10] P. Censi, S. E. Spoto, F. Saiano et al., "Heavy metals in coastal water system. A case study from the Western Gulf of Thailand," *Chemosphere*, vol. 64, no. 7, pp. 1167–1176, 2006.

[11] M. Topal, B. Karagözoğlu, and E. Öbek, "Planted batch system treating leachate," *Nevşehir University Journal of Science and Technology*, vol. 1, no. 2, pp. 87–97, 2012.

[12] P. K. Rai, "Heavy metal pollution in aquatic ecosystems and its phytoremediation using wetland plants: an eco-sustainable approach," *International Journal of Phytoremediation*, vol. 10, no. 2, pp. 133–160, 2008.

[13] K. R. Kim and G. Owens, "Potential for enhanced phytoremediation for landfills using biosolids—a review," *Journal of Environmental Management*, vol. 91, no. 4, pp. 791–797, 2010.

[14] R. Chandra and S. Yadav, "Phytoremediation of Cd, Cr, Cu, Mn, Fe, Ni, Pb and Zn from aqueous solution using *Phragmites cummunis*, *Typha angustifolia* and *Cyperous esculentus*," *International Journal of Phytoremediation*, vol. 13, no. 6, pp. 580–591, 2011.

[15] P. Miretzky, A. Saralegui, and A. F. Cirell, "Aquatic macrophytes potential for the simultaneous removal of heavy metals," *Chemosphere*, vol. 57, no. 8, pp. 997–1005, 2004.

[16] M. A. Rahman and H. Hasegawa, "Aquatic arsenic: phytoremediation using floating macrophytes," *Chemosphere*, vol. 83, no. 5, pp. 633–646, 2011.

[17] E. P. Smits and M. Pilon, "Phytoremediation of metals using transgenic plants," *Crititcal Reviews in Plant Sciences*, vol. 21, no. 5, pp. 439–456, 2002.

[18] L. Marchand, M. Mench, D. L. Jacob, and M. L. Otte, "Metal and metalloid removal in constructed wetlands, with emphasis on the importance of plants and standardized measurements: a review," *Environment Pollution*, vol. 158, no. 12, pp. 3447–3461, 2010.

[19] D. Singh, R. Gupta, and A. Tiwari, "Potential of duckweed (*Lemna minor*) for removal of lead from wastewater by phytoremediation," *International Journal of Food Science and Technology*, vol. 2, no. 1, pp. 10–26, 2012.

[20] P. J. C. Favas and J. Pratas, "Uptake of uranium by native aquatic plants: potential for bioindication and phytoremediation," *E3S Web of Conferences*, vol. 1, p. 13007, 2013.

[21] V. C. Pandey, "Phytoremediation of heavy metals from fly ash pond by *Azolla caroliniana*," *Ecotoxicology and Environmental Safety*, vol. 82, pp. 8–12, 2012.

[22] A. Sood, P. L. Uniyal, R. Prasanna, and A. S. Ahluwalia, "Phytoremediation potential of aquatic macrophyte, Azolla," *AMBIO*, vol. 41, no. 2, pp. 122–137, 2012.

[23] A. L. Charles, S. J. Markich, and P. Ralph, "Toxicity of uranium and copper individually, and in combination, to a tropical freshwater macrophyte (*Lemna aequinoctialis*)," *Chemosphere*, vol. 62, no. 8, pp. 1224–1233, 2006.

[24] N. R. Axtell, S. P. K. Sternberg, and K. Claussen, "Lead and nickel removing using *Microspora* and *Lemna minor*," *Bioresource Technology*, vol. 89, no. 1, pp. 41–48, 2003.

[25] X. Zhang, Y. Hu, Y. Liu, and B. Chen, "Arsenic uptake, accumulation and phytofiltration by duckweed (*Spirodela polyrhiza* L.)," *Journal of Environmental Science*, vol. 23, no. 4, pp. 601–606, 2011.

[26] T. O. Ajayi and A. O. Ogunbayio, "Achieving environmental sustainability in wastewater treatment by phytoremediation with water hyacinth (*Eichhornia crassipes*)," *Journal of Sustainable Development*, vol. 5, no. 7, pp. 1–11, 2012.

[27] A. F. A. Baker, I. Yusoff, N. T. Fatt, F. Othman, and M. A. Ashraf, "Arsenic, zinc, and aluminium removal from gold mine wastewater effluents and accumulation by submerged aquatic plants (*Cabomba piauhyensis, Egeria densa*, and *Hydrilla verticillata*)," *BioMed Research International*, vol. 2013, Article ID 890803, 7 pages, 2013.

[28] M. Topal, B. Karagözoğlu, and E. Öbek, "Natural treatment of leachate," *Afyon Kocatepe University Journal of Sciences*, vol. 11, no. 2, pp. 1–16, 2011.

[29] W. A. El-Kheir, G. İsmail, F. A. El-Nour, T. Tawfik, and D. Hammad, "Assesment of the efficiency of duckweed (*Lemna gibba*) in wastewater treatment," *International Journal of Agriculture and Biology*, vol. 9, pp. 681–687, 2007.

[30] S. Radic, D. Stipanicev, P. Cvjetko et al., "Ecotoxicological assessment of industrial effluentusing duckweed (*Lemna minor* L.) as a test organism," *Ecotoxicology*, vol. 19, no. 1, pp. 216–222, 2010.

[31] APHA, *Standard Methods for the Examination of Water and Wastewater*, American Public Health Association/American Water Works Association/Water Environment Federation, Washington, DC, USA, 21st edition, 2005.

[32] P. Tanhan, M. Kruatrachue, P. Pokethitiyook, and R. Chaiyarat, "Uptake and accumulation of cadmium, lead and zinc by Siam weed (*Chromolaena odorata* L. King & Robinson)," *Chemosphere*, vol. 68, no. 2, pp. 323–329, 2007.

[33] A. Zayed, S. Gowthaman, and N. Terry, "Phytoaccumulation of trace elements by wetland plants: I. Duckweed," *Journal of Environmental Quality*, vol. 27, no. 3, pp. 715–721, 1998.

[34] S. Saygideger, "*Lemna gibba* L.ve *Lemna minor* L.(Lemnaceae)' nin morfolojik anatomk, ekolojikve," *Fizyzolojik Ozellikleri.Ekoloji*, vol. 18, pp. 8–11, 1996.

[35] P. Huang, B. Han, and Z. Lin, "Floating-leaved macrophyte (*Trapa quadrispinosa* Roxb) beds have significant effects on sediment Resuspension in lake Taiho, China," *Hydrobiologia*, vol. 581, no. 1, pp. 189–193, 2007.

[36] National Environmental Quality Standards (NEQS), *Pakistan Environmental Legislation, Ministry of Environment, Government of Pakistan*, National Environmental Quality Standards (NEQS), Pakistan, 2000.

[37] N. M. Azeez and A. A. Sabbar, "Efficiency of duckweed (*Lemna minor* L.) in phytotreatmen of wastewater pollutants from basrah oil refinery," *Journal of Applied Phytotechnology in Environmental Sanitation*, vol. 1, no. 4, pp. 163–172, 2012.

[38] O. R. Zimmo, N. P. Van Der Steen, and H. J. Gijzen, "Effect of organic surface load on process performance of pilot scale Algae and duckweed based waste stabilization ponds," *Journal of Environmental Engineering*, vol. 131, no. 4, pp. 587–594, 2005.

[39] C. Mant, S. Costa, J. Williams, and E. Tambourgi, "Phytoremediation of chromium by model constructed wetland," *Bioresource Technology*, vol. 97, no. 15, pp. 1767–1772, 2007.

[40] Z. Leblebici and A. Aksoy, "Growth and lead accumulation capacity of *Lemna minor* and *Spirodela polyrrhiza (Lemnaceae)*: interactions with nutrient enrichment," *Water, Air, and Soil Pollution*, vol. 214, no. 1–4, pp. 175–184, 2011.

[41] A. Loveson and R. Sivalingam, "Aquatic macrophyte *Spirodela polyrrhiza* as a phytoremediation tool in polluted wetland water from Eloor, Ernakulam District, Kerala," *Journal of Environmental Analytical Toxicology*, vol. 5, no. 1, pp. 51–58, 2013.

[42] M. S. Al-Khafaji, F. H. Al-Ani, and A. F. Ibrahim, "Removal of some heavy metals from industrial wastewater by *Lemna minor*," *KSCE Journal of Civil Engineering*, vol. 22, no. 4, pp. 1077–1082, 2017.

[43] V. Mazzei, G. Longo, M. V. Brundo, C. Copat, G. OliveriConti, and M. Ferrante, "Effects of heavy metal accumulation on some reproductive characters in *Armadillidium granulatum* Brandt (Crustacea, Isopoda, Oniscidea)," *Ecotoxicology and Environmental Safety*, vol. 98, pp. 66–73, 2013.

[44] E. Lahive, J. Michael, A. O'Callaghan, A. Marcel, K. Jansen, and J. O'Halloran, "Uptake and partinioning of zinc in lemnaceae," *Ecotoxicology*, vol. 20, no. 8, pp. 1992–2002, 2011.

[45] E. Lesage, D. P. Rousseau, E. Meers, F. M. Tack, and N. De Pauw, "Accumulation of metals in a horizontal subsurface flow constructed wetland treating domestic wastewater in Flanders Belgium," *Science of The Total Environment*, vol. 380, no. 1–3, pp. 102–115, 2007.

[46] J. Vymazal, J. Švehla, L. Kröpfelová, and V. Chrastny, "Trace metals in phragmites australis and phalaris arundinacea growing in constructed and natural wetlands," *Science of the Total Environment*, vol. 380, no. 1–3, pp. 154–162, 2007.

[47] S. P. Mcgrath, Z. G. Shen, and F. J. Zhao, "Heavy metal uptake and chemical changes in the Rhizosphere of *Thlaspi caerulescens* and *Thlaspi ochroleucum* grown in contaminated soils," *Plant and Soil*, vol. 188, no. 1, pp. 153–159, 1997.

[48] D. D. Yilmaz and H. Akbulut, "Effect of circulation on wastewater treatment by *Lemna gibba* and *Lemna minor* (floating aquatic macrophytes)," *International Journal of Phytoremediation*, vol. 13, no. 10, pp. 970–984, 2011.

[49] A. Piotrowska, A. Bajguz, B. Godlewska-Zyłkiewicz, R. Czerpak, and M. Kamińska, "Jasmonic acid as modulator of lead toxicity in aquatic plant *Wolffia arrhiza* (Lemnaceae)," *Environmental and Experimental Botany*, vol. 66, no. 3, pp. 507–513, 2009.

[50] R. Singh, R. D. Tripathi, S. Dwivedi, A. Kumar, P. K. Trivedi, and D. Chakrabarty, "Lead bioaccumulation potential of an aquatic macrophyte Najas indica are related to antioxidant system," *Bioresource Technology*, vol. 101, no. 9, pp. 3025–3032, 2010.

[51] M. Chen, L. L. Zhang, J. Li, X. J. He, and J. C. Cai, "Bioaccumulation and tolerance characteristics of a submerged plant (*Ceratophyllum demersum* L.) exposed to toxic metal lead," *Ecotoxicology and Environmental Safety*, vol. 122, pp. 313–321, 2015.

[52] M. Sasmaz, E. Obek, and A. Sasmaz, "Bioaccumulation of uranium and thorium by *Lemna minor* and *Lemna gibba* in Pb-Zn-Ag tailing water," *Bulletin of Environmental Contamination and Toxicology*, vol. 97, no. 6, pp. 832–837, 2016.

[53] E. L. Walker and E. L. Connolly, "Time to pump iron: iron-deficiency-signaling mechanisms of higher plants," *Current Opinion in Plant Biology*, vol. 11, no. 5, pp. 530–535, 2008.

[54] E. Mateos-Naranjo, A. Gallé, I. Florez-Sarasa et al., "Assessment of the role of silicon in the Cu-tolerance of the C4 grass spartina densiflora," *Journal of Plant Physiology*, vol. 178, pp. 74–83, 2015.

[55] M. Wu, X. Jiang, Y. Lv et al., "Long-term effect of Cu 419 (ii) on the phosphorous removal performance in enhanced biological phosphorous 420 removal systems," *Chemical Engineering Journal*, vol. 281, pp. 164–173, 2015.

[56] O. Halloran, T. V. Culotta, and V. C. Metallochaperones, "An intracellular shuttle service for 422 metal ions," *Journal of Biological Chemistry*, vol. 275, no. 33, pp. 25057–25060, 2000.

[57] C. Goswami and A. Majumder, "Potential of *Lemna minor* in Ni and Cr removal from aqueous solution," *Pollution*, vol. 1, no. 4, pp. 373–385, 2015.

[58] C. Goswami, A. Majumder, A. K. Misra, and K. Bandyopadhyay, "Arsenic uptake by *Lemna minor* in hydroponic system," *International Journal of Phytoremediation*, vol. 16, no. 12, pp. 1221–1227, 2014.

[59] A. Sasmaz, I. M. Dogan, and M. Sasmaz, "Removal of Cr, Ni and Co in the water of chromium mining areas by using *Lemna gibba* L. and *Lemna minor* L," *Water and Environment Journal*, vol. 30, no. 3-4, pp. 235–242, 2016.

[60] L. Kaur, K. Gadgil, and S. Sharma, "Comparative evaluation of salicylic acid and EDTA chelant induced phytoremediation of lead and nickel using *Lemna minor* L.," *Tropical Plant Research*, vol. 2, no. 3, pp. 264–270, 2015.

[61] S. H. Bokhari, I. Ahmad, M. Mahmood-Ul-Hassan, and A. Mohammad, "Phytoremediation potential of *Lemna minor* L. for heavy metals," *International Journal of Phytoremediation*, vol. 18, no. 1, pp. 25–32, 2016.

[62] Y. Gopalapillai and B. A. Hale, "Internal versus external dose for describing ternary metal mixture (Ni, Cu, Cd) chronic toxicity to *Lemna minor*," *Environmental Science & Technology*, vol. 51, no. 9, pp. 5233–5241, 2017.

[63] R. Othman, R. Ramya, Z. M. Baharuddin, K. S. Has-Yun Hashim, and M. Yaman, "Response of *Lemna minor* and *Salninia natans* as phyroremediation agents towards Fe, Cu and Zn toxicities via in vivo model system," *Jurnal Teknologi*, vol. 77, no. 30, pp. 101–109, 2015.

[64] F. Duman, Z. Leblebici, and A. Aksoy, "Bioaccumulation of nickel, copper, and cadmium by *Spirodela polyrhiza* and *Lemna gibba*," *Journal of Freshwater Ecology*, vol. 24, no. 1, pp. 177–179, 2009.

[65] T. G. Krupnova, I. V. Mashkova, A. M. Kostryukova, N. O. Egorov, and S. V. Gavrilkina, "Bioconcentration of heavy metals in aquatic macrophytes of South Urals region lakes," *Biodiversitas Journal of Biological Diversity*, vol. 19, no. 1, pp. 296–302, 2018.

[66] K. K. Victor, M. Ladji, A. O. Adjiri, Y. D. A. Cyrille, and T. A. Sanogo, "Bioaccumulation of heavy metals from

wastewaters (Pb, Zn, Cd, Cu and Cr) in water hyacinth (*Eichhornia crassipes*) and water lettuce (*Pistia stratiotes*)," *International Journal of ChemTech Research*, vol. 9, no. 2, pp. 189–195, 2016.

[67] R. Verma and S. Suthar, "Lead and cadmium removal from water using duckweed—*Lemna gibba* L.: impact of pH and initial metal load," *Alexandria Engineering Journal*, vol. 54, no. 4, pp. 1297–1304, 2015.

Hindawi
Journal of Chemistry
Volume 2018, Article ID 6758794, 11 pages
https://doi.org/10.1155/2018/6758794

Research Article

Three-Dimensional Excitation and Emission Fluorescence-Based Method for Evaluation of Maillard Reaction Products in Food Waste Treatment

Jiaze Liu,[1,2] Jun Yin,[1,2] Xiaozheng He,[1,2] Ting Chen,[1,2] and Dongsheng Shen[1,2]

[1]*School of Environmental Science and Engineering, Zhejiang Gongshang University, Hangzhou 310012, China*
[2]*Zhejiang Provincial Key Laboratory of Solid Waste Treatment and Recycling, Hangzhou 310012, China*

Correspondence should be addressed to Jun Yin; jun.yin77@gmail.com

Received 12 July 2018; Revised 5 September 2018; Accepted 30 September 2018; Published 19 November 2018

Guest Editor: Gassan Hodaifa

Hydrothermal treatment (HT) of food waste (FW) can form Maillard reaction products (MRPs), the biorefractory organic matter due to the occurrence of Maillard reaction. However, the integrating qualitative and quantitative approach to assess MRPs is scarce. The goal of this study was to develop a method to characterize and quantify MRPs created by HT of FW. MRPs were identified by molecular weight fractionation, indirect spectrometric indicators, and three-dimensional excitation-emission fluorescence (3DEEM) analysis. The 3DEEM method combined with fluorescence regional integration (FRI) and parallel factor (PARAFAC) analyses was able to differentiate clearly between MRPs and other dissolved organic compounds compared to other approaches. The volume of fluorescence Φ from FRI and maximum fluorescence intensity F_{max} from PARAFAC were found to be suitable quantitative parameters for determination of MRPs in the hydrothermal FW system. These two parameters were validated with samples from hydrothermal FW under various operating temperatures and pH.

1. Introduction

In China, the stacking of FW has become a major issue to cause environmental problems. Recently, anaerobic digestion (AD) as an attractive waste treatment practice has been used to decrease the amount of biowaste and recover energy [1]. Due to the high biodegradability and water content of FW, it becomes a good candidate for AD [2]. During the process of the AD, the hydrolysis step is generally considered as the rate-limiting step for complex organic substrates degradation. Therefore, hydrothermal treatment (HT) was ordinarily used as a pretreatment to promote the solubilization of complicated macromolecular solid organic matters, thus improving the AD process [3].

Despite the acceleration of dissolved properties of FW, it has been documented that HT is responsible for the formation of Maillard reaction products (MRPs) [4]. On the one hand, the formation of MRPs can lead to the substrate loss during the HT of FW. On the other hand, the influence of MRPs themselves on AD merits further investigation [5]. Therefore, to optimize the HT process and enhance the efficiency of AD, it is essential to provide an integrating quantitative and qualitative approach to assess the MRPs production.

Numerous methods have been developed to characterize the occurrence of MRPs by using the precision analysis instrument [6, 7]. However, the quantitative determination could not be achieved because there is no pure standard for the measurement of MRPs [6]. In addition, these devices are time-consuming and labor-intensive, limiting their application and spreading. Thus, some easy-to-use and convenient characterization techniques became most commonly used methods, including the UVA_{254} and color intensity [8, 9].

Nowadays, three-dimensional excitation and emission fluorescence (3DEEM) is regarded as a promising tool to offer characteristic information for signature chemical structures in a complex mixture of chromophores [10]. And,

the qualitative characterization of MRPs has been achieved by the traditional 3DEEM method [11]. However, a quantitative determination could not be realized because only one excitation/emission intensity value can be used for analysis. Recent studies have demonstrated that fluorescence regional integration (FRI) method and parallel factor analysis (PARAFAC) method were developed to integrate the area beneath EEM spectra and semiquantitatively assess the specific components in a complex system [12–14]. However, the application of 3DEEM to the semiquantitative characterization of MRPs in the complicated hydrothermal FW system is scarce. Therefore, the utilization of 3DEEM to distinguish between MRPs and other dissolved organic matter under various hydrothermal conditions is supposed to be further explored.

This study aimed at developing a method to characterize and quantify MRPs created by HT of FW. Firstly, MRPs were characterized and evaluated with different methods. Then, MRPs production was further assessed by the applicability of 3DEEM combined with FRI and PARAFAC, hence exploring the suitable fluorescence parameters for semiquantifying the MRPs in the hydrothermal FW system.

2. Materials and Methods

2.1. Food Waste Sample Preparations. The FW, containing rice (44%), noodles (16%), vegetables (23%), meat (6%), and tofu (11%), was compounded based on the characteristics similar to FW collected from a canteen of Zhejiang Gongshang University (Hangzhou, China) in our previous study [15]. The five components came from the same vendor at Cui Yuan farmers' market (Hangzhou, China). The FW was cut into small pieces first by hand-breaking and then crushed using a mangler. The untreated FW sample was stored at −18°C before the HT. The main characteristics of the FW are listed in Table S1.

2.2. Hydrothermal Treatment. Hydrothermal treatment of FW was performed in an 80 mL airtight pressure digestion vessel as described by our previous study [16] at separate batch operations at each temperature. During HT, about 30 g crushed FW was placed in the vessel. Each batch was processed for 30 min. In the first experiment, the temperature manipulations were made at 110, 120, 130, 140, 150, and 160°C in an oil bath to explore the effect of temperature on MRPs production. In the second experiment, the different initial pH values (3.0, 4.0, 5.0, 6.0, 7.0, 8.0, 9.0, and 10.0) were tested at 130°C for 30 min. The time was measured from when the oil bath reached the set temperature. The vessels were cooled to ambient temperature after HT. Each treatment was performed in triple vessels.

2.3. Extraction of WEOM. WEOM was obtained with deionized water (solid-to-water ratio of 1 : 10 w/v), and the mixture was shaken for 1 h in a horizontal shaker at 35 ± 2°C. The extracts were separated from the mixture by centrifugation at 10,000 rpm for 5 min and filtered using the microfiltration membrane (0.45 μm).

2.4. Synthetic MRPs Solution. The synthetic MRPs solution was made by a concentrated solution of melanoidins, which are defined as brown substances formed during the final stage of the Maillard reaction. The formula of the concentrate was made with a 1 : 1 molar ratio of glucose and glycine with a buffer of 0.5 M Na_2CO_3 according to the previous research [17]. The solution was heated at 120°C for 3 hours as the record [17]. This synthetic MRPs solution has been used as model MRPs to analyze the properties of MRPs [9], and it was employed to examine the availability of MRPs characterization method in the present study.

2.5. Analytical Methods of MRPs

2.5.1. Spectrometric Indicators. (1) UVA_{254}. UVA was a measure of absorbance at 254 nm, measured in a 1 cm path length quartz cell. It can measure unsaturated bonds or aromaticity within dissolved organic matters [18]. Therefore, this spectrometric index was useful for this study as MRPs were linked to the presence of unsaturated double bonds and aromatic compounds and expressed as cm^{-1}·mL/g dry weight.

(2) Color Intensity. A spectrophotometer at a wavelength of 475 nm was used to determine color intensity in a 1 cm path length cell. The absorbance at this wavelength was characteristic of brown color. Characteristic color intensity was recorded in a platinum-cobalt (PtCo) unit as previously described [9].

(3) Browning Index. The Browning index of the FW solid was measured by an enzymatic digestion method which releases the brown pigments. Samples were dried for 24 h and grounded to a smaller size before use. The proposed method was modified based on pronase proteolysis created by Palombo et al. [19]. The procedure was as follows: 0.3 g of the dried sample was added into a test tube which contains 5 mL deionized distilled water at 45°C and mixed thoroughly. Then, another 0.4 mL of pronase solution was added into the mixture. After that, the test tubes were placed in a water bath, incubated for 120 min at 45°C, and then cooled in ice water, and 1 mL trichloroacetic acid (80% TCA) was added to each tube. Finally, centrifugation (20 min at 7000 rpm) and filtration were used before the spectrometric determination. The optical density of the filtrates was determined on a spectrophotometer. Samples were measured in a 1 mL cuvette with 1 cm pass length. The OD of the brown index was calculated as $OD = OD_{420nm} - OD_{550nm}$ and expressed as OD/g dry weight.

2.5.2. Molecular Weight Fractionation. Molecular weight fractionation was applied for a better separation and characterization of dissolved organic matters. Fractionation of samples was performed using an ultrafiltration centrifuge tube with different molecular weight cutoffs: 3 kDa, 10 kDa, and 30 kDa. The samples were filtered in series from 30 kDa to 3 kDa.

2.5.3. 3DEEM Analyses. The 3DEEM of WEOM was measured in a 1 cm cuvette using a Hitachi F-4600 fluorescence spectrometer at room temperature (25 ± 2°C). The scanning ranges were 200–500 nm for excitation and 250–500 nm for emission. Scanning was recorded at 5 nm intervals for excitation and 1 nm steps for emission, respectively, using a scanning speed of 2400 nm/min. The Milli-Q water blanks were subtracted in order to eliminate the effect of Raman scattering. In addition, exported EEMs were normalized by the Raman area and eliminated the primary and second Rayleigh scattering.

(1) Peak-Picking Method. A peak-picking method is used for the detection of the fluorescence intensity of easily-identifiable peaks and their locations within the EEMs. And then, the observed peaks were analyzed by comparing their fluorescence properties with the change of operating condition.

Besides, as an important humification index in EEM, HIX can reflect the degree of humification of the sample. HIX was calculated by dividing the emission intensity into the 435–480 nm regions by intensity in 300–345 nm when excitation intensity is at a wavelength of 255 nm and is shown as follows:

$$\mathrm{HIX} = \frac{\sum I_{(435-480)}}{\sum I_{(300-345)}}. \quad (1)$$

(2) FRI Analysis Method. The FRI approach was employed in this work to characterize the five excitation-emission regions of EEM spectra [12]. According to previous studies, EEM spectra are usually divided into five areas (Table S2): aromatic protein-like fluorophores (regions I and II), fulvic acid-like fluorophores (region III), soluble microbial product-like fluorophores (region IV), and humic acid-like fluorophores (region V). By normalizing the cumulative excitation-emission area volumes to relative regional areas (nm^2), the volume of fluorescence ($\Phi_{(i)}$) was calculated according to Chen et al. [12] within each region (i), applying the following equation:

$$\Phi_{(i)} = \mathrm{MF}_{(i)} \sum\sum I(\lambda_{ex}\lambda_{em})\Delta\lambda_{ex}\Delta\lambda_{em}, \quad (2)$$

where $\mathrm{MF}_{(i)}$ is a multiplication factor calculated by Equation (3); $\Delta\lambda_{ex}$ is the excitation wavelength interval (taken as 5 nm); $\Delta\lambda_{em}$ is the emission wavelength interval (taken as 1 nm); and $I(\lambda_{ex}\lambda_{em})$ is the fluorescence intensity at each excitation-emission pair (Raman units):

$$\mathrm{MF}_{(i)} = \frac{\text{total spectra area}}{\text{specific region area}_{(i)}}. \quad (3)$$

And the normalized excitation-emission area volumes referred to the value of region i. The entire region was calculated, and the percent fluorescence response was then determined using the following equation:

$$P_{i,n} = \frac{100 \times \Phi_{i,n}}{\Phi_{T,n}}. \quad (4)$$

(3) PARAFAC Component Analysis Method. PARAFAC is a method that decomposes EEMs of complex WEOM into available components. PARAFAC modeling was performed in MATLAB followed by the procedure recommended in the DOMFluor toolbox [20]. The PARAFAC models with two to seven components were computed, and core consistency was often applied to select the optimal number of components [21]. The concentration scores of each component were represented by maximum fluorescence intensity (F_{max}, R.U.).

2.6. Other Analytical Methods. The TS, volatile solids (VSs), dissolved organic carbon (DOC), soluble carbohydrate, and soluble protein were all determined. The diluent samples were operated as the same as mentioned in Section 2.3. SCOD was analyzed using standard methods [22]. The DOC concentrations of the WEOM solutions were determined with a total organic carbon analyzer (TOC-L CPH, Shimadzu, Japan). Soluble protein was quantified by the Lowry–Folin method using bovine serum albumin as the standard, and carbohydrate was determined using the phenol-sulfuric acid method with glucose as the standard [23, 24].

3. Results and Discussion

3.1. Variation of Food Waste after Hydrothermal Treatment. FW was treated under high pressure for 30 min at 110, 120,130, 140, 150, and 160°C. The SCOD concentrations of the hydrothermal-treated FW are shown in Figure S1. Increasing the temperature from 110 to 160°C caused an increase in SCOD from 85.55 g/kg to 119.91 g/kg. Although the increment of SCOD was obtained, color generation by Maillard reaction was also observed in the HT process due to the high temperature and the presence of proteins and carbohydrates [25]. Figure S2 shows that the treated solid gradually produced a darker brown color than the untreated FW with increasing treatment temperature. The significant color variation of hydrothermal FW was highly reliant on the formation of MRPs which depends on the reaction temperature. Nevertheless, owing to the complex and heterogeneous nature of the MRPs, it has not been possible to isolate or purify MRPs [26]. Therefore, there is a lack of methods for rapid, effective, and quantitative estimation of MRPs in the hydrothermal FW system.

3.2. Characterization and Evaluation of MRPs in Food Waste after Hydrothermal Treatment

3.2.1. Distribution of Soluble Organic Compounds in WEOM. Figure 1 presents the molecular weight distribution of WEOM before and after HT. DOC of the original sample was evenly in the MW analysis range and remained unchanged in each fraction after HT at 120°C. However, molecular weight fractionation distribution was modified at 140°C compared with 120°C. The total DOC content had a large promotion, but significant increase of DOC from 12 to 27 g/L only occurred in the MW > 30 kDa fraction. The

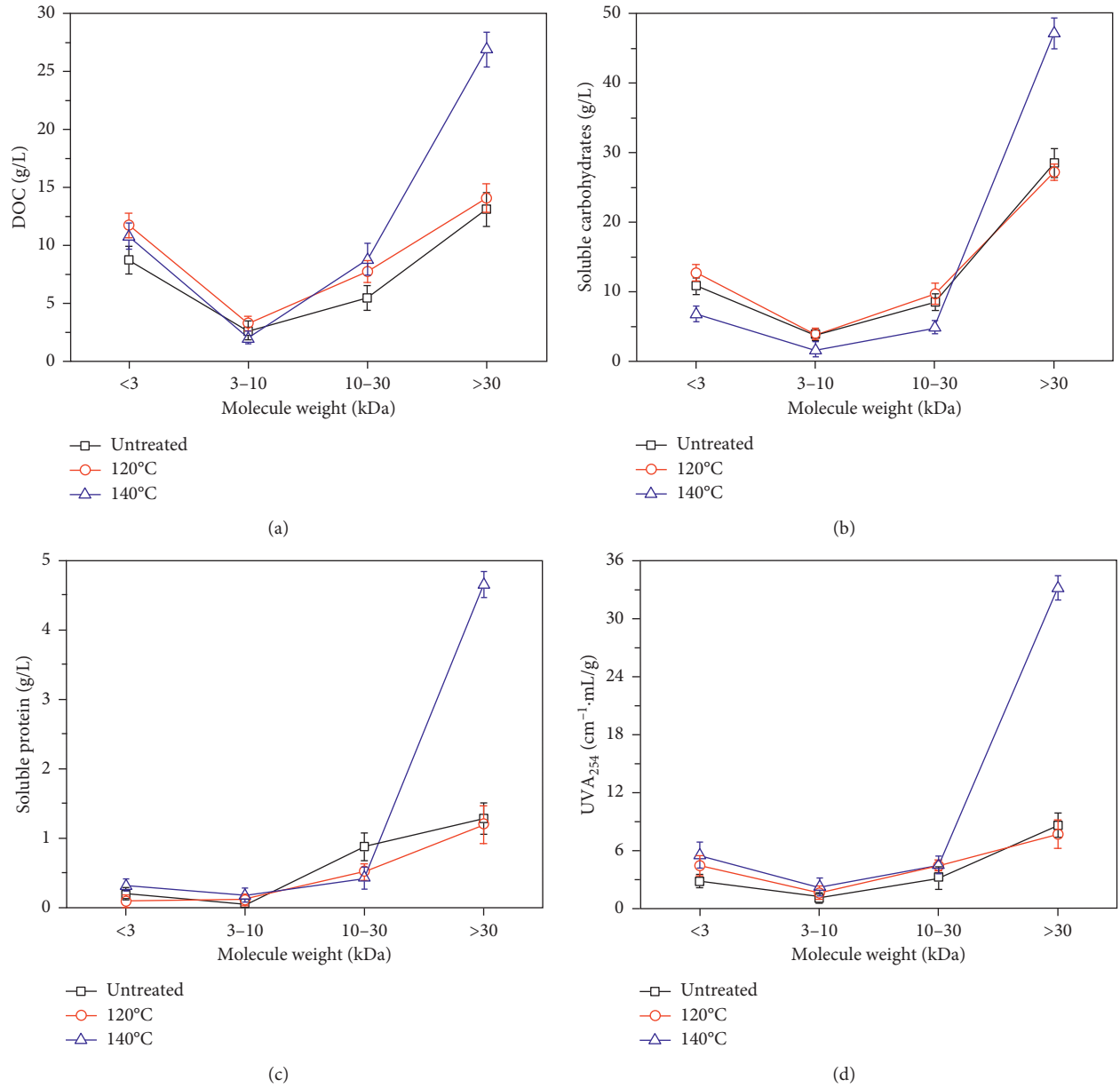

Figure 1: Different molecular weight distributions of the soluble organic compounds. (a) DOC. (b) Soluble carbohydrates. (c) Soluble protein. (d) UVA_{254}.

significant increment highlighted that dissolved organic compounds, residing in the MW > 30 kDa fraction, were expected as MRPs which have a molecular weight between 40 and 70 kDa [27]. Moreover, it is well known that the formation of MRPs has a positive relationship with the carbohydrates and proteins [28]. In 140°C group, the most prevalent fraction of soluble carbohydrates and soluble proteins also resided in the MW > 30 kDa fraction, which accounts for 78% and 83%, respectively. In addition, the characteristic absorbance UVA_{254} of WEOM in the MW > 30 kDa fraction was 8, 7.5, and 34 cm^{-1} mL/g for untreated FW, 120°C, and 140°C groups, respectively. The rise of this characteristic absorbance indicator showed that HT could result in the generation of MRPs from organic matter mixtures at 140°C. Similar conclusions were obtained by Barber [29] that MRP production occurred in the typical reaction range of thermal hydrolysis of 140–165°C.

3.2.2. Spectrometric Characterization of the MRPs from Food Waste. Nowadays, various easy-to-use quantitative spectrometric characterization methods have been applied to determine the MRP production in complicated systems [19, 30]. Three representative indicators (ΔUVA_{254}, Δbrowning index, and Δcolor intensity) were employed to demonstrate the modification of MRPs content of hydrothermal FW (Figure 2), and raw material was taken as the control. At first, ΔUVA_{254} did not vary significantly ($p > 0.05$) after HT at 110°C and 120°C. The ΔUVA_{254} increased significantly ($p < 0.05$) at 130°C, which enhanced by

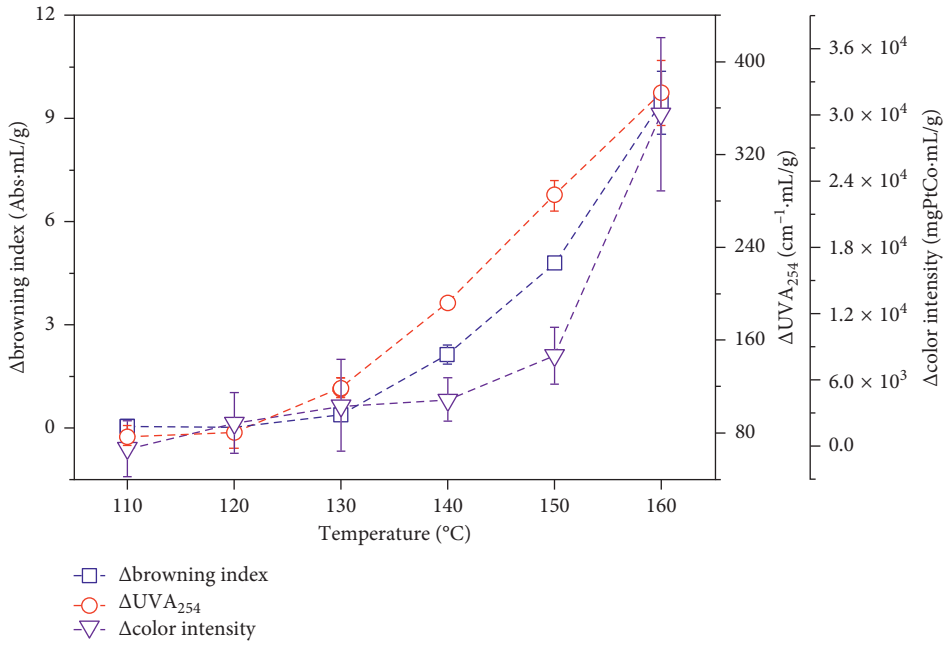

Figure 2: Three spectrometric indicators of MRPs production from FW at different temperatures.

1.5-fold compared with 120°C. Then, this surrogate index continued ascending with the increase of treatment temperature, indicating a significant number of compounds accumulated when the hydrothermal temperature above 120°C. In addition, a similar tendency was found in the result of the pronase method, and the Δbrowning index was utilized for determination of nonenzymatic browning. The changing of the Δbrowning index showed that the brown pigment production was slim to zero in 110°C and 120°C treatments and exhibited a regular increase beyond the critical temperature (120°C). The tendencies of these two parameters were consistent with the transformation of the surface color of hydrothermal-treated FW. However, the accuracy of these two indicators was still in doubt because of the complexity of hydrothermal FW systems. Moreover, the Δcolor intensity of WEOM was also recorded. Nevertheless, the relative standard deviation of Δcolor intensity was higher than other methods, and this color indicator did not demonstrate the significant difference ($p > 0.05$) between the 130°C and 140°C groups, which was different from the appearance changes of hydrothermal-treated FW. Although spectrometric characterization could quickly verify the accumulation of MRPs in an indirect way, the influence of other organic matters was still not solved.

3.2.3. Characterization of MRPs by 3DEEM Fluorescence Analysis. The objective of using 3DEEM fluorescence was to monitor the change of fluorescence properties in WEOM and to analyze the effect of temperature on MRPs generation in the hydrothermal FW system. Typical 3DEEM spectra of treated WEOM samples at different temperatures are shown in Figure 3, and detailed fluorescence properties are summarized in Table 1 by the "peak-picking" method. As expected, there were obvious differences in the 3DEEM spectra of the WEOM with the rise of temperature, and the maximal transformation was found between 130°C and 140°C groups. Moreover, Table 1 shows the change of peak intensity at the soluble microbial region ($\lambda_{ex}/\lambda_{em}$ = 285/357–361), which decreased from 3.58 R.U. (raw material) to 0.10 R.U. (160°C), and the sharp decrease trend started at the 140°C group. To the best of our knowledge, soluble microbial products (SMPs) contain various complex organic materials, such as proteinaceous material, carbohydrates, humic and fulvic substances, and organic acids [31, 32]. Thus, the organic matters resided in the region of soluble microbial by-products were considered as soluble carbohydrates and proteins because other organic matters would not appear in this region. Conversely, the peak intensity at the humic acid-like region ($\lambda_{ex}/\lambda_{em}$ = 320–360/419–438) increased from 0.43 to 3.34 R.U. as the temperature increased, and obvious transformation also occurred at 140°C group. The peak ratio (V/IV) ascended with the increase of temperature, which implied that the generation and accumulation of humic acid-like organic fluorescent molecules were attributed to the polymerization of the soluble carbohydrates and proteins during the HT. In addition, the movement of humic-like peaks location within the 3DEEM ($\lambda_{ex}/\lambda_{em}$) to longer wavelength (red-shifting), from $\lambda_{ex}/\lambda_{em}$ = 320/428 to 360/438, also indicated the humic acid-like fluorophores were concentrating and becoming more refractory [33]. Besides, the HIX value has been applied to evaluate the humification extent of dissolved organic matter [34]. From Table 1, the increase of HIX values after 140, 150 and 160°C treatments were indicative of more humic WEOM. It is generally known that MRPs are highly aromatic and resemble humic substances; it suggested that 3DEEM might serve as a good descriptor to prove the MRPs production during the HT.

Overall, compared with the 3DEEM analysis method, spectrometric approaches cannot provide a direct

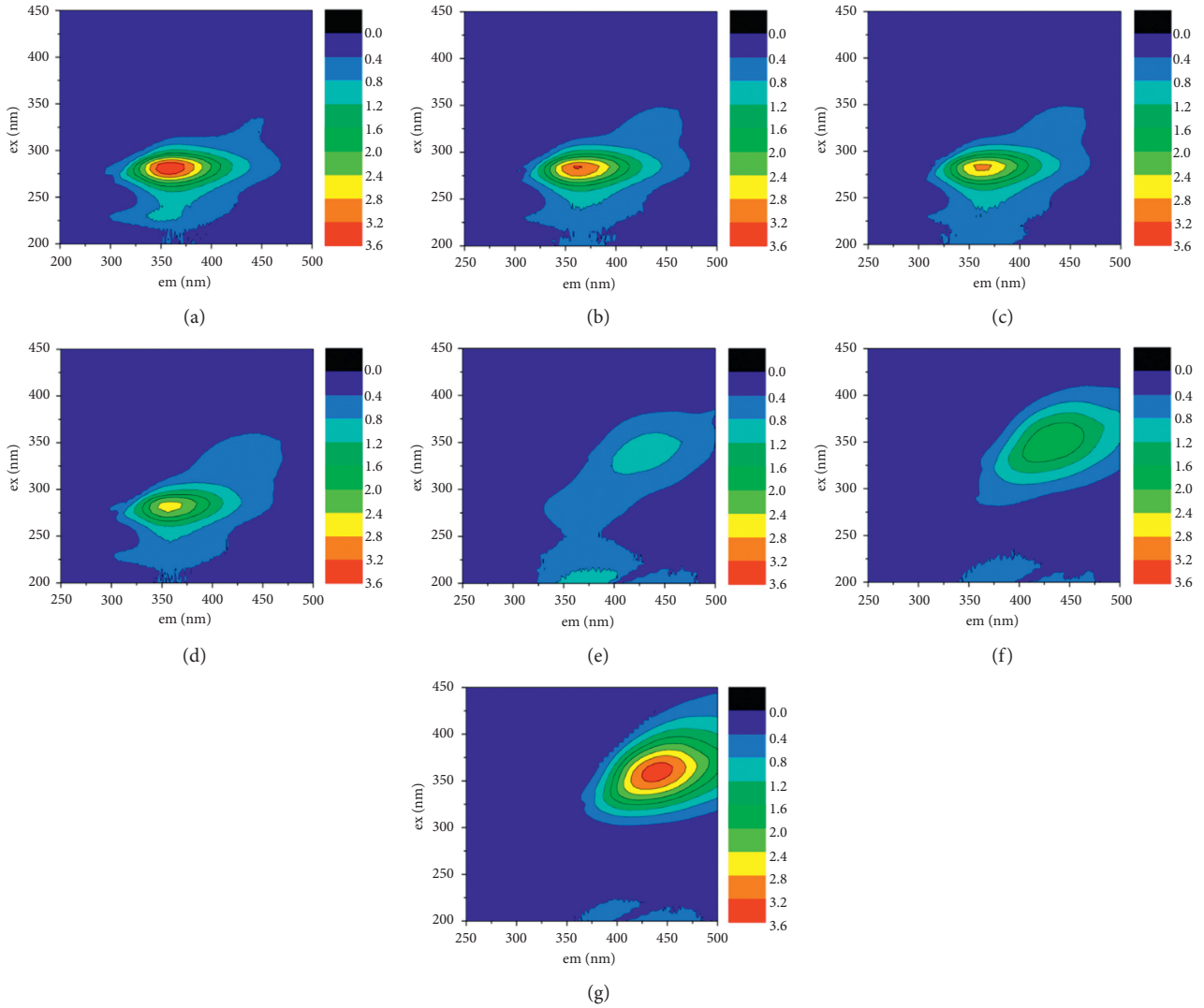

Figure 3: Typical EEM spectra of the WEOM extracted from FW treated at different temperatures. (a) Untreated, (b) 110°C, (c) 120°C, (d) 130°C, (e) 140°C, (f) 150°C, and (g) 160°C.

Table 1: Fluorescent properties of treated groups at each temperature.

Sample name	Region IV peak location		Region V peak location		Peak ratio (IV/V)	HIX
	Ex/em	Fluorescence intensity (R.U.)	Ex/em	Fluorescence intensity (R.U.)		
Untreated sample	280/357	3.58	320/438	0.43	0.12	0.49
110°C treated sample	285/360	3.24	320/434	0.58	0.18	0.62
120°C treated sample	285/360	3.67	320/436	0.52	0.14	0.62
130°C treated sample	285/359	2.56	325/419	0.60	0.23	0.45
140°C treated sample	285/359	0.75	335/421	0.96	1.28	0.88
150°C treated sample	285/361	0.42	345/430	1.96	4.67	1.68
160°C treated sample	285/360	0.10	360/438	3.43	34.30	6.70

assessment of MRPs and potentially influence the determination of MRPs due to the fluctuation from other organic or colored compounds. The molecular weight fractionation technique was used to eliminate the interference of smaller molecular weight constituents, which caused the assessment of MRPs costlier and more time-consuming. Besides, Figures 1(b) and 1(c) show that even though the molecular weight fractionation was used, the existence of organic macromolecular compounds (carbohydrates and proteins) might also affect the accuracy of UVA_{254} measurement. Accordingly, 3DEEM fluorescence analysis was simple, had good selectivity, and provided a wealth of

information about WEOM, especially helpful in characterizing WEOM and interpreting the complex information in EEM [35]. However, fluorescence information was still restricted because only one peak location and fluorescence intensity value was used for analysis, and it should be noticed that the direct quantification of MRPs using 3DEEM can be of major interest for investigation of WEOM from FW.

3.3. Quantitative Characterization of MRPs Production

3.3.1. Fluorescence EEMs-Based FRI Analysis and PARAFAC Component Estimation. Recently, FRI analysis and PARAFAC component estimation were developed to provide a more complete data analysis than the traditional "peak-picking" technique [36]. Therefore, the FRI analytical method was used to reveal the transformation of organic compounds in WEOM by integration of the volume beneath each EEM region. According to the five regions of the FRI analysis, it can be found that the obvious characteristic peaks were presented in region IV and region V. The variation of percent fluorescence response $P_{(i,n)}$ of the WEOM is shown in Figure 4. The $P_{(i,n)}$ values of region IV and region V remained almost constant in 110, 120, and 130°C groups. When temperature increased from 130 to 160°C, the $P_{(i,n)}$ value of region IV decreased from 49.8% to 16.9%, and the $P_{(i,n)}$ of region V increased from 12.1% to 66.1%. Moreover, the $P_{(i,n)}$ value of region I also had a little reduction above 130°C. These results implied that humic acid-like material regarded as MRPs in region V were efficiently accumulated when HT temperature was beyond 130°C. It was assumed that the disappearance of soluble carbohydrates and proteinaceous products (region IV) and tryptophan-like substances (region I) were the source material for the polymerization of MRPs (region V). Therefore, region IV (carbohydrates and proteinaceous products) matters and region V (MRPs) matters can be effectively differentiated based on the FRI method.

Furthermore, PARAFAC can capture the heterogeneity of WEOM samples, thereby decomposing EEM spectra into various individual fluorescent components. Two fluorescent components evaluated by PARAFAC using the CORCONDIA procedure were the soluble microbial by-product-like component (C_1) and humic acid-like component (C_2). Individual components are shown in Figure 5 as contour plots. The excitation and emission loadings are also given in Figure 5, and excitation and emission characteristics of the components identified in this study and probable source of components are depicted in Table S3. In Table S3, two PARAFAC components are pointed out in detail: C_1 with peaks of ex/em = 280/360 nm was associated with soluble microbial products, defined as carbohydrates and proteins which could be easily biodegradable [37, 38], and C_2 with specific peaks of ex/em = 360/441 nm originated from humic acid-like substances [9, 28]. In the current study, the humic acid-like component identified by PARAFAC was MRPs, which had higher ex/em than the other synthetic or isolated humic compounds [11, 27, 39]. Furthermore, the observed humic-like compounds were forcefully identified as MRPs

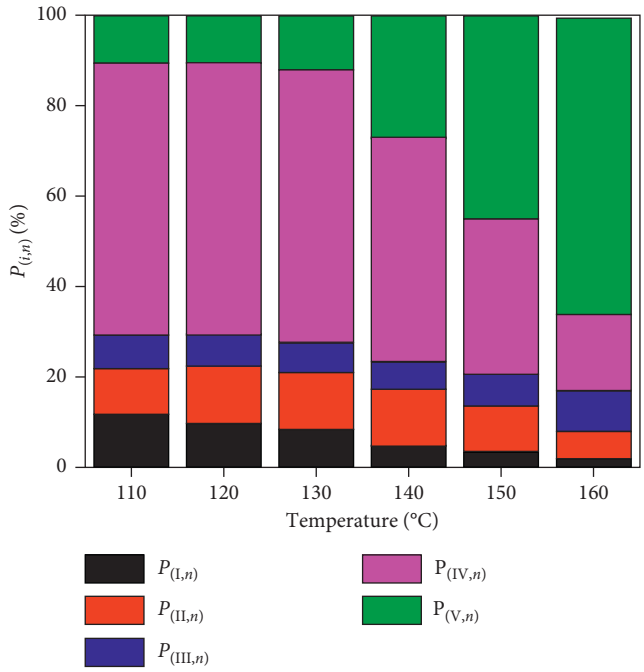

Figure 4: The distribution of FRI in WEOM from food waste after hydrothermal treatment.

by comparing its fluorescence property (ex/em) with synthetic MRPs solution created in our study (Figure S3). The maximum fluorescence intensities (F_{max}) of component C_2 remained constant at a low content when the temperature was in the range of 110°C to 130°C and then increased from 22.37 to 155.79 R.U. by further increasing the temperature from 130 to 160°C (Figure S4), which indicated little accumulation of nonbiodegradable MRPs at temperatures below 130°C and mass production of MRPs when temperature beyond 130°C. Meanwhile, the results in Figure 6 also show that the F_{max} of C_1 had a slight reduction at 110°C, 120°C, and 130°C groups but substantially dropped with the further increase of temperature. Results from PARAFAC were consistent with the FRI analysis, which suggested biodegradable organic compounds and MRPs in WEOM can be separated by PARAFAC.

As mentioned above, the distribution of $P_{(i,n)}$ and the 2-component PARAFAC estimation provided complementary information, showing that humic acid-like matter (MRPs) and SMP materials (carbohydrates and proteins) which dominated the WEOM underwent an increase and decrease, respectively, as the operating temperature increased. These results proved FRI and PARAFAC can differentiate fluorescence characteristic disparities between MRPs and other organic compounds. And, it also can be seen that Maillard reaction (C_2) was accelerated at elevated temperature by consuming organics in C_1. Therefore, 3DEEM combined with FRI/PARAFAC could be employed to analysis of MRPs generated from hydrothermal-treated FW.

3.3.2. Semiquantitative Characterization of Fluorescent Parameters for MRPs Production. The volume of fluorescence

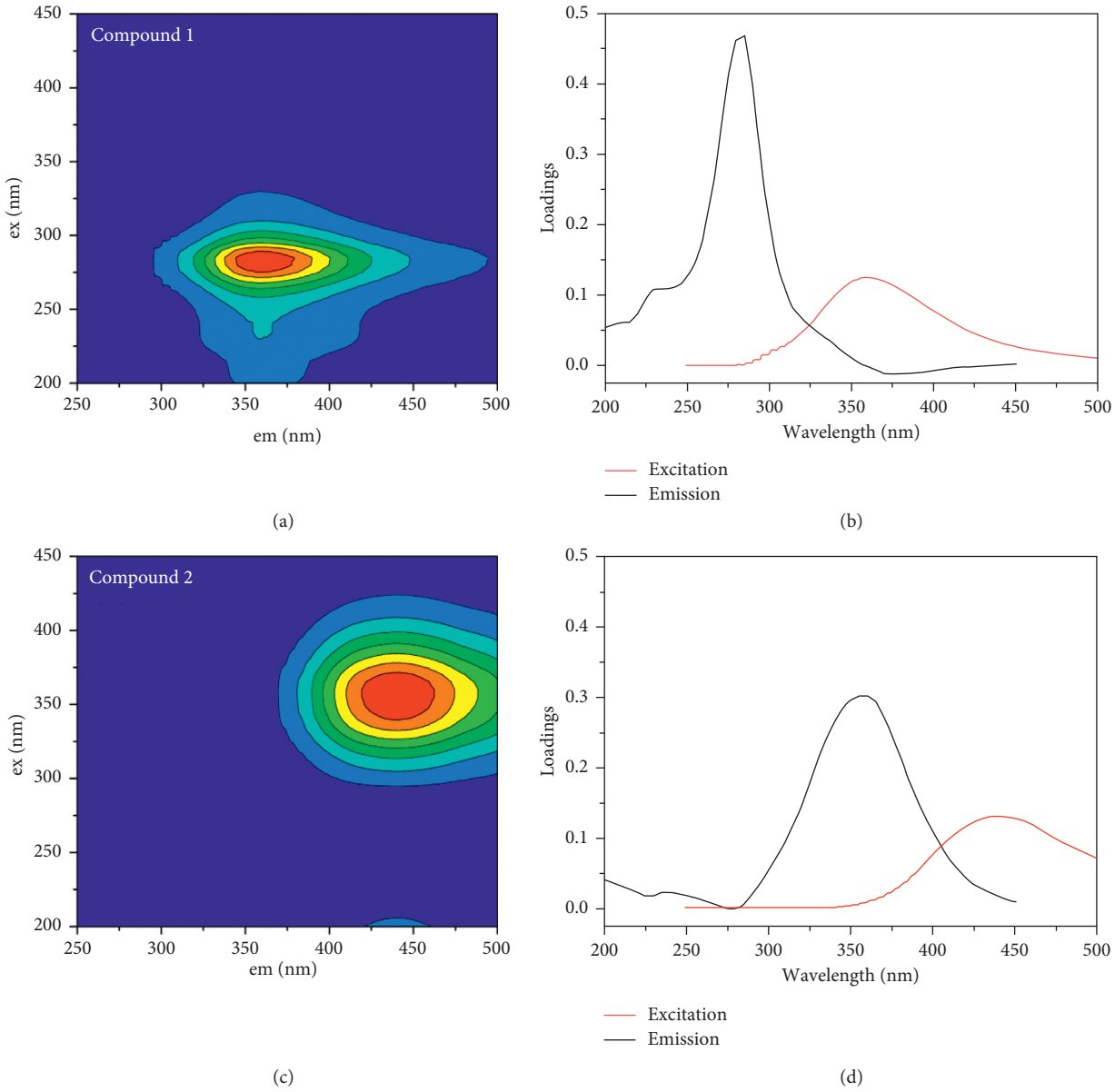

Figure 5: Two-component PARAFAC model generated from samples of WEOM: (a and b) contour plots of the spectral shapes; (c and d) line plots of the loadings.

$\Phi_{(V)}$ parameter from FRI and maximum fluorescence intensity in the C_2 component F_{max} (C_2) parameter from PARAFAC were used as the characterization parameters for assessing the generation of MRPs. All the data were based on dry weight, and raw material was taken as control. The corresponding results of fluorescent indictors are presented in Figure 6. It can be seen from Figure 5 that the impact of temperature on the $\Delta\Phi_{(V)}$ was minimal in 110, 120, and 130°C groups ($p > 0.05$), staying at a low level from 5.1×10^4 to 9.0×10^4 R.U.·nm^2·mL/g. But then $\Delta\Phi_{(V)}$ increased significantly from 2.9×10^5 (140°C) to 1.2×10^6 R.U.·nm^2·mL/g (160°C). A similar tendency was found in ΔF_{max} (C_2) (Figure 5). The ΔF_{max} (C_2) remained unchanged as temperature increased from 110 to 130°C and then went through a successive and relatively large increase from 33.5 to 141.3 R.U.·mL/g as temperature further increased. These results were consistent with the fact that MRPs are temperature dependent [29].

Besides, the correlations between 3DEEM fluorescence parameters and spectrometric parameters were analyzed to check whether fluorescence parameters could effectively characterize the MRPs in FW after HT. Pearson correlations for 3DEEM fluorescence parameters and spectrometric parameters are summarized in Table S4. Generally, spectrometric parameters were strongly correlated with 3DEEM fluorescence parameters ($r > 0.880$, $p < 0.01$), which indicated that these two fluorescent analytical techniques could be employed to monitor the generation of MRPs and semiquantitatively determine the content of MRPs in the hydrothermal FW system. In addition, these two indicators were expected to be tested at various situations, which help their generalization and application.

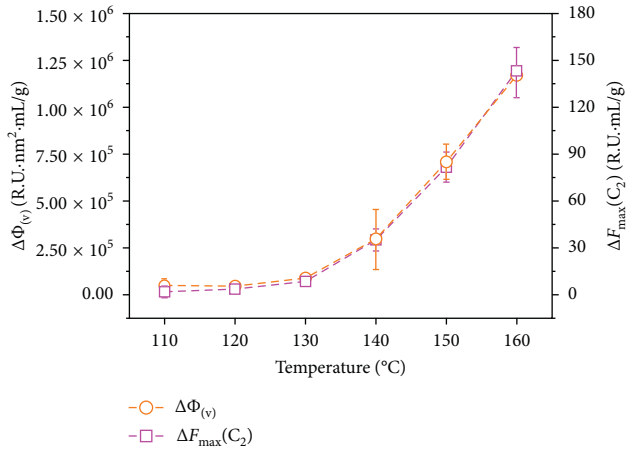

Figure 6: Semiquantitative characterization of 3DEEM fluorescent parameters for MRPs production from FW at different temperatures.

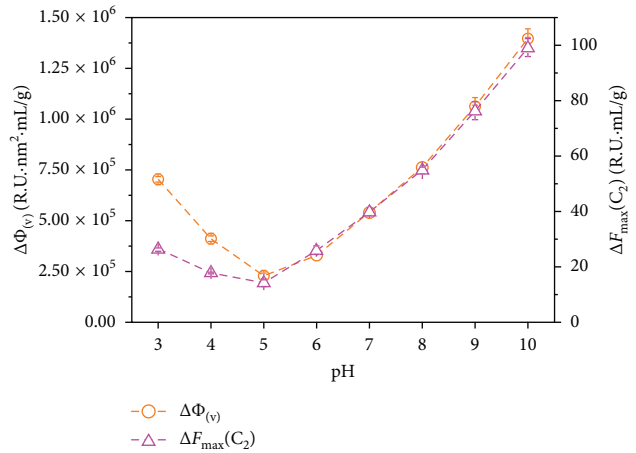

Figure 7: Fluorescence indicators of MRPs from FW at different hydrothermal-treated pH value.

3.3.3. Examples of Application for MRPs Determination by 3DEEM Semiquantitative Fluorescence Parameters. Apart from temperature, pH also has an impact on MRPs formation. From previous studies, pH and alkalinity were reported to increase the degree of polymerization, thereby causing the accumulation of MRPs [40]. Therefore, it is meaningful to evaluate the effect of pH on MRPs production during HT in FW. In order to semiquantitatively determine their production, 3DEEM-FRI/PARAFAC methods were applied. FW with initial pH from 3.0 to 10 was treated at 130°C for 30 min (Figure 7). As pH increased from 3.0 to 5.0, the mean $\Delta\Phi_{(V)}$ decreased from 7.05×10^5 to 2.29×10^5 R.U.·nm²·mL/g and reached the minimum at pH 5.0. Nevertheless, an obvious increase of MRPs was observed from a minimum of 2.29×10^5 to 1.39×10^6 R.U.·nm²·mL/g as the pH increased from 5.0 to 10.0. The ΔF_{max} (C_2) from PARAFAC analysis, which was associated with the contribution of MRPs, had a similar tendency to $\Delta\Phi_{(V)}$ and increased from the minimum of 14.24 R.U. at pH 5.0 to the maximum of 90.04 R.U. at pH 10. Previous studies have stated that high initial pH (pH > 5) could accelerate the Maillard reaction rate because Schiff-base matter formed easily [41]. Moreover, low initial pH could also cause the formation of MRPs as it favors 1,2-enolisation reaction pathway and results in the ascent of compounds like furfural or 5-hydroxymethyl-2-furaldehyde (HMF) [42]. Therefore, the results above further verified that $\Delta\Phi_{(V)}$ and ΔF_{max} (C_2) allow an effective evaluation for MRPs production in the hydrothermal FW system.

Besides, hydrothermal time and composition of FW also affect the occurrence of Maillard reaction. Thus, the effect of these hydrothermal conditions on MRPs production can be evaluated according to these two parameters. In this way, the formation of MRPs can be effectively controlled under the optimized hydrothermal condition, thus preventing the substrate loss and promoting limited hydrolysis efficiency simultaneously. Therefore, the increase of bio-converted energy can be achieved by reducing substrate consuming from MRPs formation.

4. Conclusion

Compared to traditional methods, the 3DEEM analysis is proved to be a more sensitive method to estimate the occurrence of Maillard reaction in the hydrothermal FW system, providing valuable information when the MRPs are formed. However, its utility is limited to the quantifying of the MRPs. The FRI and PARAFAC analytic methods were established to further distinguish MRPs from the other dissolved organic compounds by integration of the volume beneath each EEM region and capturing the heterogeneity of samples. And $\Delta\Phi_{(V)}$ from FRI and ΔF_{max} (C_2) from PARAFAC can be considered liable parameters for semiquantifying MRPs under various temperature and pH. The minimum MRPs were validated at temperature below 130°C and pH 5.0.

Data Availability

The data used to support the findings of this study are available from the corresponding author upon request.

Conflicts of Interest

The authors declare that they have no conflicts of interest.

Acknowledgments

The authors appreciate the National Natural Science Foundation of China (Nos. 51778580 and 51608480), Natural Science Foundation of Zhejiang Province of China (No. LQ16E080001), Open Foundation of Key Laboratory for Solid Waste Management and Environment Safety (Tsinghua University), Ministry of Education of China (SWMES 2015–07), and China Scholarship Council (iCET 2017) for providing the funding support for this project.

Supplementary Materials

Table S1: characteristics of FW. Table S2: excitation and emission (ex/em) wavelengths of fluorescence region and

their associated names. Table S3: comparison of the fluorescence component peak location in the current study with those reported in the previous literature and probable source description. Table S4: Pearson correlations among spectrometric parameters and EEM fluorescence parameters. Figure S1: SCOD of hydrothermal-treated food waste at different temperatures. The data were based on wet weight. Figure S2: the appearance of hydrothermal-treated food waste (untreated; 110°C, 120°C, 130°C, 140°C, 150°C, and 160°C treated). Figure S3: EEM spectra of the synthetic MRP solution produced by glycine and glucose after hydrothermal treatment. The peak location of synthetic MRP solution was $\lambda_{ex}/\lambda_{em}$ = 355/435; the $\lambda_{ex}/\lambda_{em}$ value is higher than the other humic isolates tested, which explains why this product was MRPs. Figure S4: F_{max} values of the two components (C_1 and C_2) in WEOM from food waste after hydrothermal treatment. (*Supplementary Materials*)

References

[1] W. Wang, H. Hou, S. Hu, and X. Gao, "Performance and stability improvements in anaerobic digestion of thermally hydrolyzed municipal biowaste by a biofilm system," *Bioresource Technology*, vol. 101, no. 6, pp. 1715–1721, 2010.

[2] Y. Li, Y. Jin, J. Li, H. Li, and Z. Yu, "Effects of thermal pretreatment on the biomethane yield and hydrolysis rate of kitchen waste," *Applied Energy*, vol. 172, pp. 47–58, 2016.

[3] B. Grycová, I. Koutník, and A. Pryszcz, "Pyrolysis process for the treatment of food waste," *Bioresource Technology*, vol. 218, pp. 1203–1207, 2016.

[4] X. Liu, W. Wang, X. Gao, Y. Zhou, and R. Shen, "Effect of thermal pretreatment on the physical and chemical properties of municipal biomass waste," *Waste Management*, vol. 32, no. 2, pp. 249–255, 2012.

[5] L. Ding, J. Cheng, D. Qiao et al., "Investigating hydrothermal pretreatment of food waste for two-stage fermentative hydrogen and methane co-production," *Bioresource Technology*, vol. 241, pp. 491–499, 2017.

[6] R. Chandra, R. N. Bharagava, and V. Rai, "Melanoidins as major colourant in sugarcane molasses based distillery effluent and its degradation," *Bioresource Technology*, vol. 99, no. 11, pp. 4648–4660, 2008.

[7] GE. Leiva, G. B. Naranjo, and L. S. Malec, "A study of different indicators of Maillard reaction with whey proteins and different carbohydrates under adverse storage conditions," *Food Chemistry*, vol. 215, p. 410, 2017.

[8] S. Pavlovic, R. C. Santos, and M. B. A. Glória, "Maillard reaction during the processing of 'Doce de leite'," *Journal of the Science of Food and Agriculture*, vol. 66, no. 2, pp. 129–132, 2010.

[9] J. Dwyer, D. Starrenburg, S. Tait, K. Barr, D. J. Batstone, and P. Lant, "Decreasing activated sludge thermal hydrolysis temperature reduces product colour, without decreasing degradability," *Water Research*, vol. 42, no. 18, pp. 4699–4709, 2008.

[10] M. Uchimiya, J. E. Knoll, W. F. Anderson, and K. R. Harris-Shultz, "Chemical analysis of fermentable sugars and secondary products in 23 sweet sorghum cultivars," *Journal of Agricultural and Food Chemistry*, vol. 65, no. 35, pp. 7629–7637, 2017.

[11] P. G. Coble, "Characterization of marine and terrestrial DOM in seawater using excitation-emission matrix spectroscopy," *Marine Chemistry*, vol. 51, no. 4, pp. 325–346, 1996.

[12] W. Chen, P. Westerhoff, J. A. Leenheer, and K. Booksh, "Fluorescence excitation-emission matrix regional integration to quantify spectra for dissolved organic matter," *Environmental Science and Technology*, vol. 37, no. 24, p. 5701, 2003.

[13] L. J. Zhu, Y. Zhao, Y. N. Chen et al., "Characterization of atrazine binding to dissolved organic matter of soil under different types of land use," *Ecotoxicology and Environmental Safety*, vol. 147, no. 2, pp. 1065–1072, 2018.

[14] L. J. Zhu, H. X. Zhou, X. Y. Xie et al., "Effects of floodgates operation on nitrogen transformation in a lake based on structural equation modeling analysis," *Science of the Total Environment*, vol. 631-632, pp. 1311–1320, 2018.

[15] K. Wang, J. Yin, D. Shen, and N. Li, "Anaerobic digestion of food waste for volatile fatty acids (VFAs) production with different types of inoculum: effect of pH," *Bioresource Technology*, vol. 161, pp. 395–401, 2014.

[16] J. Yin, K. Wang, Y. Yang, D. Shen, M. Wang, and H. Mo, "Improving production of volatile fatty acids from food waste fermentation by hydrothermal pretreatment," *Bioresource Technology*, vol. 171, pp. 323–329, 2014.

[17] E. C. Bernardo, R. Egashira, and J. Kawasaki, "Decolorization of molasses' wastewater using activated carbon prepared from cane bagasse," *Carbon*, vol. 35, no. 9, pp. 1217–1221, 1996.

[18] J. Dwyer, L. Kavanagh, and P. Lant, "The degradation of dissolved organic nitrogen associated with melanoidin using a UV/H_2O_2 AOP," *Chemosphere*, vol. 71, no. 9, pp. 1745–1753, 2008.

[19] R. Palombo, A. Gertler, and I. Saguy, "A simplified method for determination of browning in dairy powders," *Journal of Food Science*, vol. 49, no. 6, p. 1609, 2010.

[20] C. A. Stedmon and R. Bro, "Characterizing dissolved organic matter fluorescence with parallel factor analysis: a tutorial," *Limnology and Oceanography Methods*, vol. 6, no. 11, pp. 572–579, 2008.

[21] D. Zhu, B. Ji, H. L. Eum, and M. Zude, "Evaluation of the non-enzymatic browning in thermally processed apple juice by front-face fluorescence spectroscopy," *Food Chemistry*, vol. 113, no. 1, pp. 272–279, 2009.

[22] APHA, *Standard Methods for the Examination of Water and Wastewater*, American Public Health Association/American Water Works Association/Water Environment Federation, Washington, DC, USA, 20th edition, 1998.

[23] O. H. Lowry, N. J. Rosebrough, A. L. Farr et al., "Protein measurement with the Folin phenol reagent," *Journal of Biological Chemistry*, vol. 193, no. 1, pp. 265–275, 1951.

[24] D. Herbert, P. J. Philipps, and R. E. Strange, "Carbohydrate analysis," in *Methods in Enzymology*, vol. 5B, pp. 265–277, Elsevier, Amsterdam, Netherlands, 1971.

[25] C. Bougrier, J. P. Delgenès, and H. Carrère, "Effects of thermal treatments on five different waste activated sludge samples solubilisation, physical properties and anaerobic digestion," *Chemical Engineering Journal*, vol. 139, no. 2, pp. 236–244, 2008.

[26] A. Adams, K. A. Tehrani, M. Kersiene, R. Venskutonis, and N. De Kimpe, "Characterization of model melanoidins by the thermal degradation profile," *Journal of Agricultural and Food Chemistry*, vol. 51, no. 15, pp. 4338–4343, 2003.

[27] J. Dwyer, P. Griffiths, and P. Lant, "Simultaneous colour and DON removal from sewage treatment plant effluent: alum coagulation of melanoidin," *Water Research*, vol. 43, no. 2, pp. 553–561, 2009.

[28] S. I. F. S. Martins and M. A. J. S. van Boekel, "Melanoidins extinction coefficient in the glucose/glycine Maillard reaction," *Food Chemistry*, vol. 83, no. 1, pp. 135–142, 2003.

[29] W. P. Barber, "Thermal hydrolysis for sewage treatment: a critical review," *Water Research*, vol. 104, pp. 53–71, 2016.
[30] J. Dwyer and P. Lant, "Biodegradability of DOC and DON for UV/H_2O_2 pre-treated melanoidin based wastewater," *Biochemical Engineering Journal*, vol. 42, no. 1, pp. 47–54, 2008.
[31] J. Li, J. Wei, H. H. Ngo et al., "Characterization of soluble microbial products in a partial nitrification sequencing batch biofilm reactor treating high ammonia nitrogen wastewater," *Bioresource Technology*, vol. 249, pp. 241–246, 2017.
[32] C. Le and D. C. Stuckey, "Impact of feed carbohydrates and nitrogen source on the production of soluble microbial products (SMPs) in anaerobic digestion," *Water Research*, vol. 122, p. 10, 2017.
[33] M. Esparza-Soto, S. Núñez-Hernández, and C. Fall, "Spectrometric characterization of effluent organic matter of a sequencing batch reactor operated at three sludge retention times," *Water Research*, vol. 45, no. 19, pp. 6555–6563, 2011.
[34] J. Hur and G. Kim, "Comparison of the heterogeneity within bulk sediment humic substances from a stream and reservoir via selected operational descriptors," *Chemosphere*, vol. 75, no. 4, pp. 483–490, 2009.
[35] W. T. Li, S. Y. Chen, Z. X. Xu, Y. Li, C. D. Shuang, and A. M. Li, "Characterization of dissolved organic matter in municipal wastewater using fluorescence PARAFAC analysis and chromatography multi-excitation/emission scan: a comparative study," *Environmental Science and Technology*, vol. 48, no. 5, pp. 2603–2609, 2014.
[36] H. Wu, Z. Zhou, Y. Zhang, T. Chen, H. Wang, and W. Lu, "Fluorescence-based rapid assessment of the biological stability of landfilled municipal solid waste," *Bioresource Technology*, vol. 110, no. 2, pp. 174–183, 2012.
[37] X. Jia, B. Xi, M. Li et al., "Evaluation of biogasification and energy consumption from food waste using short-term hydrothermal pretreatment coupled with different anaerobic digestion processes," *Journal of Cleaner Production*, vol. 152, pp. 364–368, 2017.
[38] J. Sun, L. Guo, Q. Li et al., "Structural and functional properties of organic matters in extracellular polymeric substances (EPS) and dissolved organic matters (DOM) after heat pretreatment with waste sludge," *Bioresource Technology*, vol. 219, pp. 614–623, 2016.
[39] M. Zhang, Z. Wang, P. Li, H. Zhang, and L. Xie, "Biorefractory dissolved organic matter and colorants in cassava distillery wastewater: characterization, coagulation treatment and mechanisms," *Chemosphere*, vol. 178, pp. 272–279, 2017.
[40] M. Coca, M. T. Garcia, G. Gonzalez et al., "Study of coloured components formed in sugar beet processing," *Food Chemistry*, vol. 86, no. 3, pp. 421–433, 2004.
[41] W. Jiang, Y. Chen, X. He, S. Hu, S. Li, and Y. Liu, "A study of the tyramine/glucose Maillard reaction: variables, characterization, cytotoxicity and preliminary application," *Food Chemistry*, vol. 239, pp. 377–384, 2017.
[42] C. Rannou, D. Laroque, E. Renault, C. Prost, and T. Sérot, "Mitigation strategies of acrylamide, furans, heterocyclic amines and browning during the Maillard reaction in foods," *Food Research International*, vol. 90, pp. 154–176, 2016.

Hindawi
Journal of Chemistry
Volume 2018, Article ID 9217815, 5 pages
https://doi.org/10.1155/2018/9217815

Research Article

Comparison of Diazinon Toxicity to Temperate and Tropical Freshwater *Daphnia* Species

Thanh-Luu Pham[1] and Ha Manh Bui[2]

[1]*Institute of Research and Development, Duy Tan University, Da Nang, Vietnam*
[2]*Department of Environmental Science, Saigon University, 273 An Duong Vuong Street, District 5, Ho Chi Minh city, Vietnam*

Correspondence should be addressed to Ha Manh Bui; manhhakg@yahoo.com.vn

Received 12 June 2018; Revised 16 August 2018; Accepted 19 September 2018; Published 11 November 2018

Guest Editor: Gassan Hodaifa

The presence of pesticides in water bodies presents unique challenges to the ecosystem and all the life forms. Biological methods have been widely used to examine the toxic effects of various toxicants including pesticides. The present study aims at determining the adverse effects of diazinon, a nonsystemic organophosphate insecticide, on two cladoceran species including the temperate *Daphnia magna* (*D. magna*) and the tropical *Daphnia lumholtzi* (*D. lumholtzi*). The 48 h LC_{50} values demonstrated higher toxicity of diazinon for *D. lumholtzi* at a concentration of 3.41 $\mu g \cdot L^{-1}$ compared to *D. magna* at a concentration of 4.63 $\mu g \cdot L^{-1}$. After 14 days of exposure to diazinon, the survival capacity as well as the reproduction potential of the two cladoceran species clearly reduced and their rate of population increase (RPI) decreased at concentrations >0.1 $\mu g \cdot L^{-1}$. The present study indicated that the tropical cladoceran (*D. lumholtzi*) was more sensitive than the temperate *D. magna*. Therefore, it could be used as an indicator for toxicity assessment in tropical environments. The presence of diazinon in water bodies can be associated with significant risk to aquatic organisms.

1. Introduction

In recent decades, most of the developed countries are shifting toward a chemical-free agriculture, also known as "organic" agriculture/farming, or in other words, decreasing the use of pesticides [1, 2]. This has resulted in substantial improvements in agronomic practices guided by stringent legislations and in the quality of natural water bodies, that is, less risk to the aquatic lives [1, 2]. Most of the developing countries in the tropical regions are increasing their use of pesticides and fertilizers as they become wealthier [3]. As a result, the concentration of pesticides in tropical environments has constantly increased, causing a decline in species diversity. Although pesticides have certain beneficial effects for agricultural crops, their use can cause a wide range of toxic effects on different nontarget organisms [4].

Diazinon (*O*,*O*-diethyl-*O*-[2-isopropyl-6-methyl-4-pyrimidinyl] phosphorothioate) is a nonsystemic organophosphate insecticide. It was commonly used for insert control in agricultural crops [4, 5]. The toxicity of diazinon results from inhibiting the enzyme acetylcholinesterase (AChE), leading to the accumulation of neurotransmitters and altered signal transmission in chemical synapses [6]. In the domestic and international markets, there are more than 500 registered products that contain diazinon as the active substance [4]. Due to its widespread use, diazinon is frequently found in freshwater ecosystems [7]. In a recent study, Montuori et al. [7] reported that diazinon is prevalent in aquatic systems all over Europe, with the highest concentration recorded to be 785 $ng \cdot L^{-1}$ in the Ebro River, Spain. Moreover, high concentrations of diazinon up to 1.5 $\mu g \cdot L^{-1}$ have been found in urban waterways in California [8]. In recent decades, diazinon has been widely used in tropical regions [9]. However, pesticide laws and regulations have not been implemented adequately in these regions despite its heavy applications. The toxic effects of diazinon are available in the literature for the temperate cladoceran *D. magna*. However, the toxic effects of diazinon on tropical zooplanktons have not been well documented and studied in the literature.

Diazinon generates high acute toxicity to a wide variety of aquatic organisms, leading to a wide range of sublethal

biochemical effects, damage to specific target organs and tissues, and adverse ecological impacts. The toxicity of diazinon has extensively studied in fish [4, 9–11] and crustaceans [6, 12, 13], and it has been reported to be moderately toxic to early life stages of zebrafish [4]. The 96 h LC_{50} values ranging from 0.32 to 1.53 $mg{\cdot}L^{-1}$ for larval and from 2.2 to 10.3 $mg{\cdot}L^{-1}$ for adult of several fish have already been recorded [10]. Yen et al. [11] reported that diazinon lowers larval swimming activity and inhibits AChE activity in zebrafish, as well as an increase in the Hsp70 content. In cladocerans, diazinon at the concentration from 0.18 to 0.30 $\mu g{\cdot}L^{-1}$ caused adverse effects on the survival of *D. magna* [6, 14]. These diazinon concentrations have been reported to cause a decrease in mean total young per female, mean brood size, and rate of population increase (RPI) and development of *D. magna*. Only the concentration above 0.25 $\mu g{\cdot}L^{-1}$ caused a delay in the time to first reproduction [14]. Toxicokinetic and toxicodynamic models of diazinon and its by-product 2-isopropyl-6-methyl-4-pyrimidinol in crustacean species were investigated by Kretschmann et al. [15]. Results suggested that the oxidative dearylation of diazinon to pyrimidinol is a crucial cellular detoxification step which is catalyzed by the enzyme P450 [15]. However, most ecotoxicological studies use the temperate cladoceran *D. magna* as an ecotoxicological model; the toxicity of insecticide on tropical zooplankton species has not been examined to the same extent [16].

In this study, an acute 48 h assay and a chronic 14-day assay were performed to study the effects of diazinon on two cladoceran species. The toxicity of diazinon to early life stages of the temperate species *D. magna* was tested, and the toxicity on *D. magna* was compared to that on the tropical species *D. lumholtzi*. The results will provide baseline information to establish the benchmark for organophosphate insecticides in tropical waters.

2. Materials and Methods

2.1. Chemicals. Diazinon (*O*,*O*-diethyl-*O*-[2-isopropyl-6-methyl-4-pyrimidinyl] phosphorothioate) was purchased from Sigma-Aldrich. Stock solutions of 1 mM were prepared by diluting in dimethyl sulfoxide (DMSO) prior to the experiment and kept at 4°C.

2.2. Test Organisms. Two cladocerans species were used in the present study: *D. lumholtzi* was isolated from a fish pond in the north of Vietnam. *D. magna* was obtained from MicroBioTest Inc. (Belgium). Both daphnids were grown in 1 L beakers filled with COMBO medium [17] and kept at a temperature of 25 ± 1°C under a light : dark cycle of 12 h : 12 h. The animals were fed with microgreen alga (*Chlorella* sp.) and a 1 : 1 : 1 mixture of yeast, cerrophyl, and trout chow digestion (YTC) [18]. The food and culture medium were renewed every two days.

2.3. Acute Toxicity Assay. The acute immobilization test was performed according to Protocol 202 of the Organization for the Economical Cooperation and Development [19]. This assay was performed to evaluate the sensitivity of the species and to establish the range of concentrations to be used in chronic assays. Briefly, *Daphnia* neonates (<24 h old) were maintained in 50 mL beakers containing 30 mL COMBO medium spiked with diazinon at a concentration range of 0, 0.5, 1, 2, 5, and 10 $\mu g{\cdot}L^{-1}$. In each exposure concentration, 15 neonates were exposed per concentration of diazinon and blank control. All test exposures were prepared in triplicate. The test containers were placed at a controlled temperature of 25 ± 1°C under a light : dark cycle of 14 h : 10 h during 48 h of incubation. The assessed response for this assay was the immobility or death of the cladocerans. The criterion for test acceptance was a survival rate greater than or equal to 90% in the control group. Finally, the mortality data recorded at the end of the toxicity tests (48 h) were used to determine the median lethal concentration (48 h LC_{50}).

2.4. Chronic Toxicity Assay. Based on the acute toxicity results and environmentally relevant concentrations of diazinon in previous studies [7, 8], daphnids were exposed during 14 days to the following sublethal diazinon concentrations: 0 (control), 0.05, 0.1, 0.2, 0.5, and 1.0 $\mu g{\cdot}L^{-1}$. The reproduction test was conducted according to the standard protocol described in APHA [20] with minor modifications. Briefly, neonates of less than 24 h old were individually incubated in 50 mL beakers containing 20 mL control medium or exposed to diazinon concentrations. Diazinon concentrations and food (a mixture of green algae *Chlorella* sp., at a density of 5×10^6 $cells{\cdot}mL^{-1}$, and YTC) were renewed every two days. The survival, reproduction (fecundity), time for the first reproduction, total number of neonates per female, number of broods, and brood size were recorded daily. The body length of parent daphnids was measured at the end of the experiment.

2.5. Statistical Analysis. The 48 h median lethal concentrations (48 h LC_{50}) were predicted by probit analysis as previously reported by Stephan [21]. The rate of population increase (RPI) was calculated according to the method suggested by Euler–Lotka [22]: $\sum e^{-rx} l_x m_x = 1$, where l_x = the proportion of surviving to age x, m_x = age-specific fecundity, and x = time in days. All the calculations were based on 14-day experiments [23]. The differences between treatment groups and controls were determined through one-way analysis of variance (ANOVA). Significant differences ($p < 0.05$) were distinguished by using Dunnet's test method. All data are presented as median ± SD.

3. Results and Discussion

3.1. Acute Toxicity. No mortality occurred in the control during the experimental time of acute test. The highest tested concentration of diazinon resulted in 100% mortality of both daphnids. However, diazinon showed higher toxicity to *D. lumholtzi*. The 48 h LC_{50} values of diazinon for *D. magna* and *D. lumholtzi* under the tested experimental conditions, at 95% confidence interval, were 4.63 and 3.41 $\mu g{\cdot}L^{-1}$, respectively.

The toxic effects of pesticides on aquatic organisms are often investigated using the temperate *D. magna* under

laboratory conditions. However, there is still little understanding about the acute and chronic effects of diazinon on crustaceans, especially to species that originated from tropical regions. The 48 h LC_{50} values of diazinon reported in this study were in the range with the 48 h LC_{50} values reported for nauplius of copepod *Eodiaptomus* (48 h LC_{50} = 2.8 $\mu g.L^{-1}$), *Mesocyclops* (48 h LC_{50} = 2.9 $\mu g{\cdot}L^{-1}$), and *Thermocyclops* (48 h LC_{50} = 4.1 $\mu g{\cdot}L^{-1}$) [24]. However, the values were lower than the 48 h LC_{50} values for adults of *Eodiaptomus* (48 h LC_{50} = 46.8 $\mu g{\cdot}L^{-1}$), *Mesocyclops* (48 h LC_{50} = 30.6 $\mu g{\cdot}L^{-1}$), and *Thermocyclops* (48 h LC_{50} = 40.2 $\mu g{\cdot}L^{-1}$) [24], or higher than 48 h LC_{50} values for other cladocerans such as *Ceriodaphnia dubia* (48 h LC_{50} = 0.21 $\mu g{\cdot}L^{-1}$) [12]. Results from acute assays documented higher sensitivity of tropical *D. lumholtzi* neonates to diazinon when compared to the temperate *D. magna*. From a practical application perspective, these results clearly showed that the *D. lumholtzi* may serve as a suitable surrogate for the temperate species *D. magna*, that is, as a toxicity indicator species, under tropical conditions.

3.2. Chronic Toxicity. The effects of sublethal diazinon concentrations on the survival and reproduction of *D. magna* and *D. lumholtzi* during 14 days of incubation are shown in Table 1 and Figure 1. The survival of both daphnids decreased with increasing concentrations of diazinon during the 14-day test. Significant decreases in life history responses were observed for *D. magna* and *D. lumholtzi* when exposed to diazinon. Both daphnids grew well in the control incubation (the length of *D. magna* and *D. lumholtzi* increased up to 4.1 and 2.4 mm, respectively, at the end of the experiment). All individuals in the control survived throughout the experimental period (14 days) and produced numerous offspring (27.4 ± 3.6 juveniles per *D. magna* and 18.2 ± 2.1 per *D. lumholtzi*).

Diazinon caused significant effects and dose-dependent increases on the reproduction (number of broods per female) of both daphnids (Table 1). For *D. magna*, diazinon at the concentration up to 0.1 $\mu g{\cdot}L^{-1}$ or higher resulted in a significant decrease in reproduction (number of broods per female), while for *D. lumholtzi*, a significant reduction of reproduction was recorded from the lowest concentration tested (0.05 $\mu g{\cdot}L^{-1}$). The reproduction of both daphnids was significantly delayed ($p < 0.05$), from 6.5 days for the control to 9.6 days for *D. magna* (as the diazinon concentration up to 0.1 $\mu g{\cdot}L^{-1}$ or higher), and from 3.5 days in the control to 5.4 days for *D. lumholtzi* (as the diazinon concentration up to 0.05 $\mu g{\cdot}L^{-1}$ or higher) (Table 1). The results of both tested species indicated that the number of neonates born per female significantly declined at the diazinon concentration of 0.1 $\mu g{\cdot}L^{-1}$ or higher (Table 1). The mean body length significantly decreased in those daphnids (as the diazinon concentration up to 0.2 $\mu g{\cdot}L^{-1}$ or higher) within the 14-day test period, from 4.1 to 3.1 mm and from 2.4 to 1.9 mm in *D. magna* and *D. lumholtzi*, respectively.

The results of the life-response history of both *D. magna* and *D. lumholtzi* species. Exposure to sublethal concentrations of diazinon under laboratory conditions showed that diazinon significantly reduced the number of offspring produced per female and delayed in the age at first brood. The obtained results are in agreement with previous observations which showed a decrease in the mean offspring production and suppression of growth in *D. magna* or *Ceriodaphnia dubia* following exposure to diazinon [12, 14, 25].

The results from the chronic assay showed that *D. lumholtzi* was a sensitive species to diazinon. Sánchez et al. [25] suggested that crustaceans are closely related to insects, more than other invertebrates. Hence, they are more sensitive to pesticides than other invertebrates. Modra et al. [5] indicated that the toxicity of diazinon is affected by many factors such as the biotransformation ability of the organism itself, water temperature, presence of other pollutants, and other nonidentified environmental variables. On the other hand, by using a toxic kinetic and dynamic model for studying diazinon toxicity, Kretschmann et al. [13] suggested that the sensitivity of test species to diazinon may depend on the detoxification ability of diazinon and diazoxon (a toxic metabolite of diazoxon). These authors revealed that, when compared to *D. magna*, the amphipod crustacean *Gammarus pulex* is less sensitive to diazinon because the detoxification of diazinon and diazoxon is six times faster which in turn causes less damaging effects. The authors also suggested that mechanistic-based effect models should be used to explain the actual causes, effects, and the minor differences among different aquatic invertebrates [13].

3.3. Effects of Diazinon on Rate of Population Increase. The effects of diazinon on the RPI are shown in Figure 2. Diazinon concentrations equal and/or greater than 0.1 $\mu g{\cdot}L^{-1}$ significantly reduced the RPI of both daphnids during the 14-day chronic test ($p < 0.05$). It can be observed that both daphnids exposed to diazinon showed a nearly similar trend during the 14-day chronic test. In natural environments, diazinon is known to cause adverse effects on many zooplankton species including *Daphnia*, even at low concentrations (from 5.3 to 26.3 nM) [6, 15]. The RPI of the *Daphnia* population is an important indicator for prediction population trends. The survival rate, number of offspring per female, and age of fecundity are all crucial for the prediction [26]. A reduction in the RPI indicated chronic toxicant stress of pesticides on *Daphnia* [27].

Our results indicated that both test species were sensitive to diazinon and could be employed to predict the risk of insecticides. The present results clearly suggest that the growth rates of *D. magna* and *D. lumholtzi* in the control treatments were within the range reported in the literature [25, 26]. In tropical countries, it is necessary to establish the benchmark for organophosphate insecticides. To minimize environmental risk associated with pesticides in tropical ecosystems, we strongly recommend further studies on short- and long-term toxic effects of organophosphate insecticides on different tropical groups of organisms.

4. Conclusions

The present study confirmed that diazinon poses significant risk to aquatic organisms, namely, nontarget *Daphnia*

Table 1: Fecundity, survival, and body length of *D. magna* and *D. lumholtzi* after exposure to different concentrations of diazinon for 14 days.

Diazinon ($\mu g \cdot L^{-1}$)	Number of broods per female	Age at first reproduction (days)	Number of offspring per female	Longevity (days)	Length (mm)
D. magna					
CT	4.9 ± 0.2	6.5 ± 0.3	27.4 ± 3.6	14	4.1 ± 0.05
0.05	4.5 ± 0.1	7.2 ± 0.2	24.7 ± 3.2	14	4.0 ± 0.07
0.1	3.2 ± 0.2*	7.8 ± 0.2*	19.6 ± 4.3*	14	3.9 ± 0.08
0.2	2.0 ± 0.0*	8.6 ± 0.3*	12.2 ± 2.5*	14	3.8 ± 0.04*
0.5	1.8 ± 0.1*	9.3 ± 0.6*	3.7 ± 4.6*	11	3.3 ± 0.07*
1	1.6 ± 0.1*	9.6 ± 0.3*	3.1 ± 2.6*	10	3.1 ± 0.09*
D. lumholtzi					
CT	4.2 ± 0.3	3.5 ± 0.3	18.2 ± 2.1	14	2.4 ± 0.05
0.05	3.7 ± 0.1*	3.4 ± 0.5	18.4 ± 1.3	14	2.4 ± 0.06
0.1	3.6 ± 0.1*	4.2 ± 0.2*	16.2 ± 1.5*	14	2.3 ± 0.07
0.2	3.0 ± 0.1*	4.7 ± 0.4*	9.6 ± 1.9*	11	2.0 ± 0.05*
0.5	2.5 ± 0.2*	5.1 ± 0.3*	5.4 ± 1.3*	9	2.1 ± 0.08*
1	2.2 ± 0.1*	5.4 ± 0.2*	4.1 ± 1.2*	6	1.9 ± 0.05*

Note. * $p < 0.05$.

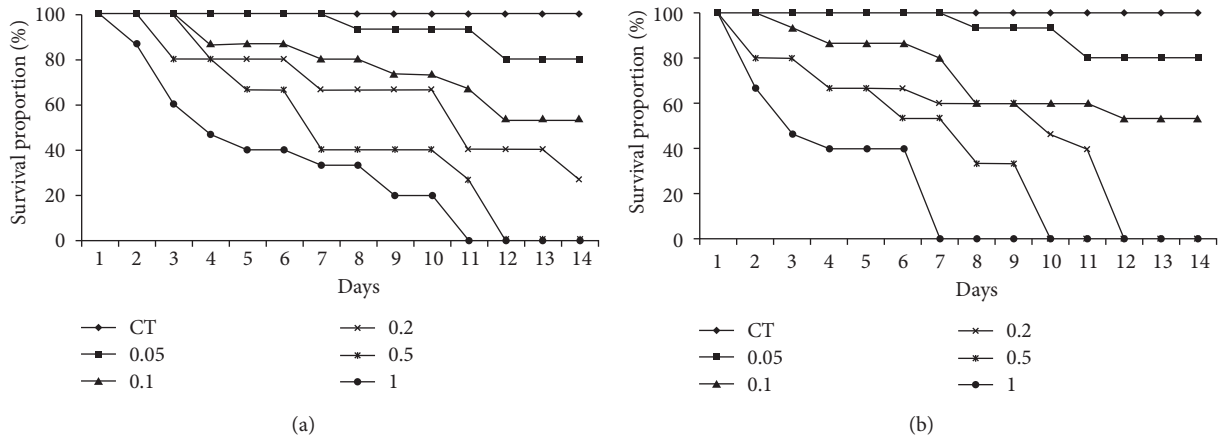

Figure 1: Survival results after exposure to different diazinon concentrations ($\mu g \cdot L^{-1}$). (a) *D. magna* and (b) *D. lumholtzi*.

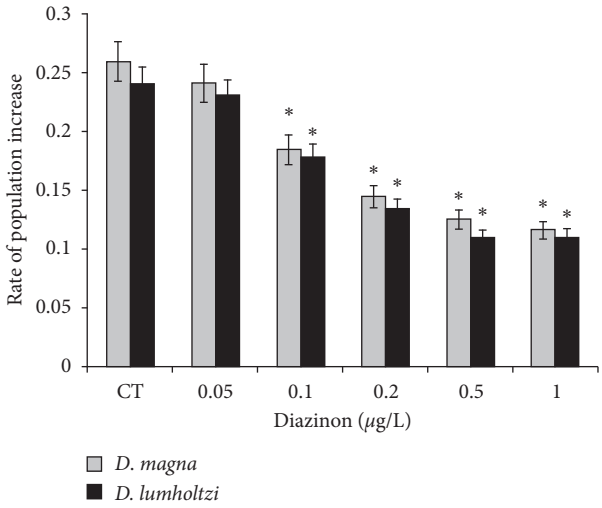

Figure 2: The effect of diazinon on the rate of population increase of *Daphnia*. *Significant difference with the control ($p < 0.05$).

species. The population growth of *D. magna* and *D. lumholtzi* was adversely affected by diazinon after a chronic exposure period. Compared with *D. magna*, *D. lumholtzi* showed even higher sensitivity to diazinon in the acute test. The results of this study are important for prediction of toxic effects and environmental risk associated with insecticides. Further studies using additional organophosphate insecticides, different tropical test species, and test conditions are needed to assess the possible environmental risk associated with pesticides in tropical aquatic ecosystems.

Data Availability

The data used to support the findings of this study are available from the corresponding author upon request.

Conflicts of Interest

The authors declare that they have no conflicts of interest.

Acknowledgments

The authors would like to thank Associate Professor Thanh-Son Dao for his technical support.

References

[1] C. E. Handford, C. T. Elliott, and K. Campbell, "A review of the global pesticide legislation and the scale of challenge in reaching the global harmonization of food safety standards," *Integrated Environmental Assessment and Management*, vol. 11, no. 4, pp. 525–536, 2015.

[2] A. Tal, "Making conventional agriculture environmentally friendly: moving beyond the glorification of organic agriculture and the demonization of conventional agriculture," *Sustainability*, vol. 10, no. 4, p. 1078, 2018.

[3] F. Sanchez-Bayo and R. V. Hyne, "Comparison of environmental risks of pesticides between tropical and nontropical regions," *Integrated Environmental Assessment and Management*, vol. 7, no. 4, pp. 577–586, 2011.

[4] M. Velki, C. Di-Paolo, J. Nelles, T. B. Seiler, and H. Hollert, "Diuron and diazinon alter the behavior of zebrafish embryos and larvae in the absence of acute toxicity," *Chemosphere*, vol. 180, pp. 65–76, 2017.

[5] H. Modra, D. Vrskova, S. Macova et al., "Comparison of diazinon toxicity to embryos of *Xenopus laevis* and *Danio rerio*: degradation of diazinon in water," *Bulletin of Environmental Contamination and Toxicology*, vol. 86, no. 6, pp. 601–604, 2011.

[6] M. A. Zein, S. P. McElmurry, D. R. Kashian, P. T. Savolainen, and D. K. Pitts, "Toxic effects of combined stressors on *Daphnia pulex*: interactions between diazinon, 4-nonylphenol, and wastewater effluent," *Environmental Toxicology and Chemistry*, vol. 34, no. 5, pp. 1145–1153, 2015.

[7] P. Montuori, S. Aurino, A. Nardone, T. Cirillo, and M. Triassi, "Spatial distribution and partitioning of organophosphates pesticide in water and sediment from Sarno River and Estuary, Southern Italy," *Environmental Science and Pollution Research*, vol. 22, no. 11, pp. 8629–8642, 2015.

[8] H. C. Bailey, L. Deanovic, E. Reyes et al., "Diazinon and chlorpyrifos in urban waterways in Northern California, USA," *Environmental Toxicology and Chemistry*, vol. 19, no. 1, pp. 82–87, 2000.

[9] V. C. Nguyen, N. T. Phuong, and M. Bayley, "Sensitivity of brain cholinesterase activity to diazinon (BASUDIN 50EC) and fenobucarb (BASSA 50EC) insecticides in the air-breathing fish *Channa striata* (Bloch, 1793)," *Environmental Toxicology and Chemistry*, vol. 25, no. 5, pp. 1418–1425, 2006.

[10] V. Scheil, C. Kienle, R. Osterauer, A. Gerhardt, and H.-R. Köhler, "Effects of 3,4-dichloroaniline and diazinon on different biological organisation levels of zebrafish (*Danio rerio*) embryos and larvae," *Ecotoxicology*, vol. 18, no. 3, pp. 355–363, 2009.

[11] J. Yen, S. Donerly, E. D. Levin, and E. Linney, "Differential acetylcholinesterase inhibition of chlorpyrifos, diazinon, and parathion in larval zebrafish," *Neurotoxicology and Teratology*, vol. 33, no. 6, pp. 735–741, 2011.

[12] K. E. Banks, P. K. Turner, S. H. Wood, and C. Matthews, "Increased toxicity to *Ceriodaphnia dubia* in mixtures of atrazine and diazinon at environmentally realistic concentrations," *Ecotoxicology and Environmental Safety*, vol. 60, no. 1, pp. 28–36, 2005.

[13] A. Kretschmann, R. Ashauer, J. Hollender, and B. I. Escher, "Toxicokinetic and toxicodynamic model for diazinon toxicity - mechanistic explanation of differences in the sensitivity of *Daphnia magna* and *Gammarus pulex*," *Environmental Toxicology and Chemistry*, vol. 31, no. 9, pp. 2014–2022, 2012.

[14] A. Fernández-Casalderrey, M. D. Ferrando, and E. Andreu-Moliner, "Chronic toxicity of diazinon to *Daphnia magna*: effects on survival, reproduction and growth," *Toxicological and Environmental Chemistry*, vol. 49, no. 1-2, pp. 25–32, 1995.

[15] A. Kretschmann, R. Ashauer, T. G. Preuss, P. Spaak, B. I. Escher, and J. Hollender, "Toxicokinetic model describing bioconcentration and biotransformation of diazinon in *Daphnia magna*," *Environmental Science and Technology*, vol. 45, no. 11, pp. 4995–5002, 2011.

[16] S. L. Ghose, M. A. Donnelly, J. Kerby, and S. M. Whitfield, "Acute toxicity tests and meta-analysis identify gaps in tropical ecotoxicology for amphibians," *Environmental Toxicology and Chemistry*, vol. 33, no. 9, pp. 2114–2119, 2014.

[17] S. S. Kilham, D. A. Kreeger, S. G. Lynn, C. E. Goulden, and L. Herrera, "COMBO: a defined freshwater culture medium for algae and zooplankton," *Hydrobiologia*, vol. 377, no. 1/3, pp. 147–159, 1998.

[18] US Environmental Protection Agency (US EPA), *Methods for Measuring the Acute Toxicity of Effluents and Receiving Waters to Freshwater and Marine Organisms*, EPA-821-R02-012, 5th edition, 2002.

[19] OECD, *Daphnia sp. Acute Immobilization Test: OECD Guideline for Testing of Chemicals No. 202*, Organization for the Economical Cooperation and Development (Publisher), Paris, France, 2004.

[20] American Public Health Association (APHA), *Standard Methods for the Examination of Water and Wastewater*, American Public Health Association, Washington DC, USA, 2005.

[21] C. Stephan, *Methods for Calculating an LC50*, Vol. 634, ASTM (American Society for Testing and Materials) Special Technical Publication, West Conshohocken, PA, USA, 1977.

[22] A. J. Lotka, "A natural population norm," *Journal of the Washington Academy of Sciences*, vol. 3, no. 241–248, pp. 289–293, 1913.

[23] M. J. Villarroel, E. Sancho, M. D. Ferrando, and E. Andreu, "Acute, chronic and sublethal effects of the herbicide propanil on *Daphnia magna*," *Chemosphere*, vol. 53, no. 8, pp. 857–864, 2003.

[24] H. Takahashi, K. H. Chang, and T. Hanazato, "Acute toxicity of the insecticide diazinon and carbaryl to calanoid and cyclopoid copepoda (*Eodiaptomus, Mesocyclops* and *Thermocyclops*) in different life stages," *Japanese Journal of Environmental Toxicology*, vol. 9, no. 2, pp. 133–139, 2006.

[25] M. Sánchez, M. D. Ferrando, E. Sancho, and E. Andreu-Moliner, "Evaluation of a *Daphnia magna* renewal life-cycle test method with diazinon," *Journal of Environmental Science and Health, Part B*, vol. 33, no. 6, pp. 785–797, 1998.

[26] E. Sancho, M. J. Villarroel, and M. D. Ferrando, "Assessment of chronic effects of tebuconazole on survival, reproduction and growth of *Daphnia magna* after different exposure times," *Ecotoxicology and Environmental Safety*, vol. 124, pp. 10–17, 2016.

[27] J. R. Sánchez-Ortíz, S. S. S. Sarma, and S. Nandini, "Comparative population growth of *Ceriodaphnia dubia* and *Daphnia pulex* (Cladocera) exposed to zinc toxicity," *Journal of Environmental Science and Health, Part A*, vol. 45, no. 1, pp. 37–41, 2010.

Hindawi
Journal of Chemistry
Volume 2018, Article ID 7918583, 9 pages
https://doi.org/10.1155/2018/7918583

Research Article

Co-composting of Olive Mill Waste and Wine-Processing Waste: An Application of Compost as Soil Amendment

Z. Majbar,[1] **K. Lahlou**,[1] **M. Ben Abbou**,[2] **E. Ammar**,[3] **A. Triki**,[4] **W. Abid**,[3] **M. Nawdali**,[5] **H. Bouka**,[2] **M. Taleb**,[1] **M. El Haji**,[6] **and Z. Rais**[1]

[1]*Laboratory of Engineering, Electrochemistry and Modeling Environment (LEEME), Faculty of Sciences, Fez, Morocco*
[2]*Laboratory of Natural Resources and Environment, University Sidi Mohammed Ben Abdallah, Faculty Polydisciplinary, Taza, Morocco*
[3]*Research Unity: Urban and Costal Environments, University of Sfax, National Engineering School of Sfax, Sfax, Tunisia*
[4]*Research Laboratory: Improvement and Protection of Olive Tree Genetic Resources, Institute of the Olive Tree, Sfax BP1087, Tunisia*
[5]*Laboratory of Chemistry of Condensed Matter (LCCM), University Sidi Mohammed Ben Abdallah, Faculty of Sciences and Technology, Fez, Morocco*
[6]*Laboratory Engineering Research-OSIL Team Optimization of Industrial and Logistics Systems, University Hassan II, Superior National School of Electricity and Mechanic (ENSEM), Casablanca, Morocco*

Correspondence should be addressed to Z. Majbar; zinebmajbar@gmail.com

Received 4 May 2018; Revised 22 July 2018; Accepted 8 August 2018; Published 23 September 2018

Academic Editor: Gassan Hodaifa

In order to decrease the environmental harm produced by the agro industries' wastes', an investigation of the co-composting of olive mill waste (olive mill wastewater (OMW), olive mill sludge (OMS)) and wine by-products (grape marc and winery wastewater) was done. Three aerated windrows of variable compositions were performed; these windrows differ in terms of their initial composition and the liquid used for their humidification; OMW and wastewater winery were used for humidification to replace water for windrow moistening. Moreover, the main physicochemical parameters (temperature, pH, electrical conductivity, and C/N) were monitored to evaluate the co-composting process. The latter lasted around three months. The elaborated composts were characterized by low C/N ratio, and they were rich in fertilizing and nutriment elements and of low heavy metal contents. The humidification of the windrows with OMW showed effectiveness in improving the windrows temperature, reflected by the high temperatures monitored during the composting process in comparison with the windrow humidified with winery wastewater. Furthermore, a longer thermophilic phase was held in windrows carrying OMS. The valorization of the produced composts for soil amendment significantly improved the soil fertility. Indeed, field experiments showed an increase in radish yield by 10%, the composts were harmless and did not have any phytotoxic effect on radish growth.

1. Introduction

The activity of the agro-food industries causes a lot of harm to environment due to the production of huge amounts of waste. In Morocco, the industrial sector generates yearly more than 1.2 million tons of wastes, among which the agro-food industry represents 67% [1]. Consequently, the management and the valorization of these harmful residues are necessary for the environment''s preservation.

The olive oil extraction is an important activity that generates a huge amount of effluent, namely, olive mill wastewater, estimated to 400 000 m^3 per year [2]. The OMW is an acidic and dark liquid effluent, with a high organic matter load and high conductivity [3, 4]; its composition varies both qualitatively and quantitatively according to the olive variety, climate condition, cultivation and harvesting practices, the olive storage time, and the olive oil extraction system [3].

In Morocco, the OMW management practice regulated and adopted by the majority of olive oil industries is the storage in evaporation ponds. However, this technique does not reduce the OMW toxicity since large quantities of olive mill sludge (OMS) are produced. These huge quantities represent a significant problem in olive oil industries; therefore, more effective solutions must be developed to remedy this problem.

The wine industry is another activity that generates significant quantity of waste; this activity produces large amount of by-products that are represented by solid organic residues (grape marc) and wastewater. The production of one hectoliter of wine produces 18 kg of grape marc [5], which gives an annual production of 7200 tons [6]. Still, the quantity of wine wastewater depends largely on the process used in the industry. The different residues from the wine industry are characterized by low pH and electrical conductivity and high organic matter content [7]. The richness of these by-products in organic matter allows their use for soil fertility improvement [8, 9]. The direct incorporation of these residues could cause serious environmental problems if they are added excessively to the soil in an uncontrolled manner. Consequently, their treatment is crucial before their discharge or use for agricultural purposes. The suitable management of these agro-food wastes is an important strategy for the environment protection. Many investigations have focused on the study of treatment and valorization techniques of these residues at an experimental scale [10–16]. At the industrial level, the treatment of these residues is rare, and the problem of all the available wastes has not yet been solved.

Recently, researchers have shown that composting is one of the effective alternatives for the recycling and the valorization of organic wastes [8, 17–22]. It is a degradation process of the organic matter, allowing the achievement of a stable product, rich in humic substances and in fertilizing elements, serving as soil organic amendment [23–25]. The application of compost can have strong ecological environmental values, allowing not only the removal of very expensive chemical fertilizers but also the improvement of the quality of agricultural soils and carbon sequestration [8, 9, 26].

Diverse studies had developed composting of organic waste, such as OMW [19, 24, 27–30], sludge from wastewater treatment [31], and agro-industrial waste [32]. While other studies on the co-composting of olive mill wastewater with poultry manure [25, 27, 33], olive mill wastewater with solid organic waste [20, 34], and date palm with activated sludge [35] have been carried out. The evaluation of the composting process and the study of its environmental impact due to gas emissions have also been the subject of numerous studies [35–38].

Considering the fact that co-composting olive oil waste (OMW and OMS) and wine industry have not gained much attention in previous studies; the aims of this work are as follows: firstly, to valorize the olive mill wastes (OMW and OMS) and by-products wine industry by co-composting; secondly, to study the evolution of the parameters describing the co-composting of mixtures of OM, OMS, and green waste; and lastly, to test the effect of the different composts produced on the performance and yield of radish in the field.

2. Materials and Methods

2.1. Raw Materials. The organic wastes used as substrates for the composting procedure included OMW, OMS, grape marc, winery wastewater, and household waste. The OMW and OMS were collected from a natural evaporation basin of continuous three-phase olive oil extraction unit located in Meknassa Ben Ali (8 km form Taza, Morocco). The basin was made of concrete with a storage capacity of 240 m^3. The collected OMW had a maximum storage time of 30 days; the OMS were collected at the end of August, after a total evaporation of the quantities of water contained in the OMW. The grape marc and the winery wastewater were collected from an industrial company "Celliers de Meknès" located in Meknes (Morocco), and the green waste was gathered from markets located in Taza (Morocco). They are composed mainly of fruit and vegetable residues. The waste physicochemical characterization is presented in Table 1.

2.2. Composting Procedure. The raw materials were mixed in order to be co-composted in open area, using 3 windrows of 0.6 m height, 2 m length, and 1.2 m diameter base [30]. These windrows differed in terms of their initial composition and the liquid used for their humidification (Table 2). The proportions of the raw materials were calculated according to the methods described by Proietti et al. and Soudi [26, 39] to obtain a physicochemical characterization of the initial mixture for starting the composting process.

The moisture content was adjusted to around 50–60% (optimal moisture content for composting); this operation was performed during the turning of the windrows. The windrows were turned once every 3 days at the beginning of the process, then once every 7 days, and once every 15 days for the remaining composting period.

Representative and homogenous samples were collected during the composting procedure from the windrows for analysis. Each sample was obtained by mixing 6 subsamples taken from six different points of windrows, according to ISO 8633 [40].

2.3. Physicochemical Analysis. The raw materials and compost samples were analyzed for pH and electrical conductivity (EC) in a 1 : 5 (w/v) water soluble extract in [41, 42]. The dry matter content was assessed by drying at 105°C for 24 h using a drying oven type WTB Binder ED 115, and the OM was determined by measuring the loss of ignition at 550°C for 4 h using muffle furnace type Lenton EF11/8B. The organic carbon (OC) was calculated using the following equation:

$$\mathrm{CO}\,(\%) = \frac{\%\mathrm{MO}}{1,724}. \quad (1)$$

The total Kjeldahl nitrogen (TKN) was analyzed using the Kjeldahl method according to AFNOR standard (1981) [43]. The determination of heavy metals and oligoelements were first extracted by heating 2 g of compost with HNO_3, and then the filtrate was analyzed using ICP-AES method (inductively coupled plasma atomic emission spectroscopy).

Table 1: Physicochemical characteristics of the raw materials used for composting process.

Parameters	OMS	OMW	Grape marc	Winery wastewater	Green waste
pH	5.42 ± 0.03	5.43 ± 0.05	7.42 ± 0.20	6.66 ± 0.02	5.88 ± 0.02
EC ($mS{\cdot}cm^{-1}$)	8.72 ± 0.02	8.02 ± 0.02	4.81 ± 0.03	0.76 ± 0.02	1.63 ± 0.02
Moisture (%)	22.66 ± 3.69	92.47 ± .0.56	72.42 ± 0.58	99.86 ± 0.01	36.98 ± 4.59
Dry matter (%)	77.34 ± 3.69	7.53 ± 0.56	27.58 ± 0.58	0.14 ± 0.01	63.02 ± 4.59
Mineral matter (%)	15.05 ± 5.91	25.25 ± 5.46	30.19 ± 1.65	45.20 ± 6.63	35.15 ± 1.95
Organic matter (%)	84.95 ± 5.91	74.75 ± 5.46	69.81 ± 1.65	54.80 ± 6.63	64.85 ± 1.95
Organic carbon (%)	49.28 ± 3.43	43.36 ± 3.16	40.49 ± 0.96	31.78 ± 3.84	37.61 ± 1.13
TKN (%)	0.74 ± 0.12	0.86 ± 0.15	0.97 ± 0.10	3.75 ± 0.30	1.53 ± 0.06
C/N	67.77 ± 9.73	ND	42.06 ± 3.47	ND	24.69 ± 1.19
COD ($g{\cdot}O_2/l$)	ND	96.07 ± 0.5	ND	14.07 ± 0.1	ND
BOD ($g{\cdot}O_2/l$)	ND	25.67 ± 0.51	ND	14.40 ± 0.4	ND

ND: not determined.

Table 2: Composition of the different windrows.

Windrow	A (600 kg)	B (600 kg)	C (1 ton)
Proportion of solid raw materials*			
(i) OMS	1/3	1/3	0
(ii) Grape marc	1/3	1/3	1/2
(iii) Green waste	1/3	1/3	1/2
Humidification effluent	OMW	Winery wastewater	OMW
Total volume used (m^3)	0.8	1.0	1.3

*Proportion expressed in weight/weight.

The characterization of the effluents was performed according to the experimental protocols described by Rodier et al. [44]. pH and electrical conductivity were directly measured using multiparameter consort C335. The chemical oxygen demand (COD) was determined according to NF T90-101 standard [45]. The biological oxygen demand (BOD) was determined using BOD meter-type OxiTop.

The windrow temperature was measured using multiparameter consort C535 daily during the mesophilic and the thermophilic composting phases and weekly until its maturity. The presented temperature value consists of a mean of 6 measurements at different points and depths of the windrow.

2.4. Phytotoxicity Test. The compost phytotoxicity was determined by evaluating its aqueous extract on seed germination. The germination test was carried out on 10 seeds of cress (*Lepidium sativum)* experimented at different dilutions in Petri dishes, including filter paper soaked in the compost extract. The test was conducted in dark at 25°C for 72 hours [32, 33]. Three repetitions were performed.

The germination index (GI) was determined considering the number of sprouts and root growth, using the following equation:

$$GI(\%) = \frac{GB}{GT} * \frac{LB}{LT} * 100, \quad (2)$$

where GB is the number of germinated seeds in the case of aqueous extract, GT is the number of germinated seeds in the case of the control where the distillated water was used, LB is the root length on compost extract, and LT is the root length control.

2.5. Radish Production. The effects of the different produced composts were assessed on radish (*Raphanus sativus)*, of a *National* variety. Nine parcels of 1.5 m^2 arranged in a random design were tested using compost and different combinations of compost mixed with farm manure, according to Table 3. These various combinations of composts and manure were used for the soil amendment at a rate of 6 t/ha; they were incorporated in the soil not only spread on the surface. The parcel, which was only amended with farm manure, was considered as the control. No mineral fertilization has been done in the parcels.

The radish seeds were sowed on 29 November 2015, and the radish was harvested on 24 January 2016. The composts effects were assessed by measuring radish yield at the end of the crop cycle.

2.6. Statistical Analysis. Statistical analyses of data were made by IBM SPSS Statistics Version 20. The analysis of the means comparison was carried out by Student's *t*-test to compare the evolution profiles of the composting parameters for the different windrows. The Duncan test was used to calculate the variance and to compare the average values of germination indices for the different composts produced.

All analyses were performed in triplicate. However, for agronomic yields, the results were obtained in the form of one replicate due to the limitation of the plots to a single field. Also, minerals and fertilizing elements and heavy metals were in only one replicate because of the limited cost of investigation of the analysis.

3. Results and Discussion

3.1. Composting Process

3.1.1. Temperature Evolution. During the composting process, the evolution of the temperature in the different windrows is presented in Figure 1. The temperature profiles allow the observation of four conventional stages: a mesophilic, a thermophilic, a cooling, and a maturation stage.

Table 3: Treatments used for parcel amendment.

Parcel	P_0	P_1	P_2	P_3	P_4	P_5	P_6	P_7	P_8	P_9
Compost (%)	0	100	100	100	75	75	75	50	50	50
Compost type		C_A	C_B	C_C	C_A	C_B	C_C	C_A	C_B	C_C
Farm manure (%)	100	0	0	0	25	25	25	50	50	50

C_A, C_B, and C_C are the different mature composts prepared, respectively, from the windrows A, B, and C.

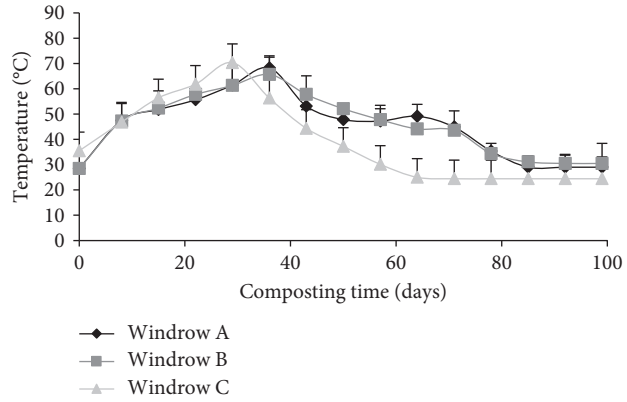

Figure 1: The windrows' temperature profiles during the composting process.

In the first stage, an increase of the temperature to 47°C was recorded during the first week. This observation resulted from the rapid colonization and activity of the mesophilic microorganisms, which degraded organic matter and released heat, thus increasing the windrows' temperature. Then, the temperature rose progressively to reach values above 60°C, corresponding to the second stage, the thermophilic phase, and remained approximately 6 weeks. This result was due to the intense microbial activity reflecting high degradation rates occurring during the first stage [20]. The high temperatures may result in the reduction of pathogens and enhanced windrow sanitation [18]. At the 6th week, the third stage began, and the temperature decreased progressively to reach 30°C. These low temperatures were the result of the less intense microbial activity due to the depletion of easily degradable organic matter [21]. Finally, at the maturity stage, the temperature stabilized at 30°C, the process of composting reached its end, and the produced compost was mature. Moreover, the windrow temperature was highly related to the ambient temperature at this stage.

The long phases observed in windrows A and B can be attributed to the initial composition of the mixtures, in particular the presence of OMS. Indeed, the OMS presents a source of organic matter and therefore an availability of additional degradable substances in these mixtures (windrows A and B) contrary to mixture C. Hachicha et al. have found the similar results suggesting that the self-insulating capacity of OMS during the degradation process can lead to a long thermophilic phase [27]. Such a phase reflects an abnormal degradation process and a delayed transition to the stabilization phase [46].

Additionally, these results also show a significant difference between the temperature profile of windrows A and C and windrows B and C, confirmed by the means comparison test by Student's t-test ($p < 0.05$. This difference can be attributed to the activity of microorganisms during the degradation process depending on the initial composition of the substrates.

3.1.2. pH Evolution. The pH evolution of the composted materials followed the same trend in the different windrows (Figure 2). At the beginning of the process, a slight decrease in pH was noted. This result could be explained by the production of organic acids, dissolved CO_2 in the medium and by-products from the degradation of easily biodegradable compounds [46]. Then, an increase in pH from 6.5 to 6.7, from 6.44 to 6.59, and from 6.48 to 7.66 was observed for windrows A, B, and C, respectively. This could be the result of ammonia production from the degradation of amines [35, 47]. Finally, the pH decreased progressively and stabilized at a neutral pH for windrows A and B and alkali pH for C. These results suggest the formation of humic substances which act as buffers, as confirmed by Zenjari et al. and Amir et al. [48, 49].

The comparison between the three pH profiles shows a significant difference ($p < 0.05$) between windrows A and C and windrows B and C. This can be explained by the nature of the initial substrates put to compost. However, the addition of OMW during the composting process influences the pH of the mixtures.

3.1.3. EC Evolution. The progress of the electrical conductivity (EC) during the composting process is presented in Figure 3. During the first weeks of composting process, the EC values increased from 2.11 to 3.42 $mS{\cdot}cm^{-1}$, from 2.04 to 3.95 $mS{\cdot}cm^{-1}$, and from 2.09 to 3.87 $mS{\cdot}cm^{-1}$, respectively, in the windrows A, B, and C. This increase revealed the extent of mineralization of the organic substrate and the release of ions [35]. Then, a progressive decrease in the EC was observed, even in windrows moistened by OMW exhibiting salts loss by the leaching phenomenon as well as by decreasing their extractability because of their fixation on the stabilized organic matter [49].

Moreover, the EC was measured on the extract of organic matter which is sensitive to the solvent extraction ratio and the temperature at which the method was carried out. It could be noticed that each windrow composition presented a particular progress, with significant differences attributed to phenomena of mineralization, leaching, and fixation depending on the composition of the substrates and the activity of microorganisms.

3.1.4. Organic Matter Degradation. The evolution of the organic matter content of the mixture during the composting process is considered as an essential parameter of biodegradation and transformation of organic matter during composting. Figure 4 presents the organic matter contents of the three mixtures at the beginning and end of the

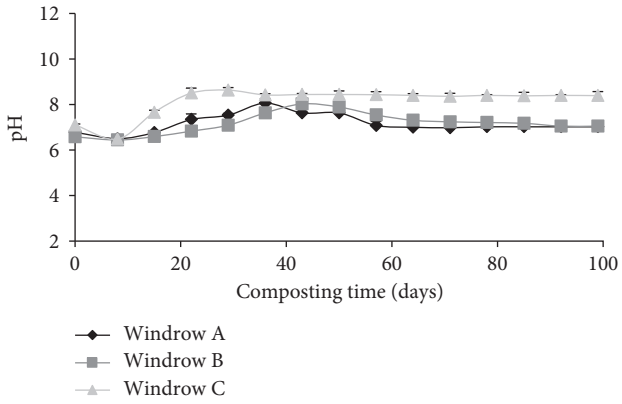

Figure 2: pH evolution during the composting process.

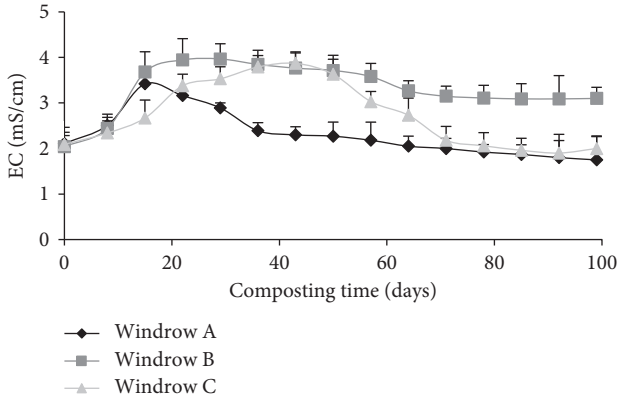

Figure 3: EC evolution during the composting process.

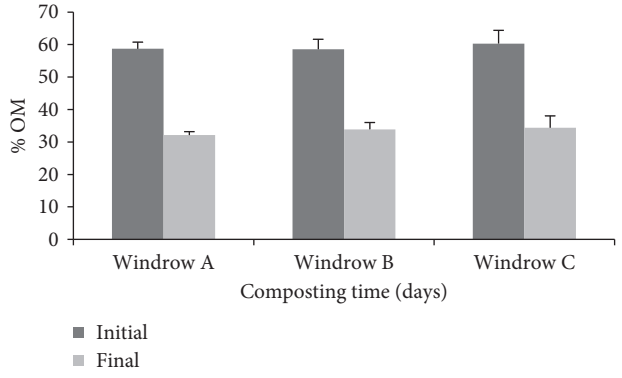

Figure 4: Organic matter degradation during the composting process.

composting process. These results show that all the experimented windrows were characterized by a high rate of organic matter (>55%) at the beginning of the composting process. It could be noticed that the windrow C has the highest organic content. During the composting process, the organic matter content gradually decreased, resulting in a degradation rate exceeding 40% for the three mixtures.

This degradation is highlighted during composting by a mass loss of the initial mixtures or even a remarkable reduction in the volumes of co-composted waste. The organic matter decomposition was the result of the microbial activity, allowing the transformation of the organic matter into stable humic substances [50]. The similar results were observed by El Fels et al., indicating a good degree of compostability of the mixtures [35].

Furthermore, no significant difference was shown by Student's t-test between the three windrows. So, one can conclude that the degradation of organic matter does not depend on the composition or nature of the co-composted waste.

3.1.5. C/N Ratio Evolution. The evolution of the C/N ratio is directly related to the biodegradation of organic matter, resulting in the lowering of the total carbon rate associated with the increase in nitrogen concentration. The initial C/N for the three windrows represented values between 25 and 35 (Figure 5). These C/N ratios were ideal for co-composting process [26, 51]. The C/N ratio evolution showed decreases of the ratios from 27.7 to 12.0, from 34.5 to 13.45, and from 34.3 to 12.2 for the windrows A, B, and C, respectively (Figure 5). This is closely related to the loss of organic carbon due to mineralization of the organic material, with a CO_2 production increasing the nitrogen concentration in the windrows during the biodegradation.

At the end of the co-composting, the C/N ratio reached values exceeding 8 for all windrows, indicating the maturity of the final compost [52]. Moreover, according to many authors, the C/N ratio is considered to be a maturity index; generally, the compost is mature if it presents a C/N ratio less than 20 [53–55].

The three profiles of the C/N ratio evolution are of the same speed and represent no significant difference between the three windrows confirmed by Student's t-test ($p > 0.05$).

3.2. Maturity and Quality of the Produced Composts

3.2.1. Characterization of the Produced Composts. The quality of the composts was assessed by comparing the final characteristics of the conceived composts to those of the French standard NF U44-051 (Table 4). The composts produced were neutral, except compost C was characterized by alkaline pH. This result is attributed to the nature of the co-composted waste. Also, they were characterized by C/N ratio around 12, exhibiting their stability.

The comparison of the three produced composts to the French standard showed significant amendment properties. Indeed, the produced composts were rich in fertilizing and mineral elements and low contents of heavy metals. These results have the same meaning with other previous studies valorizing OMW by co-composting, and the produced composts showed significant properties of organic fertilizers compared with the manure [18, 53, 56].

3.2.2. Phytotoxicity. The phytotoxicity of the produced composts was evaluated by the germination test; the result of this test is shown in Figure 6. This figure revealed the effects

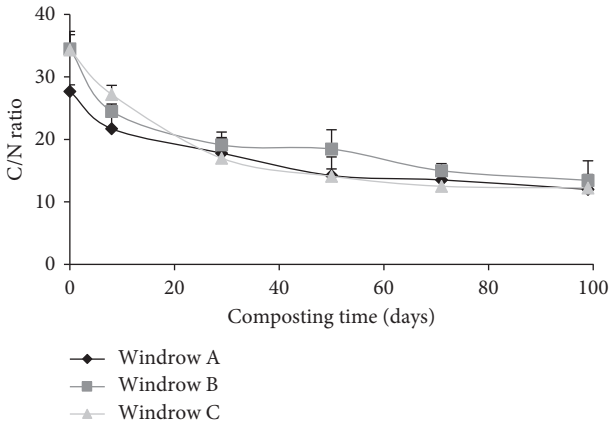

Figure 5: The C/N ratio evolution during the composting process.

Table 4: Physicochemical characteristics of produced composts.

Parameters	Compost A	Compost B	Compost C	NF U44-051
pH	7.02 ± 0.02	7.09 ± 0.03	8.30 ± 0.02	ND
CE mS·cm^{-1}	1.75 ± 0.02	3.04 ± 0.03	1.92 ± 0.03	ND
C/N	12.00 ± 1.23	13.45 ± 2.08	12.24 ± 1.15	>8
Minerals and fertilizing elements (mg/kg)				
P	855.99	158.37	346.15	ND
K	2763.56	2368.35	2264.55	ND
Mg	897.68	901.90	810.35	ND
Ca	10153.95	9237.85	9760.55	ND
Fe	5414.84	5101.55	6121.70	ND
Na	225.67	259.65	309.45	ND
Mn	49.65	31.65	33.35	ND
Heavy metals (mg/kg)				
Zn	57.83	11.6	12.2	600
Cu	22.26	5.95	6.55	300
Cr	9.35	7.60	5.95	12
Ni	<0.01	0.06	0.06	2
Cd	1.5	1.0	1.2	3
As	<0.01	<0.01	<0.01	18
Se	<0.01	<0.01	<0.01	12

ND: not determined.

of the extracts from produced composts on the germination of cress seeds at different dilutions.

The comparison between the different dilutions shows that a dilution rate of 25% shows the best germination for the different composts produced, marked by a higher rate for the compost and a significant difference between the different compost products C. However, a dilution rate of 50% shows a nonsignificant effect between the different compost products, whereas a dilution of 75% and the crude extract shows significant effects whose compost C represents the best germination index.

These differences can be explained by the nature of the raw materials, by the germination conditions of the watercress seeds and by the high conductivity of the compost extract. Indeed, high values in electrical conductivity inhibit the germination of watercress seeds, which results in low germination indices in raw compost extracts. According to Lasaridi et al., compost that is too saline can be harmful to plants; acceptable EC values should not exceed 2 to 3 mS/cm [57]. However, the three composts do not represent any phytotoxic effect because all these results showed a germination rate higher than 50%, indicating a maturity of the compost produced [38, 58].

3.2.3. Effect of the Produced Composts on Radish Production. The radish yields were assessed at the end of the crop cycle, while harvesting. The yields are presented in Figure 7. On farm manure, the yield was equal to 52.5 t/ha, but on the other parcels amended with the composts, the yield ranged from 52.8 t/ha to 57.7 t/ha. The produced composts significantly improved the productivity of the radish crop. However, the highest yields remained in parcels amended with the composts obtained from windrows C and A of 10%. It could be concluded that the OMW used for humidification played an important agronomic role. Indeed, the positive effect of composts based on olive mill waste on radish yields depends particularly on their richness in nutrients and fertilizers element particulates N, P, K, Ca, Mg, and Fe [19, 25]. These elements play a very important role in the growth of plants, thus promoting their vegetative activity, which results in an improvement in radish production yield.

However, Regni et al. suggest that long-term application of composted OMW to the soil improves vegetative activity and olive yield. They confirm that the contribution of nutrients to composted olive mill waste through their amendments associated with other indirect factors such as organic and dynamic matter content, water retention, and microbial biomass activity stimulates olive tree growth and improves olive yield and quality. These results are consistent with those found by Hachicha et al. showing the significant effect of composts based on OMS and poultry manure on potato yield [27].

4. Conclusion

The co-composting of olive mill wastes and the wine by-products with green waste has proved to be an effective means of producing an organic amendment for agricultural soils. The monitoring of the physicochemical parameters during this process has revealed a good progress of the co-composting process, a biodegradation of organic matter and a bioconversion of unstable matter into a stable product rich in humic substances. This biotransformation was also confirmed by the phytotoxicity test of the compost extracts produced, which showed that the various composts produced are mature and show no phytotoxic effect.

Moreover, the physicochemical characterization has proved that these composts are of good quality, rich in nutrients and particularly N, P, K, Ca, Mg, and Fe, and conforms to the standards of an organic amendment NF U44-051. The application of compost produced in the fields as organic soil improvers for radish cultivation has had a positive effect by increasing radish production yield by 10% compared to manure. Given the slow and complex dynamics

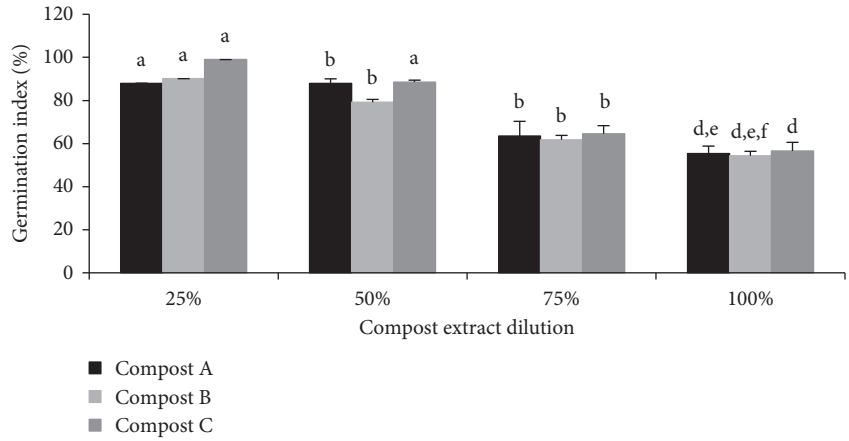

Figure 6: Effect of the compost extract on germination of cress seeds at different dilutions ($n = 5$, $p = 0.05$). Different letters (a–f) indicate significant differences ($p < 0.05$) between compost and dilution rates.

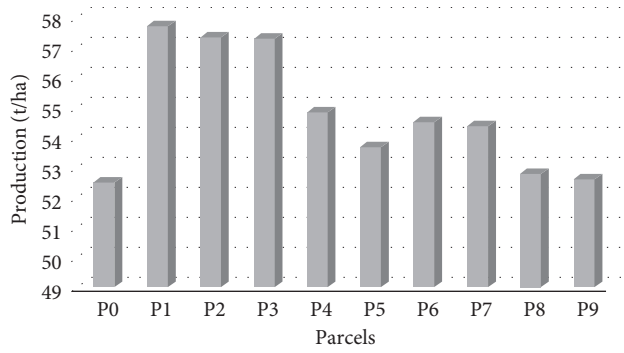

Figure 7: Production yield of harvested radish.

of organic substance transformation, long-term amendment experiments would be necessary and will be the subject of further research.

To conclude, one could say that the valorization of olive mill waste and the wine by-products is a promise strategy for the sustainable management of this type of waste allowing the transformation of environmental threats into a valuable product assuring fertility to agricultural soils.

Data Availability

The data used to support the findings of this study are available from the corresponding author upon request.

Conflicts of Interest

The authors declare that they have no conflicts of interest.

Acknowledgments

This work was supported by the funds of the PPR project type B (2015–2017) funded by the National Center for Scientific and Technical Research (CNRST). The authors would like to express their deep gratitude to all the professors and members of the doctoral research center who contributed to the improvement of this article. They extend their thanks to all of them for their advice, knowledge, insightful criticisms, and suggestions. Many thanks are also expressed to the persons who provided the material and made their laboratories available whenever needed.

References

[1] N. Perkins, A. Ajir, and L. El Ouazzani, *Rapport sur la Gestion des Déchets Solides au Maroc*, Scribd, San Francisco, CA, USA, 2014.

[2] M. Rahmani, *Examen National de l'Export vert du Maroc: Produits Oléicoles, Romarin et Thym*, United Nations, Geneva, 2017.

[3] S. Dermeche, M. Nadour, C. Larroche, F. Moulti-Mati, and P. Michaud, "Olive mill wastes: biochemical characterizations and valorization strategies," *Process Biochemistry*, vol. 48, no. 10, pp. 1532–1552, 2013.

[4] M. Ben Abbou, R. Rheribi, M. El Haji, Z. Rais, and M. Zemzami, "Effect of using olive mill wastewater by electrocoagulation process on the development and germination of tomato seeds," *Physical and Chemical News*, vol. 74, no. 10, pp. 37–43, 2014.

[5] Institut Français de la Vigne et de Vin, *Marcs de Raisins, Lies de Vin et Bourbes : Quelle Gestion des Sous-Produits Vinicoles?*, Institut Français de la Vigne et de Vin, Le Grau-du-Roi, France, 2013.

[6] Direction du Développement Des Filières de Production, *Ministère de l'Agriculture, de la Pêche Maritime, du Développement Rural et des Eaux et des Forêts Rabat*, 2016.

[7] M. A. Bustamante, R. Moral, C. Paredes, A. Pérez-Espinosa, J. Moreno-Caselles, and M. D. Pérez-Murcia, "Agrochemical characterisation of the solid by-products and residues from the winery and distillery industry," *Waste Management*, vol. 28, no. 2, pp. 372–380, 2008.

[8] L. Regni, L. Nasini, L. Ilarioni et al., "Long term amendment with fresh and composted solid olive mill waste on olive grove affects carbon sequestration by prunings, fruits, and soil," *Frontiers in Plant Science*, vol. 7, 2017.

[9] P. Proietti, E. Federici, L. Fidati et al., "Effects of amendment with oil mill waste and its derived-compost on soil chemical and microbiological characteristics and olive (*Olea europaea* L.) productivity," *Agriculture, Ecosystems and Environment*, vol. 207, pp. 51–60, 2015.

[10] E. Bertran, X. Sort, M. Soliva, and I. Trillas, "Composting winery waste: sludges and grape stalks," *Bioresource Technology*, vol. 95, no. 2, pp. 203–208, 2004.

[11] F. Hanafi, O. Assobhei, and M. Mountadar, "Detoxification and discoloration of Moroccan olive mill wastewater by electrocoagulation," *Journal of Hazardous Materials*, vol. 174, no. 1–3, pp. 807–812, 2010.

[12] N. Hytiris, I. E. Kapellakis, R. L. R. de, and K. P. Tsagarakis, "The potential use of olive mill sludge in solidification process," *Resources, Conservation and Recycling*, vol. 40, no. 2, pp. 129–139, 2004.

[13] M. Madani, M. Aliabadi, B. Nasernejad, R. K. Abdulrahman, M. Y. Kilic, and K. Kestioglu, "Treatment of olive mill wastewater using physico-chemical and Fenton processes," *Desalination and Water Treatment*, vol. 53, no. 8, pp. 2031–2040, 2015.

[14] M. Mosca, F. Cuomo, F. Lopez, G. Palumbo, G. Bufalo, and L. Ambrosone, "Adsorbent properties of olive mill wastes for chromate removal," *Desalination and Water Treatment*, vol. 54, no. 1, pp. 275–283, 2015.

[15] S. P. Tsonis, V. P. Tsola, and S. G. Grigoropoulos, "Systematic characterization and chemical treatment of olive oil mill wastewater," *Toxicological and EnvironmentalChemistry*, vol. 20-21, no. 1, pp. 437–457, 1989.

[16] A. Zirehpour, A. Rahimpour, and M. Jahanshahi, "The filtration performance and efficiency of olive mill wastewater treatment by integrated membrane process," *Desalination and Water Treatment*, vol. 53, no. 5, pp. 1254–1262, 2015.

[17] L. E. Fels, M. Hafidi, and Y. Ouhdouch, "Date palm and the activated sludge co-composting actinobacteria sanitization potential," *Environmental Technology*, vol. 37, no. 1, pp. 129–135, 2016.

[18] S. Hachicha, F. Sallemi, K. Medhioub, R. Hachicha, and E. Ammar, "Quality assessment of composts prepared with olive mill wastewater and agricultural wastes," *Waste Management*, vol. 28, no. 12, pp. 2593–2603, 2008.

[19] S. Masmoudi, R. Jarboui, H. E. Feki, T. Gea, K. Medhioub, and E. Ammar, "Characterization of olive mill wastes composts and their humic acids: stability assessment within different particle size fractions," *Environmental Technology*, vol. 34, no. 6, pp. 787–797, 2013.

[20] C. Paredes, A. Roig, M. P. Bernal, M. A. Sánchez-Monedero, and J. Cegarra, "Evolution of organic matter and nitrogen during co-composting of olive mill wastewater with solid organic wastes," *Biology and Fertility of Soils*, vol. 32, no. 3, pp. 222–227, 2000.

[21] L. Zhang and X. Sun, "Influence of bulking agents on physical, chemical, and microbiological properties during the two-stage composting of green waste," *Waste Management*, vol. 48, pp. 115–126, 2016.

[22] L. Zhang and X. Sun, "Changes in physical, chemical, and microbiological properties during the two-stage co-composting of green waste with spent mushroom compost and biochar," *Bioresource Technology*, vol. 171, pp. 274–284, 2014.

[23] C. S. Akratos, A. G. Tekerlekopoulou, I. A. Vasiliadou, and D. V. Vayenas, "Chapter 8-Cocomposting of olive mill waste for the production of soil amendments," in *Olive Mill Waste*, C. M. Galanakis, Ed., pp. 161–182, Academic Press, Cambridge, MA, USA, 2017.

[24] S. Hachicha, M. Chtourou, K. Medhioub, and E. Ammar, "Compost of poultry manure and olive mill wastes as an alternative fertilizer," *Agronomy for Sustainable Development*, vol. 26, no. 2, pp. 135–142, 2006.

[25] F. Sellami, R. Jarboui, S. Hachicha, K. Medhioub, and E. Ammar, "Co-composting of oil exhausted olive-cake, poultry manure and industrial residues of agro-food activity for soil amendment," *Bioresource Technology*, vol. 99, no. 5, pp. 1177–1188, 2008.

[26] P. Proietti, R. Calisti, G. Gigliotti, L. Nasini, L. Regni, and A. Marchini, "Composting optimization: integrating cost analysis with the physical-chemical properties of materials to be composted," *Journal of Cleaner Production*, vol. 137, pp. 1086–1099, 2016.

[27] S. Hachicha, F. Sellami, J. Cegarra et al., "Biological activity during co-composting of sludge issued from the OMW evaporation ponds with poultry manure—physico-chemical characterization of the processed organic matter," *Journal of Hazardous Materials*, vol. 162, no. 1, pp. 402–409, 2009.

[28] N. Abid and S. Sayadi, "Detrimental effects of olive mill wastewater on the composting process of agricultural wastes," *Waste Management*, vol. 26, no. 10, pp. 1099–1107, 2006.

[29] I. Aviani, Y. Laor, S. Medina, A. Krassnovsky, and M. Raviv, "Co-composting of solid and liquid olive mill wastes: management aspects and the horticultural value of the resulting composts," *Bioresource Technology*, vol. 101, no. 17, pp. 6699–6706, 2010.

[30] Z. Majbar, Z. Rais, M. El Haji, M. B. Abbou, H. Bouka, and M. Nawdali, "Olive mill wastewater and wine by-products valorization by co-composting," *Journal of Materials and Environmental Science*, vol. 8, no. 9, pp. 3162–3167, 2017.

[31] K. Lahlou, M. Ben Abbou, Z. Majbar et al., "Recovery of sludge from the sewage treatment plant in the city of Fez (STEP) through the composting process," *Journal of Materials and Environmental Sciences*, vol. 8, no. 12, pp. 4582–4590, 2017.

[32] D. Raj and R. S. Antil, "Evaluation of maturity and stability parameters of composts prepared from agro-industrial wastes," *Bioresource Technology*, vol. 102, no. 3, pp. 2868–2873, 2011.

[33] W. Abid, E. Ammar, M. A. Triki, M. Ben Abbou, and M. El Haji, "Gestion et valorisation des margines par co compostage avec les déchets verts et amendements des sols agricoles pour l'amélioration des rendements," *Brevet déposé à l'Office Marocain de la Propriété Industrielle et Commerciale*, MA 20150445 A1, 2015.

[34] C. Paredes, M. P. Bernal, J. Cegarra, and A. Roig, "Biodegradation of olive mill wastewater sludge by its co-composting with agricultural wastes," *Bioresource Technology*, vol. 85, no. 1, pp. 1–8, 2002.

[35] L. El Fels, M. Zamama, A. El Asli, and M. Hafidi, "Assessment of biotransformation of organic matter during co-composting of sewage sludge-lignocelullosic waste by chemical, FTIR analyses, and phytotoxicity tests," *International Biodeterioration and Biodegradation*, vol. 87, pp. 128–137, 2014.

[36] L. E. Fels, M. Zamama, A. Aguelmous et al., "Assessment of organo-mineral fraction during co-composting of sewage sludge-lignocellulosic waste by XRD and FTIR analysis," *Moroccan Journal of Chemistry*, vol. 5, no. 4, pp. 730–739, 2017.

[37] L. El Fels, F. Z. El Ouaqoudi, L. Lemee et al., "Identification and assay of microbial fatty acids during co-composting of active sewage sludge with palm waste by TMAH-thermochemolysis coupled with GC-MS," *Chemistry and Ecology*, vol. 31, no. 1, pp. 64–76, 2015.

[38] L. Nasini, G. De Luca, A. Ricci et al., "Gas emissions during olive mill waste composting under static pile conditions,"

International Biodeterioration and Biodegradation, vol. 107, pp. 70–76, 2016.

[39] B. Soudi, "Le compostage des déchets des cultures sous serre et du fumier," *Bullletin Mensuel d'Information et de Liaison du PNTTA*, vol. 129, pp. 1–6, 2005.

[40] ISO 8633, *Solid Fertilizers-Simple Samplingmethod for Small Lots*, ISO, Geneva, Switzerland, 1992, https://www.iso.org/standard/15994.html.

[41] International Organization for Standardization, *ISO 10390-Soil Quality-Determination of pH*, ISO, Geneva, Switzerland, 2005, https://www.iso.org/standard/40879.html.

[42] International Organization for Standardization, *ISO 11265-Soil Quality-Determination of the Specific Electrical Conductivity*, ISO, Geneva, Switzerland, 1994, https://www.iso.org/standard/19243.html.

[43] French Association for Standardization, *Determination of Nitrogen Kjeldahl-Titrimetric Determination Method after Mineralization and Distillation*, NF T90–110, French Association for Standardization, France, 1981.

[44] J. Rodier, B. Legube, N. Merlet, and R. Brunet, L'Analyse de l'Eau, Dunod, Paris, France, 9th edition, 2009, https://www.fichier-pdf.fr/2012/12/08/l-analyse-de-l-eau-9e-edition-entierement-mise-a-jour-jean-rodie/l-analyse-de-l-eau-9e-edition-entierement-mise-a-jour-jean-rodie.pdf.

[45] NF T90-101, "Water quality-determination of chemical oxygen demand (COD)-qualité de l'eau," 2001, https://www.boutique.afnor.org/norme/nf-t90-101/qualite-de-l-eau-determination-de-la-demande-chimique-en-oxygene-dco/article/778836/fa111555.

[46] C. Tognetti, M. J. Mazzarino, and F. Laos, "Improving the quality of municipal organic waste compost," *Bioresource Technology*, vol. 98, no. 5, pp. 1067–1076, 2007.

[47] L. Baeta-Hall, M. CéuSàágua, M. Lourdes Bartolomeu, A. M. Anselmo, and M. Fernanda Rosa, "Bio-degradation of olive oil husks in composting aerated piles," *Bioresource Technology*, vol. 96, no. 1, pp. 69–78, 2005.

[48] B. Zenjari, H. El Hajjouji, G. AitBaddi et al., "Eliminating toxic compounds by composting olive mill wastewater–straw mixtures," *Journal of Hazardous Materials*, vol. 138, no. 3, pp. 433–437, 2006.

[49] S. Amir, M. Hafidi, G. Merlina, and J.-C. Revel, "Sequential extraction of heavy metals during composting of sewage sludge," *Chemosphere*, vol. 59, no. 6, pp. 801–810, 2005.

[50] C. Francou, *Stabilisation de la Matière Organique au Cours du Compostage de Déchets Urbains: Influence de la Nature des Déchets et du Procédé de Compostage-Recherche d'indicateurs Pertinents*, INAPG (AgroParisTech), Paris, France, 2003, https://pastel.archives-ouvertes.fr/pastel-00000788/.

[51] J. Singh and A. S. Kalamdhad, "Assessment of compost quality in agitated pile composting of water hyacinth collected from different sources," *International Journal of Recycling of Organic Waste in Agriculture*, vol. 4, no. 3, pp. 175–183, 2015.

[52] NF U44-051, "Organic soil improvers-designations, specifications and marking," 2006, https://www.boutique.afnor.org/standard/nf-u44-051/organic-soil-improvers-designations-specifications-and-marking/article/686933/fa125064.

[53] J. A. Alburquerque, J. Gonzálvez, G. Tortosa, G. A. Baddi, and J. Cegarra, "Evaluation of "alperujo composting based on organic matter degradation, humification and compost quality," *Biodegradation*, vol. 20, no. 2, pp. 257–270, 2009.

[54] J. A. Alburquerque, J. Gonzálvez, D. García, and J. Cegarra, "Measuring detoxification and maturity in compost made from "alperujo," the solid by-product of extracting olive oil by the two-phase centrifugation system," *Chemosphere*, vol. 64, no. 3, pp. 470–477, 2006.

[55] A. K. M. Muktadirul Bari Chowdhury, C. S. Akratos, D. V. Vayenas, and S. Pavlou, "Olive mill waste composting: a review," *International Biodeterioration and Biodegradation*, vol. 85, pp. 108–119, 2013.

[56] F. Sellami, S. Hachicha, M. Chtourou, K. Medhioub, and E. Ammar, "Bioconversion of wastes from the olive oil and confectionary industries: spectroscopic study of humic acids," *EnvironmentalTechnology*, vol. 28, no. 11, pp. 1285–1298, 2007.

[57] K. Lasaridi, I. Protopapa, M. Kotsou, G. Pilidis, T. Manios, and A. Kyriacou, "Quality assessment of composts in the Greek market: the need for standards and quality assurance," *Journal of Environmental Management*, vol. 80, no. 1, pp. 58–65, 2006.

[58] M. Chikae, R. Ikeda, K. Kerman, Y. Morita, and E. Tamiya, "Estimation of maturity of compost from food wastes and agro-residues by multiple regression analysis," *Bioresource Technology*, vol. 97, no. 16, pp. 1979–1985, 2006.